




Relationships between high-K magmas and Cu–Au porphyry deposits in the Macquarie Arc, Australia

Ryan C. Dwyer¹, David B. Forster¹, Brenainn P. Simpson¹,
Phillip L. Blevin¹* and Huiqing Huang²

¹Geological Survey of New South Wales, Maitland, Australia

²James Cook University, Townsville, Australia

 RCD, 0000-0001-9495-7855; BPS, 0000-0001-9621-7092;
PLB, 0000-0001-7426-9828; HH, 0000-0002-0104-7201

*Correspondence: phil.blevin@regional.nsw.gov.au

Abstract: The Macquarie Arc is a long-lived volcanic arc terrane which began in the latest Cambrian and continued until the early Silurian. Early Silurian high-K suites associated with Cu–Au porphyry mineralization are typically considered shoshonitic; however, comparisons with well-studied examples of shoshonites in continental arcs and associated settings suggest few Macquarie Arc rocks would classify as shoshonitic. Notably, the Au-rich Cadia Intrusive Complex, which is marginally shoshonitic, and most high-K to ‘shoshonitic’ Macquarie Arc rocks are essentially high-K calc-alkaline, analogous to ‘primitive’ shoshonites generated within intraoceanic arc settings. Arc magmatism in the Macquarie Arc is consistently primitive and mantle derived prior to an increase in siliciclastic input and crustal thickening during the Silurian Benambran Orogeny, consistent with prior isotopic studies. Magma source regions can thus be interpreted as varying spatially and temporally due to variable enrichment from slab and mantle derived components, reflecting a maturing and potentially migrating arc system.

Supplementary material: A summary table of Macquarie Arc deposit characteristics, additional whole rock classification and tectonic discrimination diagrams, sample details and geochemistry, crustal thickness calculations, and LA-ICP-MS U–Pb zircon geochronology reports are available at <https://doi.org/10.6084/m9.fig-share.c.7283940>

Potassic igneous rocks, both volcanic and intrusive, have a wide range of compositions from mildly to highly potassic trachytes and latites; variably K-enriched shoshonites including primitive shoshonites (Leslie *et al.* 2009); and ultra potassic leucites, kamafugites, lamprophyres and pegmatites (Müller and Groves 2019). These rocks are typically the product of low degree partial melts of an often metasomatically enriched mantle source region and may be influenced by the incorporation of incompatible elements from subducting sediments or assimilation of crustal material during differentiation (Plank and Langmuir 1993, 1998; Pearce *et al.* 2005; Wallace 2005; Langmuir *et al.* 2006; Davidson *et al.* 2013; Krmíček and Chalapathi Rao 2022; O'Neill *et al.* 2024). These rocks occur in a convergent setting and are often associated with the formation of Cu- and Au-rich porphyry deposits and skarns (Müller 2002; Mungall 2002; Richards 2009; Müller and Groves 2019), and may provide insights into changes in arc magmatism through time and a corresponding relationship with mineralization.

Porphyry Cu–Au deposits are typically associated with oxidized intermediate or felsic calc-alkaline magmas (Pettke *et al.* 2010; Sillitoe 2010; Wilkinson 2013). Porphyry deposits host about two-thirds of the world's Cu resources, critical

for the green energy transition (Singer 2017). Mineralized porphyritic intrusions occur in oceanic, continental and post-collisional arc settings associated with the subduction of oceanic slabs (Sillitoe 1972, 1973; Ishihara 1977). The resultant melts are hydrous and enriched in incompatible trace elements, in particular large ion lithophile elements (LILEs). The enrichment of LILEs adds additional alkali metals into the magmas, which are then typically alkaline to highly alkaline, and results in the known association between potassic arc rocks and mineralized porphyries.

In the Macquarie Arc of central New South Wales (NSW), porphyry Cu–Au deposits are associated with variably K-enriched igneous suites (Blevin 2002), and various workers have proposed a link between metal endowment and high-K or shoshonitic magmatism (Müller *et al.* 1994; Holliday *et al.* 2002; Cooke *et al.* 2007; Crawford *et al.* 2007a). Shoshonites are a group of very high-K and near-SiO₂ saturated rocks that are not typically classified as alkaline or calc-alkaline (Morrison 1980). They typically occur late in the evolution of volcanic arcs, after the eruption of lower-K ocean island tholeiites and calc-alkaline rocks (Müller and Groves 2019). Because of this, shoshonitic rocks are an indicator of arc maturity and often

From: Pandey, R., Pandey, A., Krmíček, L., Cucciniello, C. and Müller, D. (eds) 2025. *Alkaline Rocks: Economic and Geodynamic Significance through Geological Time*. Geological Society, London, Special Publications, **551**, 259–300. First published online September 30, 2024, <https://doi.org/10.1144/SP551-2024-65>

© 2024 The Author(s). This is an Open Access article distributed under the terms of the Creative Commons Attribution License (<http://creativecommons.org/licenses/by/4.0/>). Published by The Geological Society of London.

Publishing disclaimer: <https://www.lyellcollection.org/publishing-hub/publishing-ethics>

associated with high-K and oxidized mineralized porphyries (Burnham and Ohmoto 1980; Carroll and Rutherford 1987; Mungall 2002; O'Neill *et al.* 2024).

In this review, we present detailed descriptions of the potassic mineralized intrusions and mineralization in the Macquarie Arc, alongside new whole-rock geochemical data for porphyry deposits and associated unmineralized intrusions and volcanic rocks, and we classify them according to published trace and major element schema. The best described of these deposits are the Cadia–Ridgeway porphyries located 20 km south of Orange, and the Northparkes porphyries 25 km NW of Parkes in NSW, Australia. Additionally, we present summary descriptions and mineralogical data for porphyry mineralization at Boda–Kaiser, Comobella, Trundle, Copper Hill, the Temora district and others, including Glendale and Junction Reefs. This study excludes major carbonate-base metal epithermal deposits, including the medium-K Lake Cowal Intrusive Complex associated with the E41, E42, E46, Galway and Regal Au deposits.

Background

Geology, evolution and setting of the Macquarie Arc

The geology of eastern Australia is dominated by a series of orogenic belts collectively referred to as the Tasmanides. These belts record the breakup of the Mesoproterozoic supercontinent Rodinia and the establishment of a Late Neoproterozoic passive margin which developed into a convergent margin during the Middle Cambrian (Glen 2005). Sequential accretion of oceanic terranes onto the Proterozoic Curnamona craton continued through to the collision of Gondwana with Laurussia and subsequent fragmentation of Pangaea in the Permian and Triassic (Veevers 2013). The Tasmanides are divided into five discrete orogens consisting of metamorphic terranes, fold and thrust belts, sedimentary basins and igneous provinces (for a recent review, the reader is directed to Rosenbaum 2018). The Tasmanides have been interpreted as an accretionary orogenic system, where the main driver of crustal growth was terrane accretion associated with a continuous, migratory subduction zone, which may have experienced polarity reversals (Glen 2013; Fergusson 2014).

The Lachlan Orogen centres on the Macquarie Igneous Province (here termed the Macquarie Arc; Fig. 1), a latest Cambrian to earliest Silurian oceanic arc characterized by quartz-rich, medium-K dacites to quartz-poor, high-K monzonites and an associated voluminous volcanic package (Crawford *et al.*

2007a; Glen *et al.* 2012). The Macquarie Arc is flanked on either side by extensive Ordovician fore- and back-arc quartz-rich turbidite sequences which comprise the bulk of the Lachlan Orogen. Subsequent extension has dismembered the Macquarie Arc into three longitudinal belts, interspersed with Silurian to Devonian I- and S-type granites and sedimentary basins (Glen 2005).

Four phases of orogenic deformation are recognized within the Lachlan Orogen (Fig. 2). These orogenic phases occurred during the Silurian (Benambran Orogeny), Early Devonian (Bindian Orogeny), Middle Devonian (Tabberabberan Orogeny) and Early Carboniferous (Kanimblan Orogeny) (Glen 2005). Although each orogenic phase has an extensional and compressional component, the extension appears to be more predominant. The Lachlan Orogen represents some of the thickest crust in the Tasmanides, proposed to be the result of significant mafic underplating (Kemp *et al.* 2020; Bello *et al.* 2021) and crustal thickening during deformation (Rosenbaum 2018). Basaltic volcanism during the Cenozoic has erupted through the Lachlan Orogen transporting phlogopite and hornblende bearing mantle xenoliths (Simpson and Sutherland 2022), indicating a metasomatized and potentially fertile lithospheric mantle.

The present-day extent of the Macquarie Arc consists of four belts of volcanic-dominated rocks that range in age from Cambrian to early Silurian. These comprise calc-alkaline to alkaline volcanic, shallow intrusive and shallow-marine sedimentary sequences. Three belts in central NSW host significant porphyry-related mineralization: the Junee–Narromine Volcanic Belt in the west, the Molong Volcanic Belt in the centre, and the Rockley–Gulgong Volcanic Belt in the east. The narrow Kiandra Volcanic Belt in southeastern NSW hosts only minor, mostly alluvial mineralization (Greenfield *et al.* 2022). The Molong Volcanic Belt and Junee–Narromine Belt host the porphyry deposits currently being mined on a large scale (Cadia and Northparkes), which are associated with rocks several authors have described as being of shoshonitic affinity (Cooke *et al.* 2007; Crawford *et al.* 2007a, b; see also Blevin 2002).

Regional metamorphism of the Macquarie Arc is mostly of lower greenschist facies or lower, including around major porphyry districts. Higher-grade facies are mostly restricted to parts of the Kiandra Volcanic Belt and Rockley Volcanic Belt, and probably relate to the arc-terminating Benambran Orogeny and/or subsequent tectonic events (Collins 1994; Glen *et al.* 2007a). Based on geochronological, stratigraphic and geochemical evidence, Percival and Glen (2007), Crawford *et al.* (2007a, b, c) and Cooke *et al.* (2007) identified four major episodes of magmatism for the Macquarie Arc, including

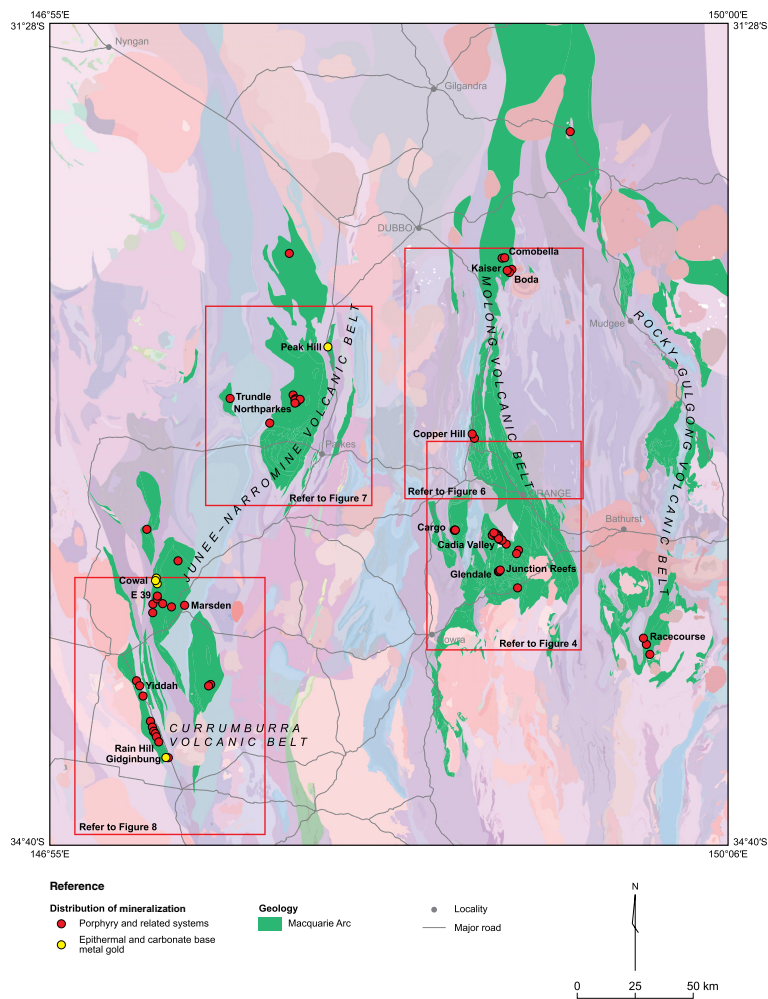


Fig. 1. Location of major Ordovician to early Silurian porphyry and related mineral systems of the Macquarie Arc. The three main longitudinal belts of Macquarie Arc rocks are shown in green. Background geology is from the *NSW Seamless Geology* (Colquhoun *et al.* 2024). The smaller Kiandra belt is located to the south of the Junee–Narromine Volcanic Belt and is not shown in this figure.

volcanism (Phases 1–4) and intrusions (Groups 1–4). The latter included the emplacement of porphyries and related Cu–Au mineralization.

Latest Cambrian to Early Ordovician Phase 1 (~490–475 Ma) was associated with calc-alkaline volcanic and shoshonitic volcanic and intrusive rocks. The basal Nelungaloo Volcanics in the Junee–Narromine Belt and Mitchell Volcanics of the Molong Volcanic Belt are among the oldest known rocks of the Macquarie Arc. They include plagioclase–augite–Fe–Ti oxide-phyric basaltic andesites and andesites of calc-alkaline to shoshonitic composition (Crawford *et al.* 2007a, b). This suggests prior enrichment in LILEs in the magmatic

source(s) of the Macquarie Arc, which may have been associated with subduction (Glen *et al.* 2007b; Fergusson 2009). Based on structural evidence, Glen *et al.* (2002) suggested that Cambrian crust underlies parts of the Macquarie Arc. This notion has been strongly supported by Pb–Pb, Hf and Nd isotopic evidence, along with U–Pb zircon geochronology (Forster *et al.* 2011; Kemp *et al.* 2020; Zhang *et al.* 2020).

Early to Middle Ordovician Phase 2 (475–466 Ma; Glen *et al.* 2011a, b) medium- to high-K calc-alkaline volcanics and minor intrusions of Phase 2 followed an inferred hiatus characterized by the Cargo and Cadia–Forest Reefs areas,

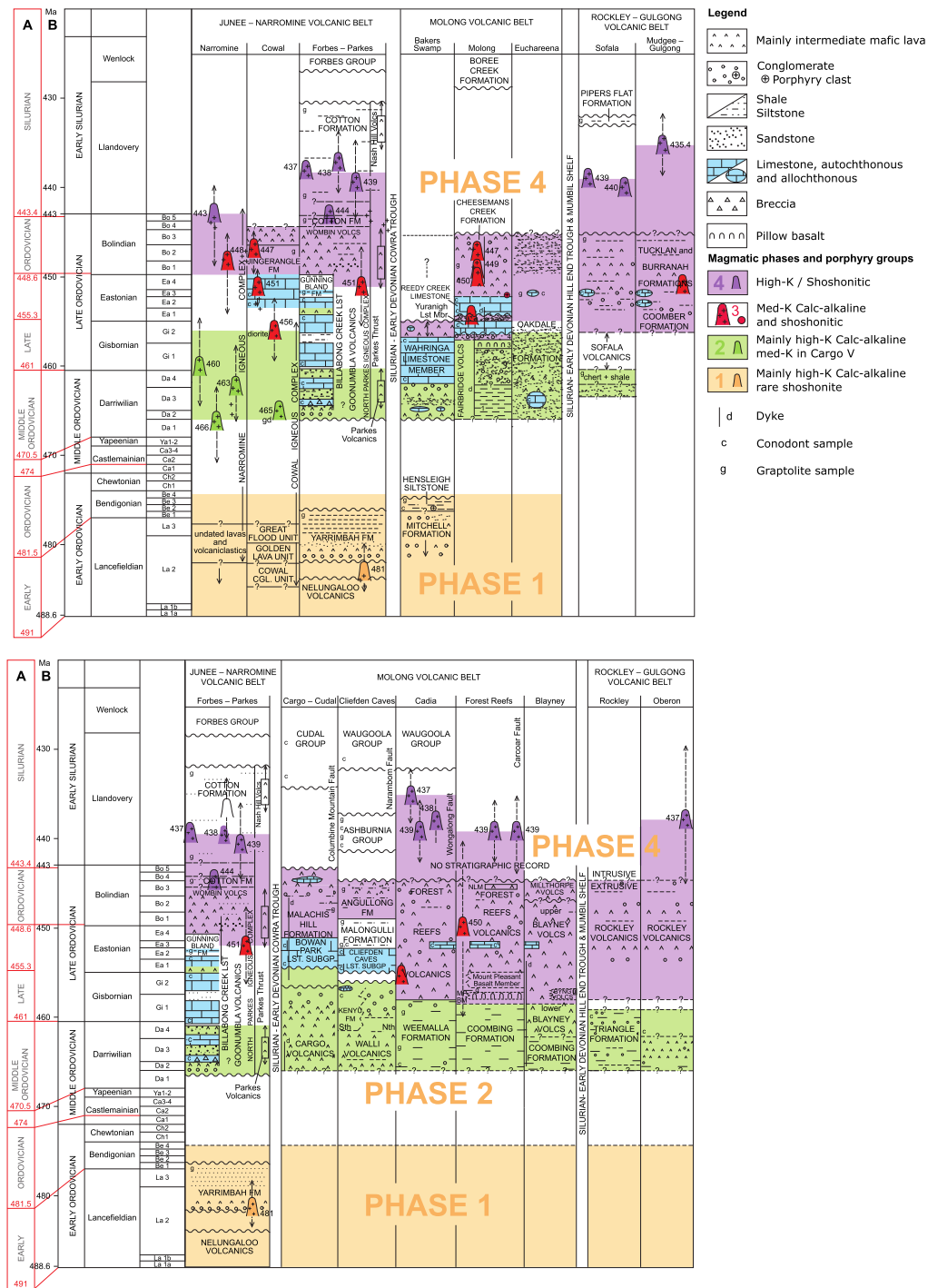


Fig. 2. Time-space plots through the northern (top) and southern (bottom) parts of the Macquarie Arc. Abbreviations: gd, granodiorite; CGL, Cowal conglomerate unit; Volcs, volcanics; LST, limestone; Mbr, member; v, volcanics; SUBGP, subgroup; NLM, Nulawonga Latite Member; MPBM, Mount Pleasant basalt member. Source: adapted from Glen and Blevin (2019).

respectively (Crawford *et al.* 2007a, b; Kemp *et al.* 2020). Volcanic and proximal volcanic-derived sedimentary sequences are predominant in the Blaney area and Cargo areas, whereas the Cadia–Forest Reefs and Sofala areas are characterized by more distal rhythmic feldspathic and variably calcareous sandstones and siltstones of the Coombing Formation and Weemalla Formation. Crawford *et al.* (2007a, b, c) and Glen *et al.* (2007b) suggested that Phase 2 was terminated by a regional uplift and erosion with a short hiatus.

Overlying Phase 3 volcanosedimentary sequences in the Cadia district are of high-K composition and are notably more proximal (Squire and Crawford 2007). Middle to Late Ordovician Phase 3 (~468–455 Ma) medium-K calc-alkaline intrusions of the Copper Hill Suite are considered to represent reversion to less potassic, medium-K magmatism in an otherwise highly potassic maturing arc system, and related to a tectonic event that led to crustal thickening of the arc (Crawford *et al.* 2007b). Group 3 intrusions (~455–445 Ma) occur as isolated medium-K calc-alkaline rocks in the Junee–Narromine and Molong Volcanic belts, most notably the Copper Hill Suite (see Blevin 2002). Crawford *et al.* (2007a, b) suggested it was the only intrusive phase emplaced during a volcanic hiatus that was associated with a period of uplift and Late Ordovician carbonate deposition, which is preserved in the Goonumbla and Cadia districts, prior to Phase 4 and Group 4 magmatism (see Butera *et al.* 2001; Forster *et al.* 2004).

Late Ordovician Phase 4 (~445–435 Ma) magmatism is mostly high-K and was more compositionally evolved, including widespread volcanics and monzodioritic to monzonitic mineralized intrusions. Phase 4 most notably includes the highly significant Cadia and Northparkes districts along with the Bodangora and Temora districts. Primitive Phase 4 lavas on the eastern side of the Molong Volcanic Belt (Byng and Blaney volcanics) are considered evidence of major extension and rifting of the arc setting (Crawford *et al.* 2007b). Magma compositional changes throughout Phase 2 through to Phase 4 are considered to reflect a shift from ‘typical oceanic arc-type lavas’ to a setting where crustal input or the influence of a thickening crust drove compositions to more evolved levels (Crawford *et al.* 2007b). Group 4 porphyry intrusions were probably syn-accretionary and emplaced at shallow levels into tilted and deformed volcanic and volcanoclastic packages during the early Silurian Benambran Orogeny (Crawford *et al.* 2007a, b; Glen *et al.* 2007c; Fox *et al.* 2015; Blevin *et al.* 2020; Groome *et al.* 2021).

Group 4 intrusions occur coevally with the termination of arc magmatism associated with the accretion of the terrane onto Gondwana during the early Silurian Benambran Orogeny. Collision and

initiation of crustal extension and dismemberment are thought to have occurred around 438 Ma (Crawford *et al.* 2007b). Parallels to the Fijian section of the Vitiaz arc were drawn by Squire and Crawford (2007), who inferred ‘pre-processing’ of the sub-arc mantle prior to collision and subsequent extension, resulting in the late subduction-modified high-K calc-alkaline to shoshonitic intrusions in the Cadia–Forest Reefs region. Stratigraphic relationships and distinctive geochemical signatures were cited to suggest that the late Bushman and Nash Hill volcanics, and the Fifield Alaskan-type complexes, likely represented a separate magmatic event unrelated to the Macquarie Arc (Crawford *et al.* 2007b).

Kemp *et al.* (2020) used new isotopic fingerprinting and age dating to extend the age range of magmatic activity to c. 503–432 Ma, including Phase 2 (477–455 Ma) and Phase 4 (~444–432 Ma, youngest ages in the Temora Belt). Those authors also suggested that Phase 3 magmatism, including Copper Hill, was older than previously thought, thus predating Late Ordovician carbonate deposition. These wider age ranges obviously call into question the intervening magmatic hiatuses.

The metal endowment of the Macquarie Arc is dominated by alkalic and calc-alkalic porphyry Au–Cu and related skarn deposits. Porphyry and related skarn deposits, which are subject to large-scale modern mining, are all Late Ordovician to early Silurian in age (Group 4). These deposits are not distributed equally throughout the volcanic belts, but typically occur in clusters or districts. Porphyry and related skarn deposits of the Macquarie Arc host over 65 Moz of gold, which is about 89% of the recoverable gold in the Macquarie Arc, the remainder hosted by carbonate–base metal (mesothermal) and high-sulfidation epithermal deposits. This represents over 50% of the gold endowment in NSW. The Macquarie Arc also hosts over 14 Mt of copper (about 80% of NSW copper endowment), almost entirely hosted by porphyry and related skarn deposits.

Summary of existing geochemical studies

Several authors, including Scheibner (1987) and Packham (1987), suggested that volcanic sequences of the Macquarie Arc formed in an intraoceanic arc setting related to west-dipping subduction. Following this, Wyborn (1992) proposed that the volcanism was related to rifting, heating and possibly foundering of the lithospheric mantle, based largely on the ‘overwhelmingly shoshonitic’ geochemical affinity of the rocks. More recently, Blevin and Morrison (1997), Blevin (1998) and Glen *et al.* (1998) have emphasized the overall calc-alkaline character of the magmatism, and again supported a contemporaneous intraoceanic island arc setting. In addition,

Blevin (2002) demonstrated that intrusions at Goonumbra and Copper Hill are largely of K-enriched calc-alkaline affinity, and that only Cadia intrusions could be considered shoshonitic by the accepted defining criteria, given that immobile elements and light rare earth elements/heavy rare earth elements (LREEs/HREEs) display only marginal enrichment and depletion compared with definitive shoshonitic series rocks (Blevin 2002). Blevin (2002) suggested that the parental magmas of the mineralizing intrusions likely represent mixing between enriched lithospheric mantle and more primitive asthenospheric sources, and that the source region was progressively enriched over time.

The most significant large-scale assessment of the geochemistry of the Macquarie Arc came from a series of papers included in the *Australian Journal of Earth Sciences* special issue 'Geological Evolution and Metallogenesis of the Ordovician Macquarie Arc, Lachlan Orogen, New South Wales' (Barron *et al.* 2007; Cooke *et al.* 2007; Crawford *et al.* 2007a, b, c; Glen *et al.* 2007a, b, c, d; Lickfold *et al.* 2007; Meffre *et al.* 2007; Percival and Glen 2007; Simpson *et al.* 2007; Squire and Crawford 2007; Squire and McPhie 2007), culminating in a synthesis of the magmatic and isotopic evolution and broad grouping of the arc in four phases (Crawford *et al.* 2007b). This synthesis divided the evolution of the Macquarie Arc into four constituent phases interspersed by inferred hiatuses in arc volcanism as described in the previous section.

Several of these papers presented geochemical data which included shoshonitic compositions for numerous volcanic and plutonic suites, including those associated with Phase 4 and Group 4 magmatism such as in the Cadia district, but also for older rocks such as in the Cowal district and in the Junee–Narromine Belt (e.g. Crawford *et al.* 2007b, c; Percival and Glen 2007; Squire and Crawford 2007). Many of the discrimination plots presented, which reported shoshonitic compositions, were based on major element whole-rock data including K_2O v. SiO_2 , P_2O_5/Al_2O_3 v. K_2O/Al_2O_3 , etc. Based on these data, along with some LREE/HREE discrimination, these papers equated many regional volcanic samples with K-enriched suites associated with Phase 4 and Group 4, including in the Goonumbra and Cadia districts.

Prior to and following the special issue, several district and regional scale geochemical studies focused on the petrogenesis, fractionation history, magmatic state and mineral potential and fertility of volcanic and intrusive suites generally associated with mineralization (Heithersay *et al.* 1990; Müller *et al.* 1994; Heithersay and Walshe 1995; Arundell 1998; Lickfold 2002; Lickfold *et al.* 2003; Wilson 2003; Chhun 2004; Zukowski 2010; Goesch 2011; Pacey 2016; Wells 2016; Hao *et al.* 2017, 2021;

Lowczak *et al.* 2018; Pacey *et al.* 2019; Zhang *et al.* 2019; Wells *et al.* 2020). These contributions substantially increased our understanding of magmatic processes within individual districts, but few studies have taken a broader view of Macquarie Arc magmatism to better understand the large-scale tectonic implications for the arc as a whole. Much of the data for the special issue were generated in the late 1990s and early 2000s, often with a limited suite of analytes and lower analytical precision than is achievable with modern instruments. Advances in characterization and discrimination, and increased understanding of petrogenesis underpinning processes within subduction systems have also outpaced this early research. New data generated with modern analytical precision and a more complete suite of analytes allow a reassessment of these pivotal works.

Summary of existing isotopic studies

Previous radiogenic isotopic studies for the Macquarie Arc include Pb–Pb, Nd and Sm–Nd (Sun 1980; Wyborn and Sun 1993; Carr *et al.* 1995; Crawford *et al.* 2007b; Kemp *et al.* 2009, 2020; Forster *et al.* 2011, 2015).

Lead isotope data for mineral deposits and limited data for rocks from the Macquarie Arc generally plot close to established mantle growth curves and are like oceanic basalts (see Sun 1980). Lead model ages for individual deposits are generally consistent with independent age constraints on mineralization. Intrusions associated with the early Silurian mineralization at Cadia and Goonumbra have narrow and distinct Pb isotope signatures that we interpret to be the result of partial melting of already LILE-enriched mantle-like sources. The data suggest that deposits of the Macquarie Arc derived Pb from one or more long-lived mantle-like Pb isotope reservoirs without significant contributions of crustal Pb prior to the Benambran Orogeny. Only slight enrichment in crustal components is evident for Cadia and Northparkes, which formed during the Benambran Orogeny (Glen *et al.* 2007c; Fox *et al.* 2015; Harris *et al.* 2020). Data for the Trundle Park and Rose Hill prospects differ markedly in that they contain significant crustal Pb and have Pb–Pb model ages on galena younger than Ordovician.

The available data also suggest the presence of mid-ocean ridge basalt (MORB)-like Pb isotope reservoirs, and that Cambrian–Early Ordovician material may be a widespread component of the Macquarie Arc (Forster *et al.* 2011; Kemp *et al.* 2020). Juvenile mantle-like epsilon Hf and U–Pb Cambrian age constraints for the monzogabbro within a basal sequence of the Temora Belt suggest that the early development of the Macquarie Arc occurred within an oceanic setting and built on mafic Cambrian crust (Kemp *et al.* 2020). Epsilon

Nd isotopes for deposits and associated rocks become progressively enriched throughout the Ordovician to early Silurian, albeit within a very narrow range consistent with mantle reservoirs (Forster *et al.* 2011; Huston *et al.* 2017).

The gradual enrichment of epsilon Nd (determined from bulk rock Sm–Nd) from primitive depleted mantle-like values of Phase 1 (+8.15 to +7.3) through to Phase 4 (+6.8 to +4.94) Macquarie Arc contrasts markedly with inferred post-subduction shoshonitic volcanics (+3.54 to +2.63) and subsequent crustal-like negative epsilon Nd of the S- to I-type granites of the Lachlan Fold Belt. A general agreement with these trends is observed in available epsilon Hf (determined from zircon Lu–Hf) data for the Macquarie Arc, and specifically for barren and mineralized intrusions (Kemp *et al.* 2009, 2020). High positive epsilon Nd and Hf suggest generation of magmas initially occurred within an intraoceanic setting with little to no sedimentary, supra-subduction zone (SSZ), or (siliciclastic) crustal inputs (Crawford *et al.* 2007b; Kemp *et al.* 2009, 2020; Forster *et al.* 2015). The trend to moderate to low positive values is interpreted to reflect the increasing contributions of felsic crust or mature sediments prior to and during accretion and subsequent orogenesis (Crawford *et al.* 2007b; Kemp *et al.* 2009, 2020).

Mineral deposits of the Macquarie Arc

The economic porphyry deposits in the Cadia–Ridgeway and Northparkes districts are of the Au (\pm Ag, Cu) type of Sillitoe (2000), with Au (g t^{-1}) v. Cu (%) ratios = 1:1 (0.2–0.6 g t^{-1} Au, 0.2–0.7% Cu) to 4:1 (Cadia Hill, Ridgeway) (see Sillitoe 1997). Based on combined, pre-mining tonnages (Table 1), the Cadia district porphyry deposits host over 1100 t Au (contained) and thus collectively rank among ‘giant’ Au–Cu porphyry deposits of Cooke *et al.* (2005). Individual deposits at Cadia, including Cadia East, rank among the largest ‘giant’ deposits, containing $>1.05 \times 10^6$ kg Au ($>37 \times 10^6$ Oz). Several deposits, most notably Ridgeway and Cadia East, may be classified as high-grade and Au-rich according to Cooke *et al.* (2005).

Cadia is also distinctly Au-rich in comparison with other mineralized districts of the Macquarie Arc. Copper/gold ratios for porphyry mineralization in the Cadia and Goonumbla districts vary markedly, being roughly four times greater at Cadia, albeit with significantly lower grades overall, with Cadia Hill and Cadia Quarry being the most gold and copper dominant, respectively. By contrast, lower-K suites associated with Cu–Au \pm Mo porphyry mineralization including Copper Hill and those in the Cowal district have Au (g t^{-1}) v. Cu (%) $<1:1$.

A selection of intrusive and host rock photographs from Cadia, Northparkes, Trundle and Kaiser is shown as a photomontage in Figure 3.

The southern Molong Volcanic Belt

Cadia district

Located about 20 km south of Orange in the Molong Volcanic Belt, Cadia is the largest porphyry system in the Macquarie Arc and in Australia, with 2023 contained resources of 45.461 MOz Au and 7610 Kt Cu (Fig. 4). Six individual deposits are known (Table 1), all of which are genetically related to porphyry intrusions of the Cadia Intrusive Complex.

Mining is currently focused on the Cadia East underground system, which hosts resources of 2900 Mt @ 0.35 g t^{-1} Au, 0.26% Cu, 0.65 g t^{-1} Ag, 66 ppm Mo (Table 1). Cadia East is a sheeted vein-style porphyry system developed above a major dyke hosted within an east-SE-striking graben. Cadia Hill and Cadia Quarry mostly occur within monzonite to quartz monzonite phases of the main pluton of the Cadia Intrusive Complex, the former, a wallrock-hosted sheeted vein system, and Cadia Quarry, breccia and vein hosted (Holliday *et al.* 2002; Wilson *et al.* 2003; Forster *et al.* 2004). Ridgeway occurs above several vertically attenuated apophyses hosted by complex stockwork vein sets, the entire system being laterally focused within a tall, box-like fault block (Wilson *et al.* 2007).

The Cadia system is hosted by Middle to Late Ordovician sedimentary rocks of the Weemalla Formation, and Late Ordovician volcanic and sedimentary rocks of the overlying Forest Reef Volcanics (Squire and Crawford 2007). Based on limited detrital zircon ages, the maximum deposition age for the lower Forest Reef Volcanics is 453 Ma, which overlaps with the protracted deposition history of the Weemalla Formation from 465 to 450 Ma (Harris *et al.* 2014).

Several calcareous feldspathic sandstone units occur within both the Weemalla Formation and Forest Reefs Volcanics. The most significant is a 40 m thick calcareous, feldspathic sandstone horizon within the Forest Reefs Volcanics containing allochthonous limestone blocks, which together host the magnetite and hematite rich Big Cadia and Little Cadia skarns that were mined historically for Cu, Fe and Au (Forster *et al.* 2004). Based on (Late Ordovician) Eastonian (Ea3) (see also Gradstein *et al.* 2012) conodonts from this unit and other evidence, Percival *et al.* (1999) and Forster *et al.* (2004) suggested that the major calcareous horizon may be associated with a regional volcanic hiatus. The upper part of the sequence above the calcareous unit consists of well-bedded volcanic-

Table 1. Recent resources for the porphyry and epithermal deposits in the Macquarie Arc district

Mine/Project name	Style	Current resources and reserves (JORC)		Contained Au (KOz)	Contained Cu ('000t)
Cadia Valley Operations	Porphyry Au–Cu	Cadia East: (indicated) 2600 Mt @ 0.35 g/t Au, 0.26% Cu, 0.65 g t ^{−1} Ag, 66 ppm Mo Cadia East: (inferred) 500 Mt @ 0.24 g/t Au, 0.17% Cu, 0.47 g t ^{−1} Ag, 25 ppm Mo Cadia East: (probable) 1200 Mt @ 0.42 g/t Au, 0.29% Cu, 0.7 g t ^{−1} Ag, 82 ppm Mo		45 461	7610
Cowal	Epithermal	Total resources: 305.3 Mt @ 0.98 g/t Au Total reserves: 138 Mt @ 1.03 g/t Au		9619	
Northparkes	Porphyry Cu–Au	Total resources: 481.52 Mt @ 0.56% Cu, 0.18% g/t Au Total reserves: 121.17 Mt @ 0.58%, 0.22 g/t Au		2787	2697
Deposit/Project name	Project status		Current resources and reserves (JORC)	Contained Au (KOz)	Contained Cu ('000t)
Boda	Porphyry Au–Cu	Exploration	Inferred: 624 Mt @ 0.26 g/t Au, 0.14% Cu	5200	900
Kaiser	Porphyry Au–Cu	Exploration	Inferred: 270 Mt @ 0.24 g/t Au, 0.18% Cu	2080	486
Bushranger/Racecourse	Porphyry Cu–Au	Exploration	Indicated and inferred: 71 Mt @ 0.44% Cu, 0.064 g/t Au	146	312
Cadia Valley Operations	Porphyry Au–Cu	Care and maintenance	Big Cadia: (inferred) 11 Mt @ 0.52% Cu, 0.7 g/t Au Ridgeway underground: (indicated) 110 Mt @ 0.57 g/t Au, 0.3% Cu, 0.74% g t ^{−1} Ag Ridgeway underground: (inferred) 41 Mt @ 0.38 g/t Au, 0.4% Cu, 0.42 g t ^{−1} Ag Ridgeway underground: (probable) 80 Mt @ 0.54 g/t Au, 0.28% Cu Cadia extended underground: (indicated) 80 Mt @ 0.35 g/t Au, 0.19% Cu Cadia Hill stockpiles: (measured) 32 Mt @ 0.3 g/t Au, 0.13% Cu Total resource: 190 Mt @ 0.28% Cu, 0.28 g/t Au, 1.3 g t ^{−1} Ag	3973	736
Copper Hill	Porphyry Cu–Au	Exploration	Inferred: 8 Mt @ 1.5 g/t Au, 0.09% Cu	895	532
Gidginbung	Epithermal	Exploration	Indicated and inferred: 122.97 Mt @ 0.27 g/t Au, 0.46% Cu	386	
Marsden	Porphyry Au–Cu	Exploration	Proprietary underground: (inferred) 1.02 Mt @ 3.29 g/t Au, 0.15% Cu	1067	566
Peak Hill	Epithermal	Exploration	Total resource: 1.519 Mt @ 1.52 g/t Au, 70 g t ^{−1} Ag The Dam: (indicated and inferred) 40 Mt @ 0.30% Cu, 0.41 g/t Au Cullingerai: (inferred) 24 Mt @ 0.30% Cu, 0.31 g/t Au Estoril: (inferred) 14 Mt @ 0.21% Cu, 0.35 g/t Au Mandamah: (inferred) 26 Mt @ 0.34% Cu, 0.38 g/t Au Yiddah: (inferred) 127 Mt @ 0.32% Cu, 0.14 g/t Au	108	2
Sorpresa	Epithermal	Exploration	(inferred) 12.8 Mt @ 0.38% Cu, 0.14 g/t Au, 120 g t ^{−1} Mo, 2.2 g t ^{−1} Ag	74	
Temora Project	Porphyry Cu–Au	Exploration		2208	721
Yeoval	Porphyry Cu–Au	Exploration		6	49

The Australasian Code for Reporting of Exploration Results, Mineral Resources and Ore Reserves (JORC code).



Fig. 3. Photomontage of intrusive and host rocks from Macquarie Arc deposits. (a) Trundle Park TD002 420.10–420.13 m. Monzonite porphyry with quartz–calcite–molybdenite vein. Dated by Re–Os method. (b) Northparkes E22D248. Hematite dusted 'red rock' alteration of partly brecciated quartz monzonite. (c) PC179 Cadia Quarry. Garnet–epidote skarn after feldspathic, calcareous sandstone near quartz monzonite intrusion. (d) Drill hole Mordialloc prospect CTD006. Feldspar-rich quartz monzonite with mafic basaltic andesite dyke. (e) PC179 Cadia Quarry. Monzonite. (f) Mordialloc prospect ERE22D248. Quartz monzonite phase – associated with mineralization. Dated by U–Pb (zircon). (g) PC302 diorite from Cadia–White Engine. (h) EL48D58 Northparkes. Silicified and slightly brecciated monzonite. (i) Kaiser NKD003. Contact between the K-altered monzodiorite/diorite intrusion and the host andesite. (j) Kaiser NKD003. Typical biotite-altered porphyritic diorite to monzodiorite comprised of plagioclase, hornblende and minor quartz. Source: photographers: David Forster, Phillip Blevin and Joel Fitzherbert.

derived rocks, including phreatomagmatic ash-fall/lapilli volcanoclastic rocks, minor mudstone and thin limestones of early Silurian, which [Harris *et al.* \(2014\)](#) suggested as being of Llandovery to Wenlock age.

The entire sequence is intruded by irregular mafic and silicic stocks, dykes and sills, including prominent feldspar porphyry dykes of the Cadia Intrusive Complex which range in composition from diorite to quartz syenite. Those closely associated with mineralization range from monzodiorite at Ridgeway to quartz monzonite with quartz syenite and pegmatitic segregations at Cadia Quarry. Key age constraints on intrusions associated with mineralization are provided in [Supplementary File 1](#). Together, they suggest that the Cadia Intrusive Complex was

emplaced 443–435 Ma which conforms with an $^{40}\text{Ar}/^{39}\text{Ar}$ age of 438.2 ± 1.3 Ma (1σ) for mica intimately associated with mineralization at Cadia Quarry. Conversely, [Wilson *et al.* \(2007\)](#) provided Middle to Late Ordovician (~456–454 Ma) U–Pb ages on zircons, reportedly from the Cadia Intrusive Complex. Together, the data suggest that the mineralized intrusions were emplaced during the early Silurian following a possible depositional hiatus marked by the largest calcareous sandstone unit ([Butera *et al.* 2001](#); [Forster *et al.* 2004](#)).

The Cadia intrusions are mineralogically distinct from those in the Northparkes district in that they are more pyroxene rich and biotite forms at the expense of pyroxene with fractionation rather than amphibole. Whole-rock geochemical data provided by

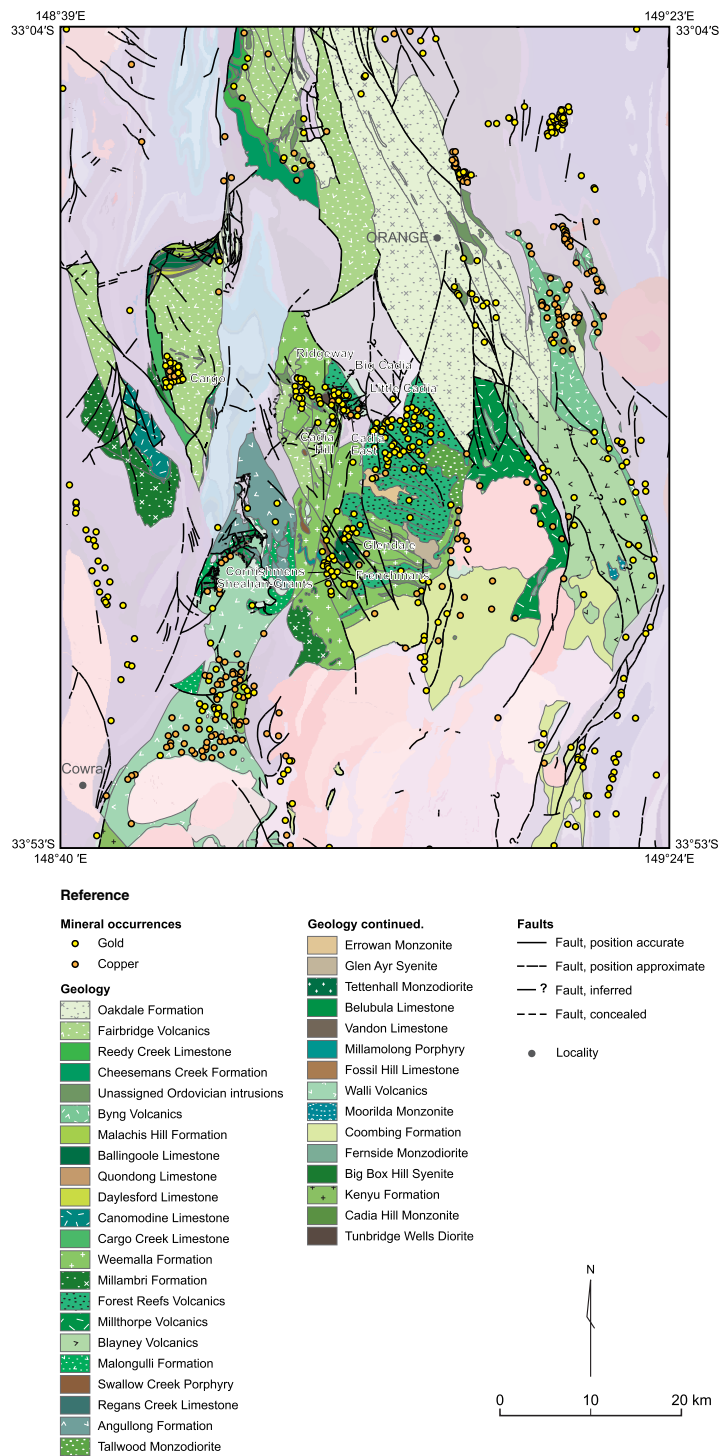


Fig. 4. Geological map of the Ordovician to early Silurian rocks of the southern Molong Volcanic Belt located south of Orange in central New South Wales. Notable deposits include Cadia–Ridgeway, Junction Reefs, Glendale and Cargo. Historic Cu and Au occurrences are shown.

Blevin (1998) and presented in this study suggest they are amongst the highest K rocks in the Macquarie Arc.

Metal abundance and zonation at Cadia. Despite the differences in gold/copper ratios between deposits at Cadia, (Supplementary File 1), the system overall is distinctly more Au-rich than Northparkes. The spatial relationships between mineralization, including alteration, and the host rocks in the Cadia district are shown in Figure 5a.

At Ridgeway, Au and Cu grades are largely coincident, being highest in bornite-rich zones adjacent to mineralizing quartz monzonite intrusions, with the extent of copper mineralization $>0.2\%$ conforming quite well with the extent of biotite-K-feldspar bearing calc-potassic alteration with gold mineralization $>0.2 \text{ g t}^{-1}$ extending slightly further outwards.

Gold and Cu at Cadia Hill correlate well with the abundance of veins. This wallrock-hosted sheeted vein system is mainly associated with propylitic alteration and has considerably higher Au/Cu ratios than the other deposits (Table 1), most notably Cadia Quarry, which is characterized by steeply dipping biotite-K-feldspar-rich breccia zones tens of metres wide, which probably reflect innermost high-temperature calc-potassic alteration zones (Holliday *et al.* 2002; Forster *et al.* 2004).

Gold- and Cu-mineralization at Cadia East is associated with sub-parallel sheeted veins developed around and above monzodiorite to quartz-monzonite dykes and stocks, most notably a dyke-like monzonite to quartz-monzonite body at depth. Mineralization occurs in two broad overlapping zones: an upper Cu-dominant disseminated zone, and a deeper, centrally located Au-rich zone associated with sheeted veins which extends to shallower depths to the west. The Au-rich zone, developed broadly around the monzonite dyke, is localized around a core of steeply dipping sheeted quartz–calcite–bornite–chalcopyrite–molybdenite \pm covellite \pm magnetite veins, with the highest Au grades associated with the widest zones of bornite-bearing veins (Holliday *et al.* 2002). Competency contrasts, including lithological boundaries in the host sequence, also have localized mineralized veins (Greenfield *et al.* 2022).

Oxidized magnetite-rich skarn deposits are associated with the porphyry mineralization at Cadia. The Big Cadia and Little Cadia skarns together host about 150 000 t of copper and 14.4 KOz of Au. While dwarfed by their parent porphyry deposits (Cadia Quarry and Cadia East), they are nonetheless important parts of the systems, having been significant historical producers in the nineteenth century, and were also key to discovering and understanding the larger porphyry deposits (Forster *et al.* 2004; Forster 2009).

Glendale and Junction Reefs

The Junction Reefs district located 39 km SSW of Orange lies within the Late Ordovician Molong Volcanic Belt. The area hosts significant Au and minor Cu mineralization associated with Late Ordovician dioritic to monzonitic intrusions.

An interbedded sequence of siltstone, shale, minor carbonate units and volcanic sandstone of the late Middle to Late Ordovician Weemalla Formation dominates the geology of the Junction Reefs area. This sequence was part of a proximal wedge of shallow marine volcanic debris on the slopes of a possibly emergent volcanic edifice (Wyborn 1997). Conformably overlying the Weemalla Formation are mafic volcanics of the Late Ordovician Forest Reefs Volcanics that outcrop to the NE of the Glendale deposit. Early Silurian intermediate igneous rocks, including the Tettenthal Monzodiorite, Junction Reefs Monzodiorite and Glendale Quartz Monzonite, intrude the older sequences.

Three different mineralization styles are present. These are distal Au–skarn mineralization (Sheahan–Grants, Frenchmans and Cornishmens), auriferous sheeted quartz arsenopyrite veins (Glendale) and intrusive breccia pipes (Prince of Wales). The deposits, including some derived alluvial Au, were mined in the nineteenth century, producing over 48 KOz Au. The geology and mineralization in these zones have been described by Overton (1990), Mandyczewsky *et al.* (1991), Perkins *et al.* (1992) and Gray *et al.* (1995). Both the Glendale deposit and the skarns are pyrrhotite-bearing, indicating relatively reduced oxidative conditions of formation for the Macquarie Arc.

A classic spatial skarn zonation is developed concentrically around the shoshonitic plugs. Calc-silicate mineralogy and parageneses are typical for gold skarns, including prograde skarn assemblages and hydrous retrograde assemblages (Gray *et al.* 1995). The calc-silicate (garnet/pyroxene $<2:1$) and sulfide ore mineralogy (Au-bearing, pyrrhotite–pyrite–chalcopyrite–arsenopyrite) are features characteristic of the category of reduced Au skarns (Meinert 1992, 1995).

The northern Molong Volcanic Belt

Bodangora district

Hosted by the northern Molong Volcanic Arc, the Bodangora district is located about 15–20 km NE of Wellington and includes numerous historic mines and modern porphyry and skarn prospects, some of which have been faulted and sheared (Fig. 6). Historic mines include the Bodangora Creek, Dicks Reward and Mitchells Creek

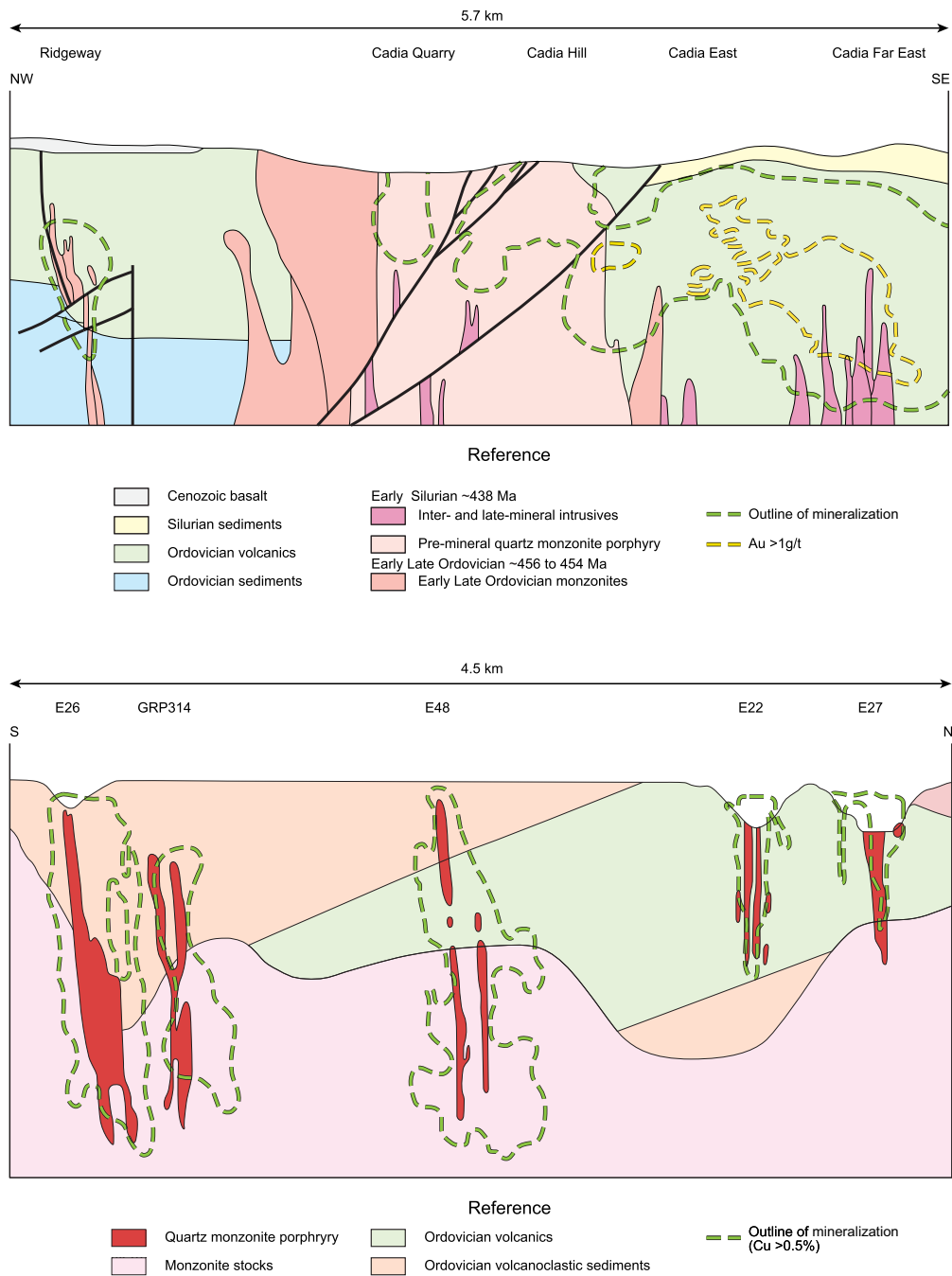


Fig. 5. Schematic cross-sections of the Cadia district (top) and Goonumbla district (bottom) deposits. Source: reproduced from [Blevin *et al.* \(2020\)](#).

mines, which produced 7.1 t Au, mainly between 1869 and World War I (c. 1914–18), with minor production in the 1930s and 1980s, along with

the Kaiser mine that produced 30–40 kg of Au and minor Cu during the 1860–70s and 1930s, respectively.

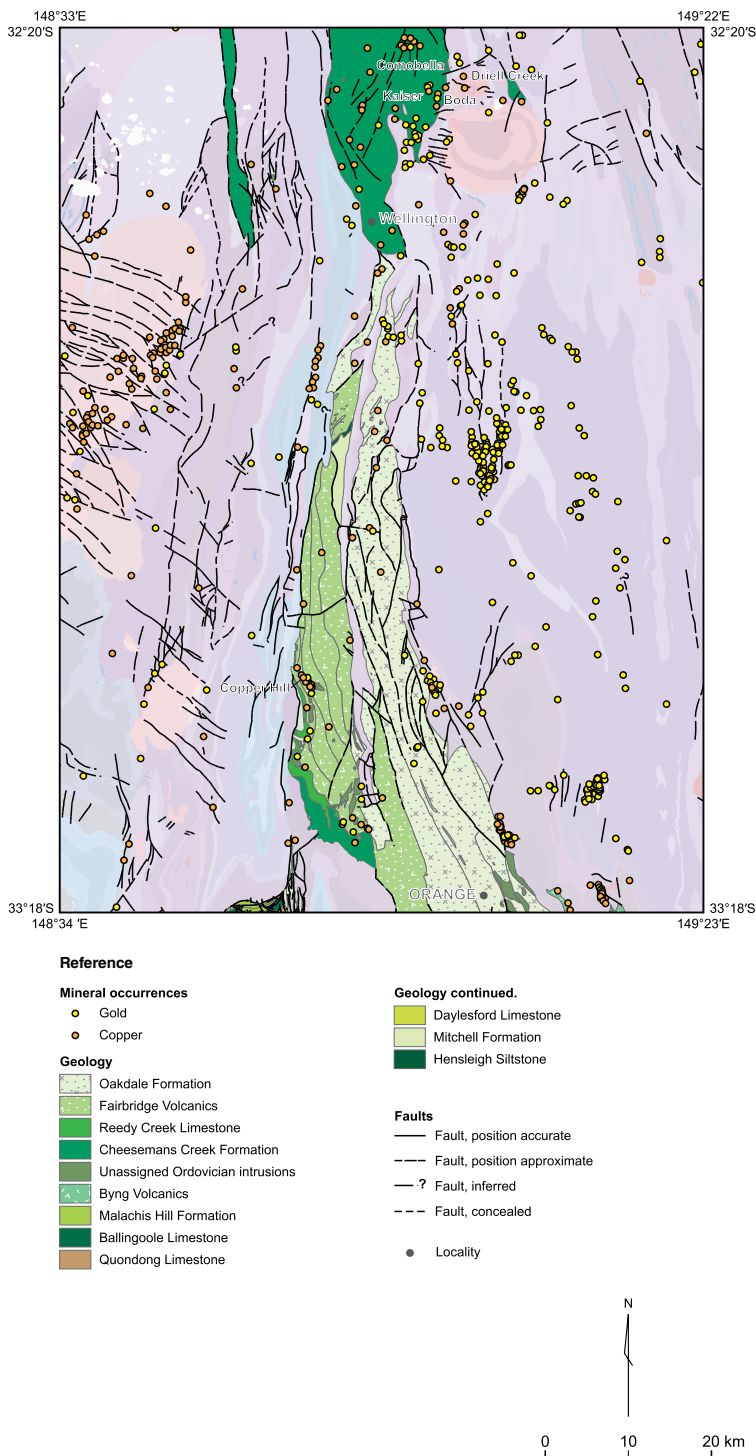


Fig. 6. Geological map of the Ordovician to early Silurian rocks of the northern Molong Volcanic Belt located north of Orange in central New South Wales. Notable deposits include Copper Hill, Boda–Kaiser and Comabella. Historic Cu and Au occurrences are shown.

There has been concerted recent exploration for porphyry and skarn-related Cu–Au mineralization in the Bodangora district, which has identified the Comobella, Finns Creek, Driell Creek and Kaiser prospects, and most notably, the large Boda system (Alkane Resources 2019, 2020, 2021).

Comobella. The Comobella area is located about 6 km NW of Kaiser. MacKenzie (1993) described several skarn, breccia and intrusive related Cu–Au occurrences over a 1.5 by 2.4 km area hosted by andesitic lavas, latites and reworked volcanic units of the Late Ordovician Oakdale Formation, which have been intruded by a series of poorly outcropping monzonitic and syenitic intrusive stocks of Late Ordovician age (447.9 ± 2.1 and 447.6 ± 2.1 Ma; Supplementary File 1; Jones *et al.* 2023). The area is interpreted to be proximal to an Ordovician intrusive complex or volcanic centre. Mineralization is preferentially developed along the margins of the intrusions and includes chalcopyrite, bornite and minor covellite with magnetite. Two alteration assemblages have been identified. These are the rimming by K-feldspar of both the clasts and the matrix and an epidote–actinolite–garnet overprint in the matrix that is part of a calc-silicate skarn assemblage (MacKenzie 1993). Prominent magnetite-rich skarns several hundred metres long occur around the area.

Boda and Kaiser. The Boda and Kaiser deposits occur within a north–south-trending structural corridor which extends for over 2.5 km including the Boda Two prospect.

Boda is by far the largest deposit in the Bodangora district and represents the most significant new discovery of the twenty-first century in the Macquarie Arc, including an intercept of 1167 m @ 0.55 g t^{-1} Au, 0.25% Cu (from 75 m). The Boda–Kaiser copper–gold deposit hosts resources of 5.2 MOz of gold and 873 Kt of copper (Supplementary File 1; Alkane Resources 2021).

Intrusive phases include various dykes and intrusive breccias, mainly monzodiorites and monzonites, which are cut by late-mineral, equigranular monzonite dykes (Greenfield *et al.* 2022). The magmatic breccias are near-vertical and transition to intensely altered hydrothermal breccias which form the highest-grade core of the Boda deposit. Chalcopyrite-rich mineralization grades outward to chalcopyrite–bornite–chalcocite-bearing mineralization over about 150 m. This is atypical of many Llandoverian porphyry systems of the Macquarie Arc, which have central, bornite-rich cores.

Distinct alteration zonation is evident, including:

- An inner calc-potassic zone consisting of fine-grained biotite–actinolite–epidote–magnetite with interfingering of a lesser potassic assemblage dominated by biotite.

- Plagioclase at the margins of this alteration is pinkish due to hematite dusting. This zone extends for over 1.5 km.
- More distal and deeper alteration consists of zoned propylitic alteration with typical mineral assemblages of epidote–chlorite–calcite–hematite–pyrite (Supplementary File 1).
- Phyllic alteration with up to 10% pyrite overprints eastern parts of the Boda system, with mineralization copper depleted and gold enriched (Greenfield *et al.* 2022).

The late mainly equigranular monzonite dykes are weakly mineralized with chalcopyrite occurring in quartz veins (Alkane Resources 2021; Greenfield *et al.* 2022). Various post-mineral dykes and sills are prominent.

Kaiser. Located about 500 m north–NW of Boda within the mineralized corridor, the Kaiser Mine was a minor historical producer of Au and Cu. Diorite, monzodiorite and monzonite dykes and sills (constrained to 437.9 ± 2.1 ; Jones *et al.* 2023) intrude the sequence, with the more felsic phases being intensely altered. Two major faults have locally cataclastically affected and upgraded mineralization. Feldspar–quartz episyenite ‘finger’ dykes have been observed, some of which contain chalcopyrite, mainly after altered ferromagnesian minerals.

The mineralization has been described by Pagen (1998) and Greenfield *et al.* (2022) as consisting of vein-controlled and disseminated pyrite, chalcopyrite, magnetite, bornite, covellite, chalcocite and gold with pyrrhotite molybdenite and rare sphalerite and galena.

Early magnetite K-feldspar veins are overprinted by a potassic assemblage which also includes biotite and actinolite (Greenfield *et al.* 2022). These are overprinted by epidote–carbonate–albite–chlorite–sulfide (chalcopyrite) veins.

Other general observations include:

- The intensity of both the hydrothermal alteration and the sulfide mineralization generally decreases outwards.
- Higher-grade Cu–Au mineralization also occurs in narrow shear zones where the sulfide-rich potassic zones have undergone post-alteration cataclasis, foliation and recrystallization.
- A late, low-temperature stage is represented by the presence of thin fracture-controlled native copper bearing carbonate veins.

Boda and Kaiser have upper zones enriched in copper and gold, respectively. These zones are notable for containing adularia–clay alteration.

While multiple zones of alteration and mineralization occur in the immediate district, the many analogous features of Kaiser and Boda and their proximity within a north–south-striking zone

together suggest they probably belong to the same, or a very closely related, mineralized system.

Copper Hill

Porphyry-style mineralization in the Copper Hill district (not to be confused with the Copper Hill/Trundle Park prospect at Trundle, NSW) is hosted by the Copper Hill Intrusive Complex, which intrudes andesitic volcanics and minor limestones of the Middle Ordovician Fairbridge Volcanics (Blevin and Morrison 1997). Skarn mineralization related to the porphyries also occurs, most notably at the Little Copper Hill prospect. Current total resources stand at 190 Mt @ 0.28% Cu, 0.28 g t⁻¹ Au, 1.3 g t⁻¹ Ag (Supplementary File 1).

The Copper Hill Intrusive Complex is dominated by dacites and tonalites. Blevin and Morrison (1997) and Blevin (2002) recognized two intrusive phases: a quartz diorite with gradational boundaries to micro-tonalite (equivalent to the early quartz diorite phase of Chivas and Nutter (1975), and a dacite porphyry that occurs as an intrusive body and as dykes (Blevin and Morrison 1997). Those authors also recognized three distinct dacite porphyry bodies based on phenocryst and matrix differences.

The geochemistry of the Copper Hill district is distinct from the other, higher-K suites that are the focus of this chapter. The district is dominated by dacites and tonalites which are of medium-K calc-alkaline affinity. This is a relatively low-K suite for the Macquarie Arc generally when compared to slightly older intrusive suites (Blevin 2002; Crawford *et al.* 2007b; Kemp *et al.* 2020). Numerous attempts have been made to date the Copper Hill Intrusive Complex and the mineralization, including 449.1 ± 1 Ma (⁴⁰Ar/³⁹Ar) and 450 ± 6 Ma (U–Pb sensitive high-resolution ion microprobe (SHRIMP)) by Perkins *et al.* (1995; see also Crawford *et al.* 2007b; Glen *et al.* 2011a). Kemp *et al.* (2020) obtained a slightly older U–Pb age based on a simple age distribution yielded by rims of zircon crystals from the medium-K Copper Hill tonalite of 458 ± 2 Ma along with two Re–Os ages on molybdenite of 455 ± 2 and 454 ± 2 Ma.

Scott (1978) observed a zoned alteration system at Copper Hill, including a quartz–magnetite–chlorite central stockwork zone that is surrounded by a sericite–quartz–pyrite inner zone with associated chlorite–calcite–rutile–illite (sericitic) alteration, and an outer chlorite dominated zone with associated propylitic (epidote–pyrite–illite–quartz–calcite) alteration. Sulfide mineralogy is also zoned, with a sulfide-rich central core dominated by pyrite, grading outwards to chalcopyrite–pyrite, with an outer zone of sphalerite, galena and tetrahedrite > chalcopyrite. Associated with this alteration are two assemblages that infill shears and fractures. These are a quartz–carbonate–

pyrite–chalcopyrite–sphalerite–galena assemblage that occurs with the deeper alteration, and a silica–pyrite–chalcocite ± base metals assemblage in shallower parts.

The northern Junee–Narromine Volcanic Belt

The Goonumbla district: Northparkes

The Goonumbla porphyry Cu–Au district, which hosts the current Northparkes, Endeavour (E) 26 mine, is located about 25 km NW of Parkes (Fig. 7) within the Junee–Narromine Belt. The area has been the subject of much research in recent decades, including studies by Jones (1985), Heithersay (1986) Heithersay *et al.* (1990), Heithersay and Walshe (1995), Hooper *et al.* (1996), Lickfold (2002), Lickfold *et al.* (2003), Müller and Groves (2019), Pacey *et al.* (2019) and Hao *et al.* (2021).

The district hosts four economic porphyry copper–gold deposits, E22, E26 North (the current Northparkes mine), E27 and E48. The district also includes several smaller porphyry Cu–Au (Wells *et al.* 2021) and skarn-type deposits, including Endeavour 44, Endeavour 6 and Endeavour 7. Current resources are listed in Table 1. The mineralization is hosted by the Late Ordovician Goonumbla Volcanic Complex, which is located within the central portion of the Early Ordovician to Late Ordovician/early Silurian Junee–Narromine Volcanic Belt.

Three major cycles of Ordovician volcanic rocks and associated intrusive complexes have been identified at Goonumbla. These are the Nelungaloo, Goonumbla and Wombin volcanics, which have been described in detail by Krynan *et al.* (1990), Simpson *et al.* (2005) and Pacey *et al.* (2019).

The Nelungaloo Volcanics are 650 to 1500 m thick and are the oldest in the district and among the oldest reliably dated sequence of rocks in the Macquarie Arc, except for parts of the Temora Belt (Kemp *et al.* 2020). The Nelungaloo Volcanics are constrained by cross-cutting monzodiorites ('Nettlebecks Lane Monzodiorite') constrained to 477 ± 2 and 477 ± 4 Ma (Kemp *et al.* 2020). The volcanics comprise a subaqueous distal apron facies suite of volcanoclastic sedimentary rocks and syn-sedimentary andesitic lavas and sills (Butera *et al.* 2001; Simpson *et al.* 2005). The Yarrimbah Formation directly overlies the Nelungaloo Volcanics (Sherwin 1976, 1996, 2000). It is described by Glen *et al.* (2007b) as a 400–600 m thick, broadly fining upwards sequence of volcanoclastic sandstones, siltstones and bedded mudstones.

The Goonumbla Volcanics are a Middle to Late Ordovician sequence up to 4000 m thick. Shallow

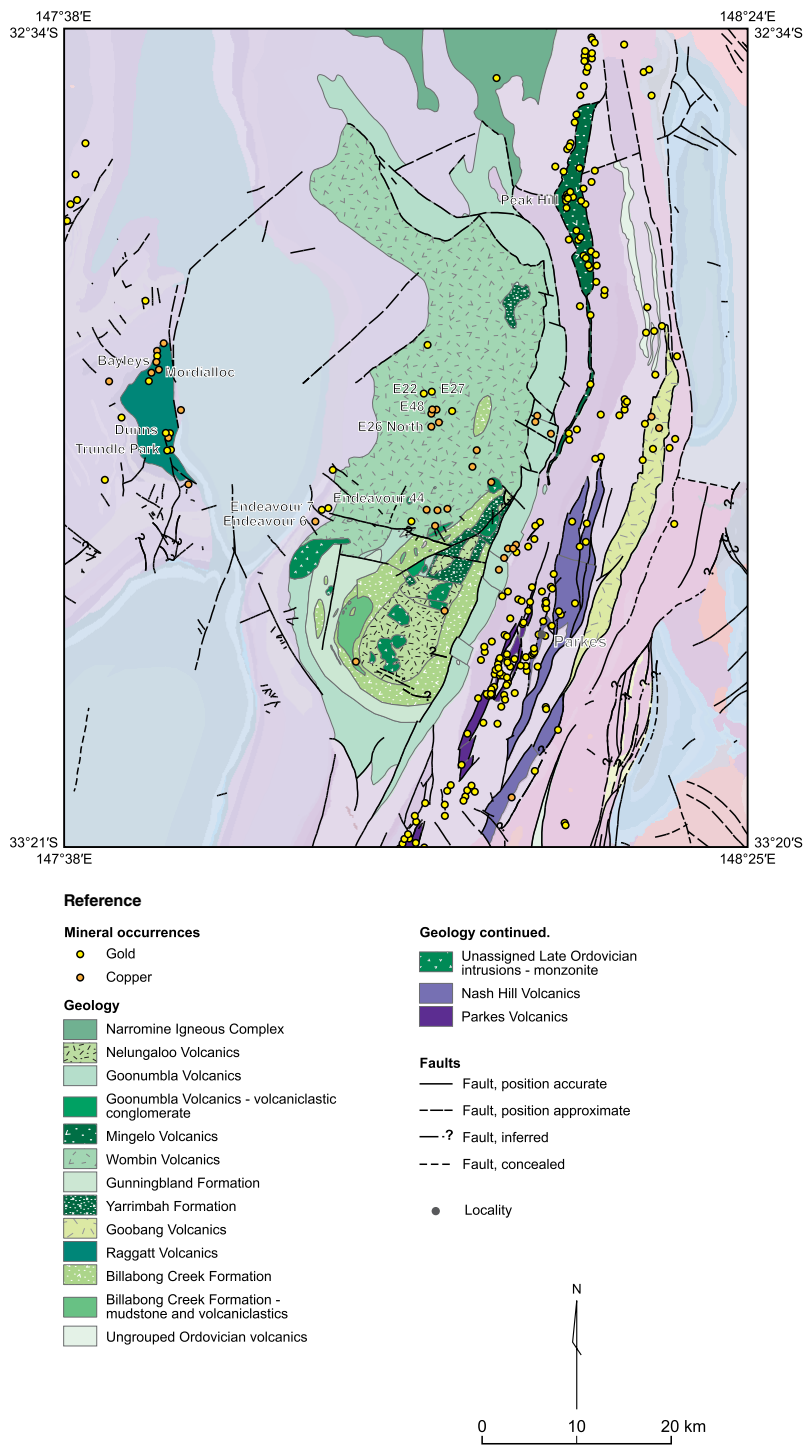


Fig. 7. Geological map of the Ordovician to early Silurian rocks of the northern Junee–Narromine Volcanic Belt located NW of Parkes in central-west New South Wales. Notable deposits include Trundle (Mordialloc and Trundle Park), Northparkes and Peak Hill.

water, bedded volcanoclastic sandstone, siltstone, minor intercalated limestones and volcanic breccia are overlain by thick volcanic conglomerate and a coeval sequence of coherent basaltic andesitic to trachyandesitic volcanic rocks, including lavas and shallow sills. The Billabong Creek Limestone and Gunningbland Formation are probably laterally equivalent to the Goonumbla Volcanics. The lower Goonumbla Volcanics are constrained by a cross-cutting monzonite dyke 450.8 ± 4.2 Ma (Butera *et al.* 2001; Lickfold *et al.* 2007).

The Late Ordovician to early Silurian Wombin Volcanics (lower constraint of 433.8 ± 3.1 Ma) (Hao *et al.* 2021; Zhen and Percival 2023) are an up to 1 km thick sequence which represents a volcanoclastic apron facies of polymict volcanic breccias intercalated with turbiditic crystal-rich sandstone and less abundant syn-sedimentary trachyandesitic sills, porphyritic trachyandesitic and flow banded trachytic lavas, which conformably overlie the Goonumbla Volcanics. Simpson *et al.* (2005) interpreted the Goonumbla and Wombin volcanics as a subaqueous volcanoclastic apron that formed on the flanks of a shallow marine to subaerial stratovolcano.

In the Northparkes district, at least nine intrusive phases have been identified, with the main stage of mineralization being associated with K-feldspar quartz monzonite porphyry pipes and dykes, and, to a lesser extent, late-mineral augite–biotite–K-feldspar quartz monzonite porphyry intrusions and their associated K-feldspar and sericite–hematite-bearing alteration assemblages (Lickfold *et al.* 2003).

Mainly ‘pencil like’ subvertical intrusions associated with mineralization include groups of pre, early, syn and post-mineralization phases (Fig. 5b). Pre-mineralization intrusions include equigranular monzodiorites, including beneath E26–26 North. Early mineralization intrusions are typically biotite-bearing, medium- to coarse-grained and equigranular to semi-porphyritic. Intrusions associated with the main stage of mineralization constrained to 441.8 ± 3.7 and 441.1 ± 2.5 Ma (Hao *et al.* 2021) are dominated by K-feldspar quartz monzonite porphyries with 30 to 40% phenocrysts of plagioclase, K-feldspar and minor magnetite, biotite and hornblende (Blevin 2002). Various late mineralization intrusions with clear cross-cutting relationships, including xenoliths of earlier phases, include plagioclase, K-feldspar and minor augite–biotite–hornblende phenocrysts with magnetite with a groundmass containing 10–50% quartz. Post-mineralization intrusions include dykes of basaltic trachyandesite, mafic monzonite porphyry and basalt. The most significant and visually striking are feldspar-dominant, mostly aphanitic ‘zero’ dykes so named since they are altogether barren (Lickfold *et al.* 2003; Blevin *et al.* 2020).

The porphyry-type mineralization in the district consists of sub-vertical pipe-like intrusions of quartz monzonite porphyry. Up to 11 stages of alteration have been identified by numerous workers (see Lickfold 2002), however, they can clearly be grouped according to the series of intrusive phases described above. The main stage of mineralization is associated with K-feldspar quartz monzonite porphyry pipes and dykes, and, to a lesser extent, late-mineral augite–biotite–K-feldspar quartz monzonite porphyry intrusions and their associated K-feldspar and sericite–hematite alteration assemblages (Lickfold *et al.* 2003). The mineralization generally occurs as disseminations, and within fractures and veins within both the intrusion and the surrounding volcanic rocks, with the strongest mineralization being associated with quartz stockwork veining within a central potassic alteration zone (Heithersay *et al.* 1990). A mineral zonation has been identified with a poorly defined outer pyritic zone surrounding a chalcopyrite-dominant zone which, in turn, surrounds an inner, higher-grade, central bornite and chalcocite-dominated oxidized zone (Heithersay *et al.* 1990). Pervasive sericitic alteration is relatively restricted (see Harris and Golding 2002), and widespread propylitic alteration is present.

Trundle district

The Trundle district is hosted by a roughly triangular 15 by 5 km block of Ordovician andesitic to trachyandesitic lavas, tuffs and volcanoclastic breccias of the Raggatt Volcanics (Fig. 7). The block is fault bounded on the eastern side. Sparse fossiliferous limestones within the sequence contain Late Ordovician corals and conodonts which correlate with carbonate units of the Goonumbla Volcanics (Pickett and Ingepen 1990).

Minor copper, gold and iron were mined during the 1930s and World War II (c. 1939–45), mainly from skarn mineralization. Modern exploration has included several prospects, most notably Trundle Park/Copper Hill, Mordialloc, Bayleys and Bloomfield, which are developed around diorite to quartz monzonite and rare syenite intrusions. Much of the early phase modern exploration focused on skarn mineralization developed after reactive host rocks including carbonates (e.g. Trundle Park), using skarn mineralogy and zonation to attempt vectoring toward porphyry mineralization (see Forster 2009). Alteration associated with mineralization extends up to about 800 m from intrusive stocks and dykes, but narrower, definable zones of alteration are evident around porphyritic intrusions.

Mineralization is centred on various diorite to quartz monzonite and minor syenite stocks and dykes. These post-date very coarsely porphyritic

plutons, including one dated at Mordialloc (443.6 ± 3.6 Ma by U–Pb on zircon; [Supplementary File 6](#)) where Cu–Au mineralization is associated with near-vertical quartz porphyritic quartz monzonite stocks.

Porphyry-style mineralization and associated alteration at Trundle generally occurred in three main stages: (i) pre-mineral halos of vein-like K-feldspar + quartz dykes with weak Cu mineralization; (ii) early-mineralization K-silicate (both i and ii apparently related to amphibole–biotite–quartz monzonite intrusions); and (iii) late-stage fault and fracture-controlled and lesser veins containing phyllic assemblages (sericite–carbonate–quartz–pyrite + anhydrite). The porphyry deposits generally have a high grade bornite (and lesser chalcocite) core, which passes outwards into a chalcopyrite dominant zone to an outer patchy pyritic (up to 3%) halo. Intense mineral destructive alteration is generally absent, with the potassic core being present as pink–red K-feldspar along fractures and vein selvages. Thin, commonly seamed quartz–carbonate veins are also associated with Cu and Au mineralization. Cu–Au bearing magnetite-rich skarn and calc-silicate skarn is present and abundant at the Trundle Park prospect, developed in at least three major carbonate units (e.g. drill hole TD002). Some late-stage zones are notably base metal-rich. In such zones, the sulfide minerals mainly consist of pyrite–chalcopyrite \pm sphalerite \pm galena and vary widely in relative abundance. Molybdenite may be associated with the late-stage mineralization, including at Trundle Park, with Mo anomalism being largely coincident with Cu hosted by late-stage monzonite intrusions, and forming a >20 ppm Mo halo in the adjacent skarn ([Kincora Copper Ltd 2020](#)). Gold occurs in these Cu- and Mo-bearing zones, but broader Au-dominant zones mainly appear to occur peripherally.

[Forster *et al.* \(2015\)](#) reported a Re–Os age on molybdenite of 418 ± 2.0 Ma from a ~ 30 m wide quartz–monzonite dyke-like intrusion at Trundle Park, which is indistinguishable from a U–Pb zircon age on the same rock (418.4 ± 1.35 ; [Supplementary File 6](#)). These significantly younger ages may be related to younger magmatism near the eastern margin of the Trundle Block, near major thrust faults which juxtapose the mid-Silurian Campbells Group and Ordovician Raggatt Volcanics. These thrust faults may have partly reactivated older, possible rift-related faults which were contemporaneous with Early Devonian magmatism.

While these quartz–monzonite intrusions share mineralogical similarities to monzonites dated as Ordovician in age, they differ primarily in texture. The monzonites typically exhibit crowded feldspars in a porphyritic texture, whereas these intrusions lack such a prominent porphyritic texture. Geochemical

and isotopic data further distinguish them (see Discussion section).

The southern June–Narromine Volcanic Belt

Temora district

The Temora district includes several porphyry Cu–Au deposits along with the Gidginbung Mine, which is of epithermal style ([Fig. 8](#)). They are hosted by a 50 km long, north–NW-striking linear belt of volcanic rocks of the Late Ordovician to early Silurian Gidginbung Volcanics, which mostly lie under shallow cover ([Perkins *et al.* 1995](#); [Lawrie *et al.* 2007](#)). The volcanic rocks consist of andesitic volcanoclastics intruded by hornblende gabbro, diorite to tonalite and late-stage monzodiorite dykes and sills. Intrusions, including those associated with mineralization, comprise porphyritic monzodiorite dykes and gabbroic, dioritic to monzodioritic porphyritic sills and stocks. Until recently, all available age constraints indicated that the rocks associated with mineralization in the Temora Belt were of Late Ordovician to early Silurian age, but recent dating by [Kemp *et al.* \(2020\)](#) suggests intrusions of similar geochemical affinity were emplaced as early as the Late Cambrian.

Significant porphyry deposits in the district include Cullingerai, The Dam, Estoril, Mandamah and Yiddah. Combined resources for the district exceed 2.2 MOz Au and 720 Kt Cu with only a few small historical workings present, mainly around Yiddah. The age of the Yiddah porphyry is constrained to the early Silurian (433.8 ± 6.4 , 438.3 ± 3.5 Ma), indistinguishable from spatially associated amphibole–feldspar porphyritic monzodiorite stocks dated to 439.2 ± 6.4 Ma ([Goesch 2011](#); [Kemp *et al.* 2020](#)).

Ore mineralogy consists of quartz–magnetite–pyrite and chalcopyrite veins with molybdenite as a weak sulfide halo to several deposits. Three major mineralization stages with corresponding alteration assemblages are described as common to all the deposits by [Cronin *et al.* \(2017\)](#), including an early generation of high-temperature quartz–magnetite \pm feldspar \pm pyrite \pm chalcopyrite associated with seamed quartz veins with selvages of magnetite–quartz–carbonate–chlorite–chalcopyrite–hematite \pm K-feldspar, followed by a crystalline to clotty quartz–carbonate–chlorite \pm chalcopyrite stage. These are overprinted by weakly mineralized quartz–white mica–pyrite alteration. These vein and alteration paragenetic relationships are characteristic of many single-phase porphyry deposits ([Blewin *et al.* 2020](#)). Of the deposits in the district, The Dam is distinct in having significant bornite as part of the porphyry-style vein assemblage and a

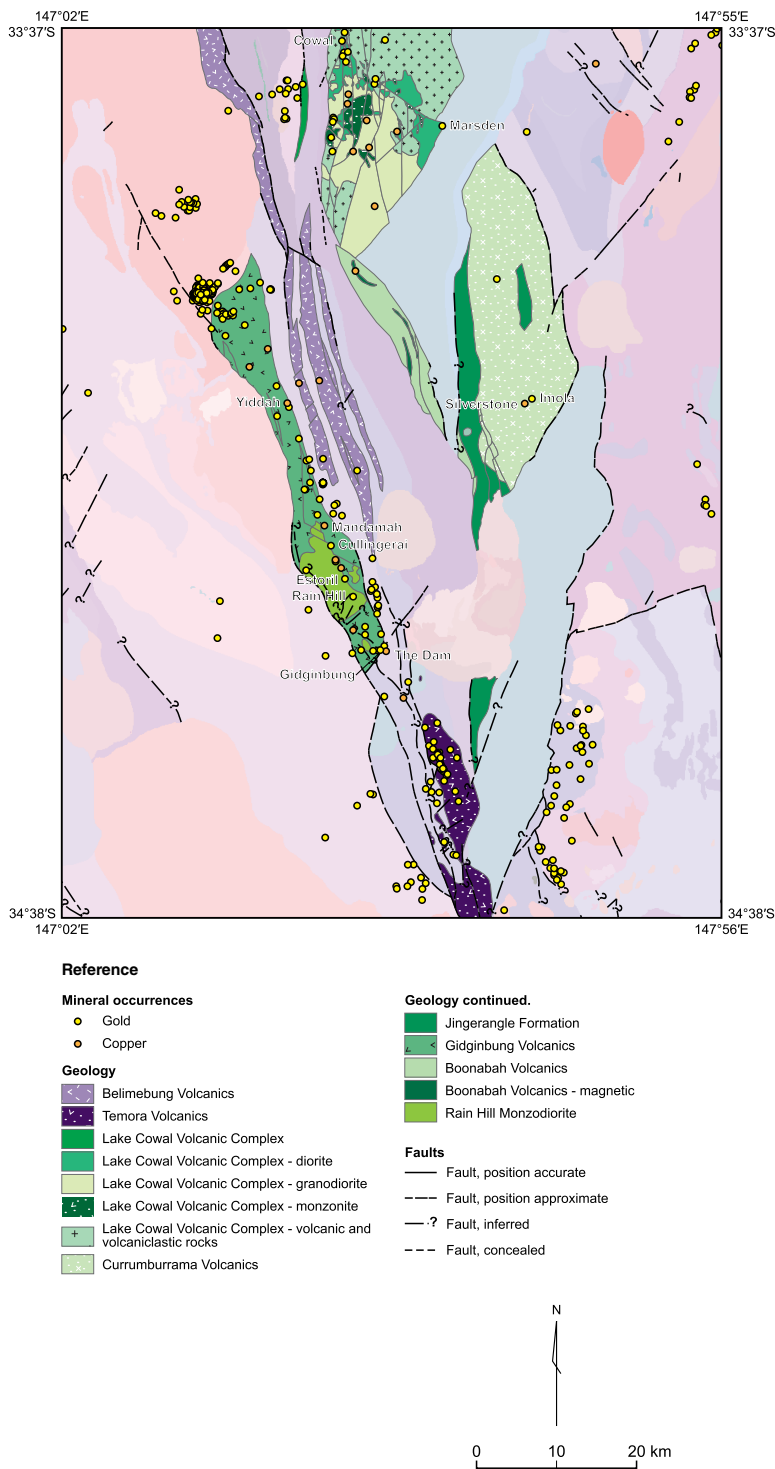


Fig. 8. Geological map of the Ordovician to early Silurian rocks of the southern Junee–Narromine Volcanic Belt located SE of West Wyalong in central-west New South Wales. Notable deposits include the Temora district (Yiddah, Rain Hill, Gidginbung) and Currumburrama district (Imola and Silverstone).

prominent late-stage, white mica–clay–sulfide–barite alteration assemblage, interpreted as being of epithermal style by [Downes *et al.* \(2004\)](#).

The Rain Hill Cu–Au–Mo prospect is hosted by the Rain Hill Monzodiorite of the Gidginbung Volcanics, which consists of subequigranular, amphibole-bearing monzodiorite to monzonite with minor quartz (<6%). The Rain Hill prospect is associated with a circular geophysical anomaly about 4 km in diameter which includes several quartz monzonite to monzogranite intrusions, composed of up to 30% quartz, 25% K-feldspar, 20% plagioclase and 5% chlorite with accessory apatite, titanite and magnetite ([Cyprus Amax Australia Corporation 1998](#)). Various porphyritic mafic dykes are also present which contain relict chromite, Cr-bearing magnetite and pyroxene ([Blevin and Morrison 1997](#)), and elevated Pt and Pd concentrations ([Wyborn 1996](#)). The intrusion has an $^{40}\text{Ar}/^{39}\text{Ar}$ age on hornblende of 434.9 ± 2.3 Ma ([Wormald 1993](#)). This conforms with the 435 ± 5 Ma zircon age for the host andesite from the Gidginbung Volcanics obtained by [Perkins *et al.* \(1990\)](#). Mineralization is both disseminated and within veins, hosted within and around the margins of the intrusions, comprising chalcopyrite, bornite and pyrite. Cuprite, chalcocite and covellite occur in weathered zones with Au grades of $3\text{--}5\text{ g t}^{-1}$ over intervals of up to 50 m – about a ten-fold enrichment over typical intersections in fresh rock. Alteration associated with mineralization includes potassic (K-feldspar–plagioclase–quartz–magnetite \pm biotite), propylitic (albite–chlorite–carbonate–illite/muscovite \pm actinolite–magnetite–hematite) and phyllic (illite–muscovite–quartz–pyrite) assemblages.

Currumburrama district

The Currumburrama district is hosted by a separate block of Ordovician to early Silurian volcanic Currumburrama latite of the Currumburrama Volcanics ([Fig. 8](#)), which has been constrained to late Sandbian to earliest Katian age based on faunal assemblages in limestones ([Zhen and Percival 2023](#)). The Late Ordovician conodonts were observed to be similar to an equivalent or slightly younger assemblage obtained in drill core from the Marsden prospect within the Lake Cowal Igneous Complex, and together comprise the only Late Ordovician biostratigraphical constraints in the southern Junee–Narromine Volcanic Belt ([Zhen and Percival 2023](#)).

The district hosts the Silverstone and Imola porphyry Cu–Au prospects drilled in the early 2000s. Intrusions associated with mineralization include quartz–magnetite–chalcopyrite veins and K-feldspar–biotite–magnetite–chalcopyrite veins in intrusions reminiscent of those described above in the Temora Belt.

The Rockley–Gulgong Volcanic Belt

Racecourse/Bushranger

The Racecourse or Racecourse Creek prospect is hosted by the Rockley–Gulgong Volcanic Belt. It occurs near the locality of Black Springs, SSW of Oberon, hosting a resource of (indicated and inferred) 71 Mt @ 0.44% Cu, 0.064 g t⁻¹ Au. Primary igneous rocks include massive equigranular diorites and monzonites, and massive to flow-foliated monzonite porphyries and micro-monzonite porphyries. The diorites contain minor or no primary K-feldspar, whereas the monzonites have abundant K-feldspar enclosing primary plagioclase prisms. The earliest hydrothermal reaction in mineralizing intrusions is biotite–quartz (potassic) replacement of ferromagnesian minerals ([Mason 2014](#)).

Three main styles of hydrothermal alteration were identified by [Mason \(2014\)](#): (1) early brittle fracturing and infiltration by silica–CO₂–S–Fe–Cu–(Mo) bearing hydrothermal fluid; (2) sodic–calcic alteration with sulfides (pyrite–chalcopyrite–pyrrhotite–molybdenite) \pm albite \pm rutile; and (3) late fracturing/shearing and infiltration by fluid under compressive structural conditions, producing sub-parallel or variably oriented thin fractures and through-going shears sealed by assemblages of sericite, chlorite, calcite, quartz and sulfides (pyrrhotite, pyrite, chalcopyrite, ?tennantite–tetrahedrite). The system is relatively reduced for a porphyry-system of the Macquarie Arc, demonstrated by the abundance of pyrrhotite.

Results

Trace element classification and shoshonite classification criteria

Whole-rock classification

Interpretation of new and existing whole-rock geochemical data for the Macquarie Arc provides key constraints on the character and classification of host volcanics and pre-, syn- and post-mineralization intrusions. Due to the mobility of alkali metals in hydrothermal systems, typical classification based on total alkalis v. silica is not broadly appropriate for rocks in the Macquarie Arc. Major element classification diagrams after [Le Maitre *et al.* \(1989\)](#) and [Middlemost \(1994\)](#) are presented in [Supplementary File 2](#). A full list of sample locations, lithologies, stratigraphic attributions and whole-rock geochemistry is included in [Supplementary File 3](#).

Utilizing the trace element classification scheme after [Pearce \(1996\)](#), most samples in this study cluster with intermediate andesitic compositions

(Figs 9a, 10a & 11a), and are typically described in hand sample as monzodiorite, monzonite and quartz monzonite or extrusive equivalents (Lickfold *et al.* 2003, 2007; Wilson *et al.* 2003, 2007; Pacey *et al.* 2019; Wells *et al.* 2021). The general composition and evolutionary trends of mineralized intrusive resemble those of the regional volcanic host rocks (Supplementary File 2). Within all districts and regions described below, there are examples of volcanic and plutonic rocks (e.g. Nelungaloo, Fairbridge and Gidginbung volcanics basalts, and the Stokefield Metagabbro) that are more primitive and depleted, as indicated by below average Nb/Y (Figs 9a, 10a & 11a).

Porphyries, including syn-mineralization intrusions, show a wider compositional range and become consistently more evolved and more alkaline with time, whilst post-mineralization intrusions, including pyroxene bearing ‘mafic’ monzonites, typically become more primitive (e.g. Goonumbla ‘mafic monzodiorites’; Fig. 9a). Syn- to post-mineralization volcanics (e.g. Wombin Volcanics) trend towards more evolved compositions, whereas volcanic rocks of late-stage post-Benambran age (e.g. Bushman Volcanics) tend to be more alkaline than older Macquarie Arc *sensu stricto* sequences.

Hydrothermal alteration of analysed samples

Feldspar Na–K GER (general element ratio) alteration diagrams (K/Al v. Na/Al) after Madeisky and Stanley (1993) indicate that many samples used in our study have experienced significant alteration and mobilization of mobile major elements, including K₂O and Na₂O (Figs 9b, 10b & 11b). Despite this, a general grouping representative of potassic calc-alkaline volcanics is evident for most districts.

Trends of decreasing K with increasing Na are suggestive of K-loss and Na-gain. Such trends are typified by data from two basaltic Nelungaloo Volcanics (Fig. 9b) and two Cadia Hill Monzonite samples (Fig. 10b) which have extremely low-K and high-Na. Yiddah (Rain Hill) and Gidginbung volcanics samples notably fall along this trend (Fig. 11b). Dislocation of these data away from the average basalt composition (Cox 1980) on a trend to the albite node of the feldspar Na–K control diagram suggests significant alteration and K-loss likely due to albitization. A few samples, most notably of the K-feldspar quartz monzonite porphyry (K–QMP), K-feldspar-augite quartz monzonite porphyry (KA–QMP) and mineralized samples from the Two-Thirty prospect Northparkes Intrusive Complex (Fig. 9b), show evidence of potassic alteration, displaying an increase in K relative to average unaltered composition. More intense alteration and loss of both K and Na are observed for a limited number of samples, for

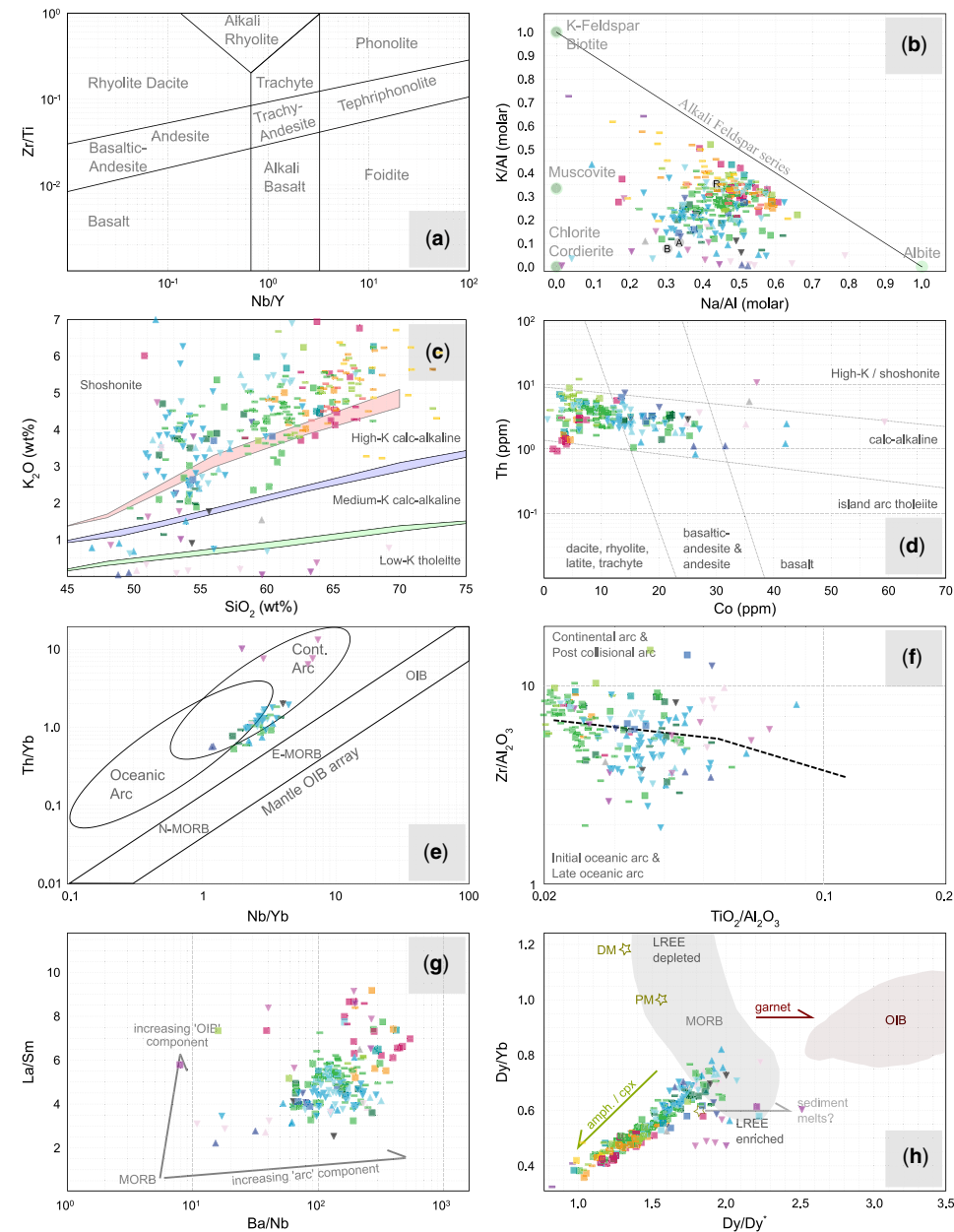
example, one result from each of the Wombin, Bushman and Fairbridge volcanics, as well as some Copper Hill Intrusive Complex volcanic rocks.

K-series classification

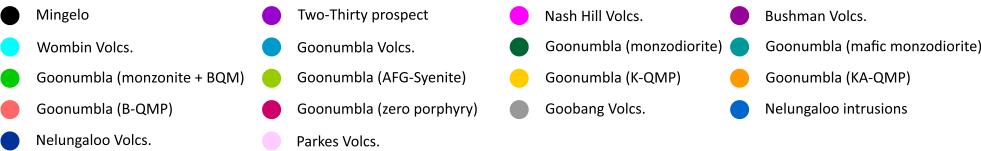
To effectively discriminate between variably K-enriched magma series, we discuss our data in the context of shoshonite discrimination diagrams after Hastie *et al.* (2007) (see Figs 9–11) and Pearce (1982) (Supplementary File 2). In this classification scheme, Th is used as a proxy for K₂O due to similar mobility to K in subduction systems, whereas Co shows an inverse correlation to SiO₂ during differentiation and is thus considered an appropriate analogue. Both diagrams rely in large part on the behaviour of Th as being mobilized during subduction, similarly to other LILEs. Additional K can be mobilized into the system from two main subduction components: fluids derived from altered oceanic crust (slab flux), and secondly from silicate melts derived from melting of mainly sedimentary material. Thorium may be mobilized in the sedimentary component, but is potentially less mobile in the aqueous fluids driven off the subducting slab (Bryant *et al.* 2003; Elliott 2003; Hastie *et al.* 2007). Depth and temperature of derivation appear to be the main controls on Th mobility in the liberated aqueous fluids (Hastie *et al.* 2007).

Whilst Th is considered to behave like K across a range of magmatic suites derived from different depths, within modern subduction systems, it may undergo partial decoupling under some conditions (Hastie *et al.* 2007). Due to the mobility of Th at upper amphibolite facies, a large proportion of Th may be transmitted to the mantle wedge prior to subducting material descending to sub-arc depths. Partial decoupling may occur during partial melting due to the less incompatible behaviour of K which partitions more strongly into magmas derived by smaller degrees of partial melting. Potassium is also more readily mobilized by hydrothermal fluids (Leitch and Lentz 1994; Hastie *et al.* 2007). Despite these limitations, the classification scheme after Hastie *et al.* (2007) gives reasonable results and has good agreement with other shoshonite classification criteria (e.g. LREE v. HREE enrichment; Morrison 1980).

Due to the observed alteration, subdivision and classification of Macquarie Arc rocks into K-series using the K₂O–SiO₂ diagram of Peccerillo and Taylor (1976) is problematic. Samples from most districts cluster in the high-K and shoshonite fields (Figs 9c, 10c & 11c). Intrusive phases associated with mineralization are generally highly potassic and classify as shoshonitic. A smaller proportion of samples plot within the medium-K and low-K fields, and often reflect K-loss. Examples of lower-K samples appear present within all districts (e.g.



Location



ROCK TYPE



Nelungaloo basalts, Stokefield Metagabbro and Coombing Formation). Copper Hill intrusive and Fairbridge volcanic samples are notable examples whose average composition is likely medium-K. Medium- to high-K results for the Yiddah (Rain Hill) and Gidginbung volcanic samples reflect probable K-loss (Fig. 11b), and composition is likely high-K to shoshonitic. This is supported by petrographic descriptions and immobile element classification schemes (Fig. 11d; Supplementary File 2; Goesch 2011).

When plotted on Hastie *et al.*'s (2007) Th–Co (Figs 9d, 10d & 11d) and Pearce's (1982) Ta/Yb–Th/Yb (Supplementary File 2) trace element classification schemes, samples from most districts classify as calc-alkaline. Only a small number of samples (e.g. Cadia and Kaiser-Dubbo) plot transitionally into the high-K and shoshonitic field of Hastie *et al.* (2007). Yiddah (Rain Hill), Gidginbung Volcanics, Mothershippton monzodiorite and late volcanics such as the Nash Hill Volcanics plot into the high-K and shoshonitic fields of Hastie *et al.* (2007) and Pearce (1982). Lower-K sequences such as the Copper Hill Intrusive Complex and the Nelungaloo basalts plot with low Th and Th/Yb–Ta/Yb transitional to the island arc tholeiite fields (Figs 9d, 10d & 11d; Supplementary File 2).

Discrimination between oceanic and continental arc settings

In addition to bulk rock classification, we utilize trace element discrimination diagrams to investigate the nature and any observable variation in magma source region. Here, we present a selection of these diagrams with additional diagrams and supporting text in Supplementary File 4.

The data presented here are consistent with an arc setting having high Th/Yb relative to Nb/Yb,

which moves the data off the 'mantle array' on the diagram of Pearce (2014). The main cluster of results for basaltic samples plots within the overlap of the 'continental' and 'oceanic' arc fields (Figs 9e, 10e & 11e). Data from many suites which plot within this overlap also have data which plot in the 'continental' field only (e.g. Ridgeway, Goomnumbla volcanics and intrusions, Cheesemans Creek Formation). Data from the Nash Hill Volcanics and the Yiddah (Rain Hill) sit exclusively within the continental arc field. Some data do not plot within either continental or oceanic arc fields (e.g. one sample from an intrusion in the Trundle Block, as well as some data from the Gidginbung and Bushman volcanics).

Müller and Groves (2019) proposed the use of a hierarchical set of discrimination diagrams and compositional criteria to satisfactorily discriminate the tectonic setting of potassic igneous rocks. The initial step of Müller and Groves's (2019) hierarchical discrimination approach uses compositional criteria (TiO₂, Hf and Zr contents) to determine if samples have within-plate affinity. All analyses have TiO₂ (<1.5 wt%), Hf (<10 ppm) and Zr (<350 ppm) contents, which suggests they were not generated in a within-plate setting (Müller and Groves 2019). When plotted on the TiO₂/Al₂O₃–Zr/Al₂O₃ discrimination diagram of Müller and Groves (2019) (Figs 9f, 10f & 11f), most analyses plot within the oceanic arc field (initial oceanic arc (IOP), late oceanic arc (LOP)) transitional to and into the continental arc (CAP) and post-collisional arc (PAP) field. Intermediate samples, from the Cadia Hill Monzonite and the Northparkes Intrusive Complex, plot within the CAP + PAP field close to the field boundary, whereas more alkaline samples (e.g. Yiddah (Rain Hill), Trundle Park and Nash Hill Volcanics) all plot within this field.

Fig. 9. Classification and discrimination diagrams of Forbes–Parkes regional and Northparkes district volcanic, intrusive and mineralizing porphyry samples. (a) Zr/Ti v. Nb/Y trace element classification scheme using volcanic nomenclature after Pearce (1996). (b) Feldspar Na–K GER diagram. Molar ratios of Na/Al v. K/Al are used to infer mobility of alkali metals in or out of the system. The B, A and R points refer to the expected composition for a basalt, andesite and rhyolite, respectively. (c) K₂O v. SiO₂ major element shoshonite affinity classification scheme. (d) Th–Co–K trace element potassium affinity classification. In some cases, Co is absent from historical data and cannot be plotted on this diagram. (e) Th/Yb v. Nb/Yb tectonic setting discrimination scheme. (f) Zr/Al₂O₃ v. TiO₂/Al₂O₃ volcanic arc setting discrimination diagram for basaltic and basaltic–andesite composition samples. (g) Ba/Nb v. La/Sm trace element source component classification scheme, which indicates degrees of arc v. OIB input. (h) Dy/Yb v. Dy/Dy* trace element source component classification scheme. Dy/Dy* serves as a proxy for MREE–HREE slope and allows inference for amphibole, clinopyroxene or garnet source input during partial melting and subsequent fractionation. Abbreviations: GER, general element ratio; OIB, ocean island basalt; LREE, light rare earth elements; MREE, middle rare earth elements; HREE, heavy rare earth elements; MORB, mid-ocean ridge basalt; Cont., continental; DM, depleted mantle; PM, primitive mantle; amph., amphibole; cpx, clinopyroxene; Volcs., volcanics; BQM, biotite quartz monzonite; QMP, quartz monzonite porphyry; AFG, alkaline feldspar granite. Source: data not generated as a part of this study for the Northparkes Intrusive Complex (a–h) is sourced from Lickfold (2002) (a–c, e–h), Pacey (2016) (a–h), and Wells *et al.* (2020) (a–c, e–h). Regional data for the Forbes–Parkes area sourced from Crawford *et al.* (2007b) (a–c, e–h).

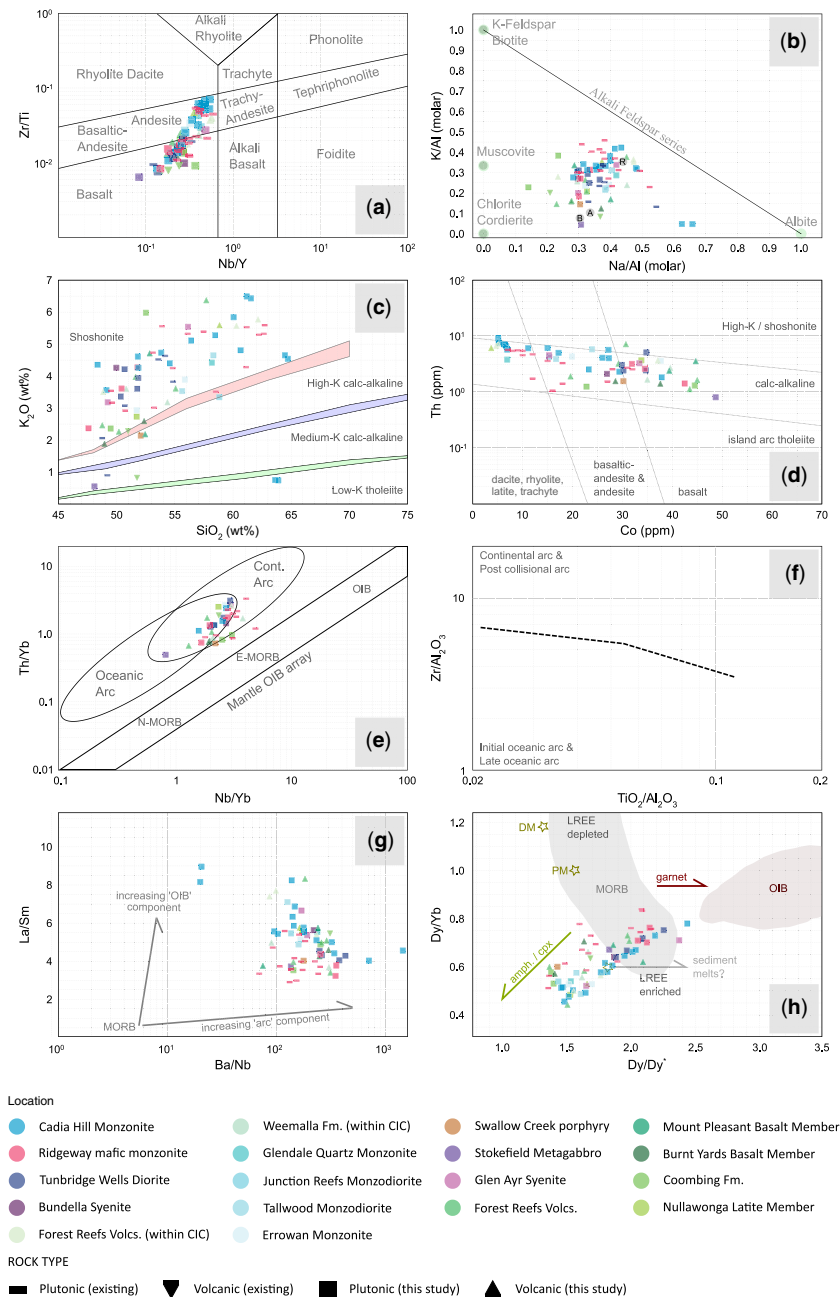


Fig. 10. Classification and discrimination diagrams of the Forest Reef regional and Cadia district and regional volcanic host and syn-mineralization intrusive rocks. Monzodiorite and quartz monzonite samples of the Junction Reefs and Glendale prospects are located within the Forest Reef region. (a) through (h) are described in the caption of Figure 9. Abbreviations: GER, general element ratio; OIB, ocean island basalt; LREE, light rare earth elements; MREE, middle rare earth elements; HREE, heavy rare earth elements; MORB, mid-ocean ridge basalt; Cont., continental; DM, depleted mantle; PM, primitive mantle; amphi., amphibole; cpx, clinopyroxene; Volcs., volcanics; BQM, biotite quartz monzonite; QMP, quartz monzonite porphyry; AFG, alkaline feldspar granite; CIC, Cadia Intrusive Complex. Source: data not generated as a part of this study for Tunbridge Wells (a–c, f) from Wilson (2003) and Ridgeway samples (a–h) from Chhun (2004). Additional Coombing samples (a–c, e–h) from Crawford *et al.* (2007b).

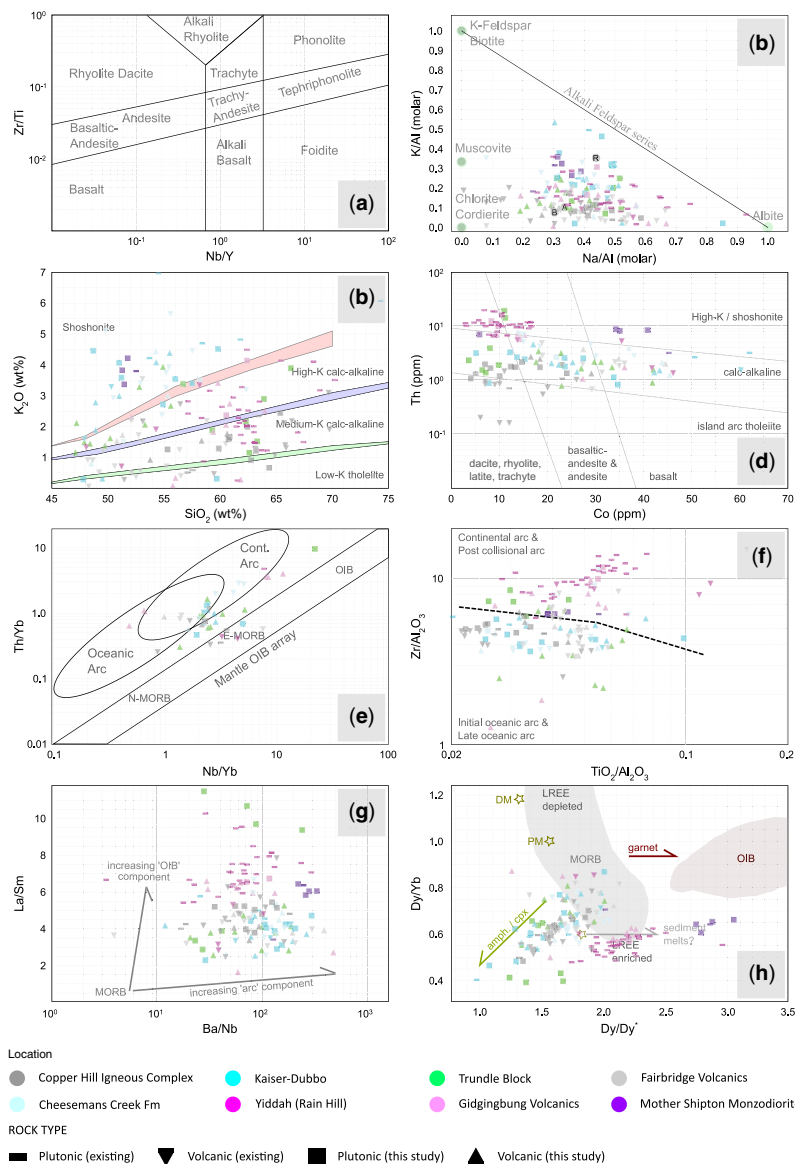


Fig. 11. Classification and discrimination diagrams of several mineralized districts including Bodangora, Trundle Block, Rainhill Intrusive Complex and Copper Hill Intrusive Complex are compared alongside stratigraphically associated regional volcanics Cheesemans Creek Volcanics, Gidginbung Volcanics and Fairfield Volcanics, respectively. Probable Raggett Volcanic host rocks are included within Trundle Block samples. The shoshonitic Mother Shipton Monzodiorite of unknown age outcrops within the Silurian Temora Volcanics and is located south–SE of the Gidginbung Volcanics. Cadia Hill Monzonite and Nelungaloo Volcanic samples are included for comparison and later discussion. (a) through (h) are described in the caption of Figure 9. Abbreviations: GER, general element ratio; OIB, ocean island basalt; LREE, light rare earth elements; MREE, middle rare earth elements; HREE, heavy rare earth elements; MORB, mid-ocean ridge basalt; Cont., continental; DM, depleted mantle; PM, primitive mantle; amph., amphibole; cpx, clinopyroxene; Volcs., volcanics; BQM, biotite quartz monzonite; QMP, quartz monzonite porphyry; AFG, alkaline feldspar granite. Source: data not generated as a part of this study for Rainhill Intrusive Complex (a–h) is sourced from [Goesch \(2011\)](#) and Copper Hill Intrusive Complex (a–h) from [Chun \(2004\)](#). Existing regional data for Fairbridge and Cheesemans Creek samples is sourced from [Crawford *et al.* \(2007b\)](#) (a–c, e–h) and historic GSNSW databases ([Geological Survey of NSW 2024](#)) (a–h). Bogandora and Mother Shipton samples (a–h) from recent GSNSW studies analysed and located with Geoscience Australia's Data Portal ([Geoscience Australia 2024](#)).

Magma source regions

In the following sections, we present Ba/Nb v. La/Sm trace element discrimination diagrams (Figs 9g, 10g & 11g) after Langmuir *et al.* (2006), alongside Dy/Dy* v. Dy/Yb diagrams (Figs 9h, 10h & 11h) after Davidson *et al.* (2013) to elucidate the possible magma source components and fractionation history of the main districts of the Macquarie Arc.

The Ba/Nb–La/Sm diagram of Langmuir *et al.* (2006) identifies subduction and supra-subduction zone-related source components. High La/Sm and low Ba/Nb represents the ocean island basalt (OIB) or alkaline end-member, whereas the inverse represents the arc component. End-member components and mixing trends can be inferred by the distribution of samples between these element pairs. Strong enrichment in fluid mobile elements such as Ba relative to conservative elements (Nb, Zr, Y, Yb) typifies the arc or slab flux component, whereas a high La/Sm ratio identifies the steep LREE enriched REE patterns typical of OIB-like components (Langmuir *et al.* 2006). Barium behaves in a similar way to K during subduction and is fluxed off the subducting slab at similar depths (Becker *et al.* 2000; Savov *et al.* 2005; Hastie *et al.* 2007).

A general progression from low to moderate Ba/Nb–La/Sm through to high Ba/Nb–La/Sm is observed in most districts (Figs 9g, 10g & 11g). The significantly lower Ba/Nb and lower La/Sm cluster of low Nb/Yb samples typified by the basaltic Nelungaloo Volcanics contrasts with the moderate La/Sm and high Ba/Nb for most volcanic and intrusive samples. Mineralized and zero porphyries of the North Parkes and Cadia intrusive complexes plot with the high Ba/Na and La/Sm. Data from the Yiddah (Rain Hill) and Trundle Park plot with high to extremely high La/Sm.

Additionally, Dy/Dy* uses the measured value of the middle rare earth element (MREE) Dy compared with the interpolated value of La and Yb to quantify the ‘concavity’ or shape of the REE value represented by Dy* (Davidson *et al.* 2013). When plotted against Dy/Yb, REEs can effectively be classified by shape. Trends of differentiation of cogenetic samples can be defined by sympathetic decreasing Dy/Yb with Dy/Dy* with preferential partitioning of MREE, controlled by fractionating phases such as amphibole or clinopyroxene. Concave up curves reflect partitioning of MREE over HREE and LREE into amphibole and, to a lesser extent, clinopyroxene.

The terms N-MORB, E-MORB and OIB/alkaline have inherent tectonic associations but are used here as a measure of enrichment with N-MORB being more depleted than primitive mantle derived magmas, and E-MORB being more enriched (Gale *et al.* 2013). ‘OIB influenced’ or ‘alkaline’ is

used to imply the input of an enriched deeper asthenosphere mantle source. OIB/alkaline or ‘OIB influenced’ samples plot with increasing to high Dy/Yb, suggesting a significant control by substitution into garnet due to the retention of Yb over Dy. Additionally, LREE depletion to enrichment can be inferred by a broad negative correlation with decreasing Dy/Dy* reflecting the ‘concavity’ of corresponding REE patterns. Known compositions of global average subduction-related sediments and the influence on REE patterns can also provide insight into sedimentary contributions to source compositions. Dy/Dy* and its use on the Dy/Yb–Dy/Dy* allow a clearer understanding of petrogenetic processes which are often obscured by the traditional use of REE multi-element diagrams.

When plotted on the Dy/Yb–Dy/Dy* diagram of Davidson *et al.* (2013), most data plot first within the ‘MORB’ field and progress along the ‘amphibole/clinopyroxene’ differentiation trend (Figs 9h, 10h & 11h). Notably, data from the Cadia Hill Monzonite have a higher Dy/Dy* and first plot towards the ‘OIB’ field consistent with the ‘garnet’ differentiation trend before progressing through the ‘MORB’ field and along the ‘amphibole/clinopyroxene’ trend (Fig. 9h). Data from some samples in the Temora district (Yiddah (Rain Hill), Gidginbung Volcanics, Mother Shipton Monzodiorite; Fig. 11h) and the Forbes–Parkes region (Nash Hill and Bushman volcanics; Fig. 10h) have distinctly high Dy/Dy* and low Dy/Yb, consistent with the inferred ‘sediment melts?’ trend used to indicate potential crustal contamination (Davidson *et al.* 2013).

Discussion

Geochemical character, subduction setting and tectonic assessment of potassic igneous suites in the Macquarie Arc

Occurrence of high-K calc-alkaline and shoshonitic rocks in the Macquarie Arc

Macquarie Arc rocks, including mineralized intrusive hosts, are often referred to as high-K to shoshonitic (Arundell 1998; Blevin 2002; Holliday *et al.* 2002; Lickfold 2002; Lickfold *et al.* 2003, 2007; Wilson *et al.* 2003; Wilson 2003; Forster *et al.* 2004; Simpson *et al.* 2005; Crawford *et al.* 2007a, b; Glen *et al.* 2007a, d; Percival and Glen 2007; Simpson *et al.* 2007; Squire and Crawford 2007; Goesch 2011; Pacey *et al.* 2019; Harris *et al.* 2020; Wells *et al.* 2020, 2021), but few terrane-wide classifications, or detailed immobile trace element studies, of these economically significant rocks have been undertaken. Utilizing simple K₂O abundance, most Macquarie Arc samples in this study should

be classified as high-K or shoshonitic (Figs 9c, 10c & 11c). Despite this, Blevin (2002) suggested that the various intrusive and volcanic suites of the Macquarie Arc, including the Cu-rich Northparkes Intrusive Complex, are not truly shoshonitic but more accurately highly potassic calc-alkaline rocks (Figs 9d, 10d & 11d). Only rare examples of shoshonites exist within the Macquarie Arc, for example, the Mother Shipton Monzodiorite and the Yiddah porphyry associated with the Rain Hill Monzodiorite (Fig. 11d; Goesch 2011). Whilst typically considered a shoshonite, the Au-rich Cadia Intrusive Complex is only marginally classifiable as shoshonitic (Blevin 2002). By most classification criteria, this assessment is fundamentally valid. Broadly, Macquarie Arc rocks are undeniably potassic and calc-alkaline but classification as shoshonitic using immobile elements such as Th (Hastie *et al.* 2007), Th/Yb (Pearce 1982), LREE/HREE and average elemental abundances (Morrison 1980; Blevin 2002; Scarrow *et al.* 2008; Torabi 2011; Müller and Groves 2019; Amaral *et al.* 2022) suggest most are only marginally shoshonitic (Figs 9–11 and Supplementary File 2).

Despite the similarities between these modern shoshonites, comparisons to well-known examples generated from deep and potentially phlogopite-bearing mantle source regions such as Bingham (Maughan *et al.* 2002; Grondahl and Zajacz 2017), Tibet (Turner *et al.* 1996; Campbell *et al.* 2014), Iran (Torabi 2011; Nayeibi *et al.* 2024) or the Sunda rear-arc (Edwards *et al.* 1994; Kirchenbaur *et al.* 2022) are difficult to make. Published whole-rock analyses for samples from these arc terranes have comparatively high Th, pronounced LREE/HREE enrichment and high Dy/Yb (as compared to Macquarie Arc samples; Fig. 12a, b), indicating low degree partial melt generation at mantle depths above phlogopite stability and often recording the influence of crustal contamination (Morrison 1980; Sun and Stern 2001; Scarrow *et al.* 2008; Torabi 2011; Li *et al.* 2013). Instead, we propose that a more apt comparison for the most potassic Macquarie Arc ‘shoshonites’ is that of ‘primitive’ shoshonites generated in intraoceanic settings with minor to absent sedimentary or crustal influence, with limited evidence for truly deep melt generation (Sun and Stern 2001; Leslie *et al.* 2009; Ishizuka *et al.* 2010; Clarke *et al.* 2022; Yutani *et al.* 2023). Examples from post-subduction shoshonites include Fiji (Leslie *et al.* 2009; Clarke *et al.* 2022), rear-arc shoshonites of the Izu–Bonin–Mariana arc (Sun and Stern 2001; Ishizuka *et al.* 2007, 2010), Baguio from the complex western Luzon arc (Hollings *et al.* 2011) and intraoceanic shoshonites of Nemuro (Yutani *et al.* 2023), which share geochemical and isotopic systematics most similar to data presented in this study, including the well-studied mineralized districts.

Results from the Trundle Park and Bayley prospects and for Mother Shipton differ notably compared to most suites within the arc (e.g. Cadia Intrusive Complex, Northparkes Intrusive Complex and other low Th Trundle (Mordialloc) samples; Figs 9–11). We present three new U–Pb zircon ages for the Trundle district. Two Late Ordovician to early Silurian ages (440.9 ± 1.76 Ma for DBF23-3-4A and 443.4 ± 1.81 for DBF23-4-12; Supplementary File 6) for the medium-K to high-K Mordialloc samples suggest emplacement coeval with the highly mineralized suites at Northparkes. Geochemical similarities between Trundle (Mordialloc) and mineralized porphyries of Northparkes suggest similar processes and source components contributed to mineralization between both districts during the Late Ordovician to early Silurian. We also present a new U–Pb zircon concordia age of 418.4 ± 1.35 Ma (lower intercept age of 417.7 ± 2.1 Ma; Supplementary File 6) sampled from shoshonitic rocks at Trundle Park. This suggests the high Th shoshonitic intrusions and related units with this geochemical composition intruded post-subduction in a probable rift setting. Prior work for Trundle Park revealed evidence of crustal contamination (Pb–Pb isotopes; Forster and Maas 2015) and Devonian Re–Os ages (418.6 Ma ± 2 Ma; Forster *et al.* 2015) from rocks we now classify as shoshonites. Although further work to better constrain the geological relationships in this area is warranted, this implies the high Th shoshonite samples at Trundle post-date the Benambran Orogeny and are consistent with emplacement during Tabberabberan extension (Glen 2005).

Prolonged arc volcanism, subduction setting and tectonic assessment

The Macquarie Arc is a long-lived volcanic arc terrane which was active for up to 70 Myr with probable but poorly defined hiatuses in volcanic activity. As a result, the variable composition and character of arc rocks in the terrane are difficult to understand without due consideration of the spatial and temporal variations in magma geochemistry and isotopic fingerprints. The enriched and high-K characteristics of volcanic and intrusive suites across the Macquarie Arc, in particular the Early Ordovician Nelungaloo Volcanics, raise questions about the tectonic setting and evolution of the arc over time. The Nelungaloo Volcanics are considered to represent some of the earliest magmatic activity within the arc (Wyborn 1992; Butera *et al.* 2001; Blevin 2002; Simpson *et al.* 2005; Crawford *et al.* 2007b; Glen *et al.* 2007b; Percival and Glen 2007). This is at odds with the traditional view of a relationship between K enrichment, time and distance from the trench (i.e. K-series zonation over time) (Morrison 1980;

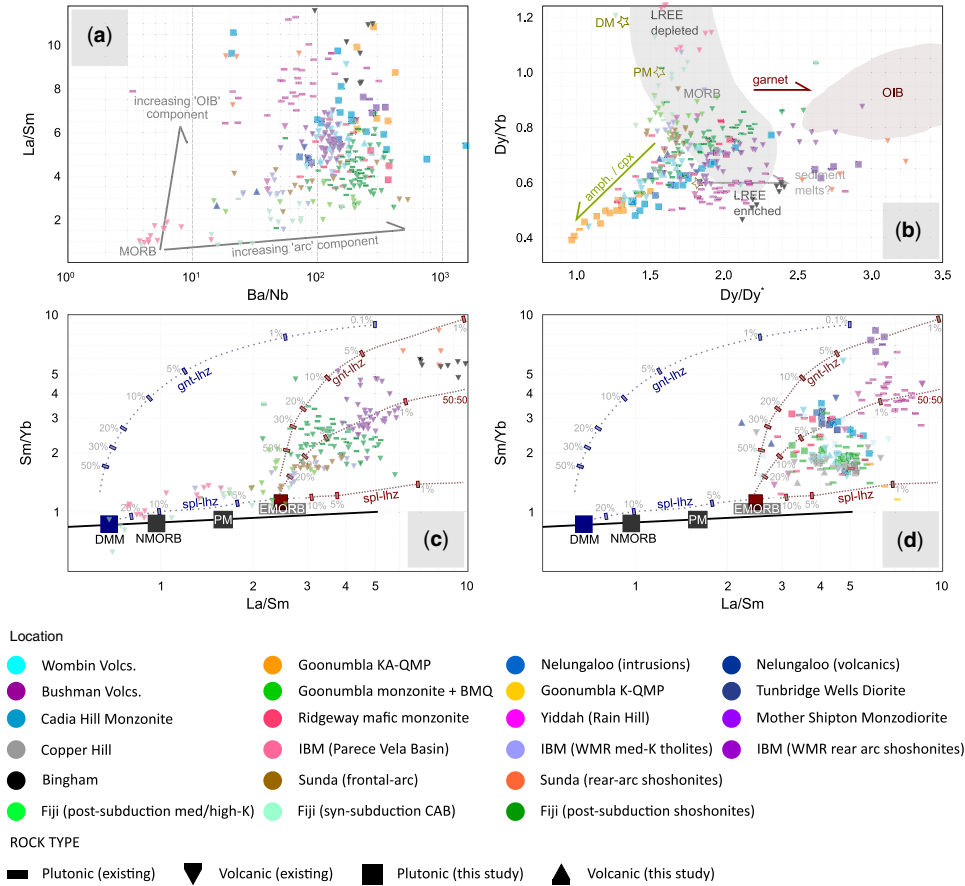


Fig. 12. Data of the Macquarie Arc contrasted against data from modern arc systems (Izu–Bonin–Mariana, Sunda, Bingham and Fiji arcs). **(a)** Ba/Nb v. La/Sm trace element source component classification. **(b)** Dy/Yb v. Dy/Dy* trace element source component classification scheme. **(c)** and **(d)** Sm/Yb–La/Sm diagrams for potential analogues (12c) compared with select Macquarie Arc data (12d). The dashed and solid lines are the non-modal batch melting trajectories for the depleted MORB mantle (DMM) and enriched mid-ocean ridge basalt mantle (E-MORB) respectively, after Aldanmaz *et al.* (2000). Degrees of partial melting are shown as thick marks on the melt trajectories. All data utilized are of basalt or basaltic andesite composition. Refer to Aldanmaz *et al.* (2000) for full methodology. N-MORB: normal mid-ocean ridge basalt; PM: primitive mantle; gnt–lhz: garnet–lherzolite; 50:50: 50% garnet–lherzolite, 50% spinel–lherzolite; spl–lhz: spinel lherzolite. Source: (a) Langmuir *et al.* (2006); (b) Davidson *et al.* (2013); (c–d) Aldanmaz *et al.* (2000).

Tatsumi and Eggins 1995; Winter 2014; Kirchenbaur *et al.* 2022). It should be noted that the relationship between K zonation through time is well defined in continental settings but is only observed in some island arc settings (Morrison 1980). There are examples of intraoceanic arcs where a spatial relationship to K enrichment is not always apparent (Morrison 1980; Müller and Groves 2019; Yutani *et al.* 2023). Whilst various researchers disagree on the details, the generally accepted interpretation is that the Macquarie Arc formed in an intraoceanic arc setting which was subsequently accreted with

Gondwana and deformed during the Benambran Orogeny (Crawford *et al.* 2007b; Glen *et al.* 2007d, 2012; Meffre *et al.* 2007; Kemp *et al.* 2009, 2020). Tectonic discrimination after Müller and Groves (2019) suggests most sequences were generated in a late intraoceanic setting that transitions to a post-collisional arc and provides support for this interpretation (Figs 9f, 10f & 11f). District scale structural and geochronological evidence suggests economic porphyry mineralization occurred during terrane accretion and orogenesis (Crawford *et al.* 2007b; Fox *et al.* 2015; Harris *et al.* 2014, 2020).

Enrichment of the sub-arc mantle via subduction related processes may have occurred prior to accretion and has implications for metal endowment (see later Discussion sub-sections).

All geochemical systematics explored as part of this study support an intraoceanic setting with little to absent subduction or crustal derived sedimentary components prior to terrane accretion. Isotopic systematics of primitive mantle-like Sm–Nd, Lu–Hf and Pb–Pb isotopes for most arc sequences support this (Wyborn and Sun 1993; Kemp *et al.* 2009, 2020; Forster *et al.* 2011, 2015; Hao *et al.* 2021). A trend to more crustal isotope values does occur during the terminal phase coeval with mineralization and accretion, and it is observed with late volcanics such as the Nash Hill and Bushman volcanics. This can be attributed to either a sediment starved setting or limited melting of subducted sediments (Stern and Arima 1998; Ishizuka *et al.* 2010).

Distribution of most data between values expected for a purely oceanic and continental setting on the Th/Yb–Nb/Yb (Pearce 2014) (Figs 9e, 10e & 11e) tectonic discrimination diagram is typical of a mature intraoceanic/volcanic arc setting with a thicker and more developed arc crust. Saccani (2015) refers to this as ‘polygenetic crust–island arc’ (Supplementary File 4). Trends of increasing Th/Yb with increasing Nb/Yb suggest coupled fractional crystallization, ‘OIB’-type enrichment and lower extent of melting (Pearce 2014; Saccani 2015).

Whilst our data broadly support an intraoceanic arc setting, there is evidence for varied contributions of slab flux across the igneous suites sampled in this study. Some results for intrusive suites from mineralized districts (e.g. Goonumbla, Trundle, Copper Hill and results for the regional Fairbridge volcanics) form a trend with lower Th/Yb, which may reflect a waning or reduced subduction influence. Lower Th/Yb and Nb/Yb for samples including the basaltic Nelungaloo samples and the Stokefield Metagabbro distinguish them from the main cluster and suggest a more depleted source composition, with higher degrees of partial melting potentially generated in a more juvenile arc setting. Steep vertical displacements of Th/Yb and significant increases in Th observed in more alkaline samples (i.e. Nash Hill, Gidginbung, Yiddah (Rain Hill) and alkaline Trundle Park) are suggestive of crustal contamination. Of this group, Yiddah (Rain Hill) is the only mineralized district with noticeable crustal influence identifiable from the bulk rock geochemistry (Fig. 11e, h) constrained to the Late Ordovician (Goesch 2011; Harris *et al.* 2014; Kemp *et al.* 2020). Its position within the southern extent of the Junee–Narromine Volcanic Belt places it apart from most other examples and may speak to previously unrecognized variations in crustal architecture and thickening along arc. Notably, this was contemporaneous with the

eruption and emplacement of the high-K Cadia district (see Harris *et al.* 2014).

Data presented in this study alongside existing data for known Macquarie Arc intrusive and volcanic suites are primarily derived from an E-MORB mantle source (Supplementary File 4), are typically calc-alkaline (Figs 9d, 10d & 11d and Supplementary File 4) and have isotopic character consistent with derivation from depleted mantle reservoirs (Sun 1980; Wyborn and Sun 1993; McDonough and Sun 1995; Kemp *et al.* 2009, 2020; Hao *et al.* 2021). A likely analogue is an intraoceanic rear-arc setting (Ishizuka *et al.* 2010; Tani *et al.* 2011; Johnson *et al.* 2021). The LILE and LREE enrichment and high-field strength element (HFSE) depletion suggest the sub-arc/lithospheric mantle has been previously enriched by fluid mobile elements, potentially in frontal-arc chains or segments (Ishizuka *et al.* 2010; Tani *et al.* 2011). High La/Sm, Dy/Yb and a generally E-MORB composition (Figs 9g, h, 10g, h, 11g & h; Supplementary File 4) suggest influence from garnet-lherzolite source, decreasing degrees of melting and provide evidence of a thickening arc crust (Fig. 12d; Pearce 2008; Saccani 2015). Crustal thickness calculations (Supplementary File 5) suggest a progressive thickening over time prior to accretion. Crustal thickness progression correlates well to Th and, by proxy, K (and other LILEs) for most sequences and supports the suggestion of a thickening and progressively more enriched arc crust.

The general E-MORB composition contrasts distinctly with many frontal-arc sequences. Most frontal-arc sequences include low-K, depleted N-MORB and tholeiite sequences with more subdued LILE and LREE enrichment and HFSE depletion (Fig. 12), which are generated with higher degrees of melting at shallower depths from MORB-type asthenosphere prior to subduction-related metasomatism (Ishizuka *et al.* 2010; Tani *et al.* 2011).

A reasonable analogue can be found in the Izu–Bonin–Mariana (IBM) medium- to high-K to shoshonitic rear-arc sequences (Fig. 12). The rifted rear-arc Western Mariana Ridge contains analogous low to moderate Th isotopically primitive potassic to shoshonitic lavas whose geochemical systematics parallel those of the Macquarie Arc lavas (Ishizuka *et al.* 2007, 2010; Tamura *et al.* 2015) and are consistent with a westward thickening crustal model for the Lachlan Orogen identified by Musgrave (2022). In detail, the IBM lavas are a partial analogue for the older, pre-accretionary sequences of the Macquarie Arc. Nonetheless, they provide reasonable context in order to better understand the general geochemical and isotopic systematics. Parallels have also been made to post-subduction high-K to shoshonitic rocks of Fiji (Crawford *et al.* 2007b; Squire and

Crawford 2007; Leslie *et al.* 2009; Clarke *et al.* 2022). Placing the Nelungaloo Volcanics within this setting during the Early Ordovician does remain problematic.

Occurrences of K-rich sequences with no apparent spatial or arc maturation relationship do exist (Müller and Groves 2019; Yutani *et al.* 2023). Müller and Groves (2019) suggest early frontal-arc K-rich magmatism can be generated due to dehydration melting of chlorite in cool subduction settings (Till *et al.* 2012). Further work is required to determine if this is a plausible suggestion for the generation of the shoshonitic rocks within the Macquarie Arc, and specifically of the Nelungaloo Volcanics early in the evolution of the terrane.

Compositional differences between the Junee–Narromine and Molong belts: implications for arc maturation

A changing arc terrane in space and time

Progressive enrichment during arc maturation produces porphyry-related magmas which are geochemically more evolved and more hydrous than preceding volcanic rocks (Richards *et al.* 2012; Loucks 2014; Jamali and Mehrabi 2015; Müller and Groves 2019; Park *et al.* 2021). Richards *et al.* (2012) suggest this process reflects maturation over tens of millions of years and is an important factor influencing mineralization potential of porphyry systems. The thickening of the arc crust, progressive fluid-induced enrichments or metasomatism and increased contributions from varied mantle sources are controls on the depths where melts are generated within the sub-arc mantle. As a result, the composition and character of arc volcanism and related sub-volcanic intrusions have an intrinsic relationship with arc maturation through time.

Broadly, this is consistent with the large-scale early Silurian mineralization within the Cadia and Northparkes porphyry districts. However, districts within the Junee–Narromine Volcanic Belt have internally similar geochemical characteristics and are somewhat distinct from districts within the Molong Volcanic Belt, which has implications for magmatic fertility (Figs 9 & 10). Broad compositional evolution is observed across all districts and regions, with the most evolved and transitionally alkaline to alkaline samples noted within mineralized intrusive complexes (Figs 9–11; Supplementary File 2). This compositional evolution is accompanied by enrichment of LILEs and LREEs and OIB (alkaline) influence (Figs 9g, 10g & 11g).

Most measures of enrichment are higher within the Cadia Intrusive Complex (Fig. 10) when compared with key mineralized districts within the

Junee–Narromine Volcanic Belt, and specifically to Northparkes Intrusive Complex samples. A notable observation is that the Cadia samples have higher La/Sm, Dy/Yb, Sm/Yb and LREE/HREE that indicate a greater contribution from a relatively deeper, garnet–lherzolite mantle source (Figs 10g, h & 12).

The porphyry districts in the Molong Belt (e.g. Bodangora (Boda–Kaiser) and associated Cheesemans Creek samples) appear most like the Cadia Intrusive Complex and regional Forest Reefs samples (Figs 10, 11 & 12d). A spatially continuous set of samples from Comobella and the Cheesemans Creek Formation along the upper Molong Belt and within the Bodangora district show a greater slab flux and residual garnet signature that includes K–Th enrichment characteristic of the Cadia Intrusive Complex. A probable example of K enrichment over time is observed within the Molong Volcanic Belt (Figs 10 & 11). The Middle to Late Ordovician medium-K Copper Hill Intrusive Complex and Fairbridge sequence are compositionally distinct, and less K-enriched when compared to the younger Late Ordovician to Silurian Forest Reefs volcanics and Cadia Intrusive Complex, as well as the Cheesemans Creek and Bodangora sequence. As a result, we propose that the Copper Hill Intrusive Complex is an end-member along a continuum of variably K-enriched suites of fundamentally medium- to high-K calc-alkaline series affinity (Figs 10d, e, 11d & e and Supplementary File 2).

The Copper Hill Intrusive Complex and Fairbridge sequence are comparatively depleted in LILE, LREE and LREE/HREE, and record less input from garnet–lherzolite mantle reservoirs when compared to the Cadia Igneous Complex (Figs 10, 11 & 12d). This distinction could suggest progressive enrichment has occurred over time and could be reasonably attributed to arc maturation (Fig. 11; Richards *et al.* 2012; Winter 2014; Saccani 2015). It is important to highlight the possibility that the differences seen in the Copper Hill Intrusive Complex could be attributed to heterogeneous mantle sources (Sun and Stern 2001). Coeval medium-K and high-K shoshonites can be generated within the same setting but within different arc segments (Peate *et al.* 1997; Sun and Stern 2001; Ishizuka *et al.* 2010; Clarke *et al.* 2022), as seen in the co-eruption of lower-K districts within the Junee–Narromine Volcanic Belt coeval with higher-K sequences within the Molong Volcanic Belt (e.g. the medium-K Late Ordovician to early Silurian Trundle ‘Mordialloc’ intrusions and the shoshonitic Cadia Intrusive Complex).

Within the Junee–Narromine Belt, the geochemical systematics suggest Trundle (Mordialloc) is most like the Northparkes Intrusive Complex. Data from Mordialloc samples support magma generation from a dominantly spinel–lherzolite mantle source

and K–Th enrichment comparable to Northparkes Intrusive Complex samples (Figs 9 & 11). Late Ordovician to early Silurian age constraints for both districts and spatial proximity may suggest generation from similar mantle sources at a similar time. High Th and LREE/HREE crustal influenced shoshonites only occur in the Junee–Narromine Volcanic Belt (Figs 9 & 11) both syn-Benambran accretion (e.g. Yiddah and Mother Shipton Monzodiorite) and post-subduction rifting (e.g. Trundle Park). This does suggest distinctive source components and a comparable but distinct setting contributed to magmatism within each volcanic belt.

Enrichment of the sub-arc crust by fluid mobile elements

In addition to variations in magma source regions during arc maturation, metasomatism of the arc crust by subduction fluids results in enrichment of fluid mobile elements in the arc crust. Parental melts of arc basalts are typically hydrous (2–6% H₂O; Plank *et al.* 2013) and record complex mixing of elements derived from the subducting slab, overlying mantle wedge and oceanic sediments (Plank and Langmuir 1993, 1998; Pearce *et al.* 2005; Langmuir *et al.* 2006; Davidson *et al.* 2013). As a result, these magmas are rich in LILE, including K and Ba, as well as volatiles such as Cl and S and metals (Wallace 2005). Base and precious metals are soluble in hot, saline fluids derived from the down-going slab, and are strongly influenced by oxidation state and sulfur fugacity (Blevin 2002; Mungall 2002; Richards 2009; Blevin *et al.* 2020). Copper-rich deposits are more often related to more typical arc-related magmas, whereas Au-rich deposits more often relate to atypical subduction or collisional settings (Richards 2009). Therefore, understanding the enrichment of LILE such as K within subduction systems may be important to understand the mineral potential and fertility of porphyry deposits.

Measures of fluid-induced enrichments (i.e. Ba/Nb) and of LREE enrichment (i.e. La/Sm) are associated with more alkaline magmas or source regions (Langmuir *et al.* 2006). A progressive increase in Ba/Nb tracked through host sequences to mineralizing intrusions supports the suggestion that fluid-induced enrichment occurred during arc maturation and strongly influenced the observed enrichments (i.e. LILE) (Figs 9g, 10g, 11g, 12a & b). Localized, district and regional scale variations of these observed enrichments (Cadia Intrusive Complex and Northparkes Intrusive Complex) are likely due to sub-arc mantle heterogeneity related to subduction derived fluxes and melts. Different degrees of partial melting, varied residual phases (influenced by bulk composition, i.e. highly potassic magmas delaying

crystallization of amphibole in favour of biotite) and magmatic oxidation state also exerted a strong influence on elemental systematics and likely influenced the fertility of ore forming fluids.

Within the Macquarie Arc, evidence of this process can be inferred. The sequence of Goonumbla–Wombin–Northparkes Intrusive Complex illustrates a clear enrichment and maturation trend over time of a compositional similar sequence (Fig. 9g). A similar trend can be seen in Cadia Intrusive Complex and regional Forest Reefs samples. Basalts within the lowermost Forest Reefs Volcanics, which intercalate with the Weemalla Formation, are distinctly less enriched than the upper Forest Reefs and Cadia Intrusive Complex sequences (Fig. 10g). Similar occurrences are noted within other districts and regions, including volcanics within Trundle, Gidginbung and Yiddah (Rain Hill), and Bodangora (Fig. 11g). An intriguing example includes the Nelungaloo Volcanics basaltic samples. These samples have lower K, lower Th and are distinctly more depleted and MORB-like (lower Nb/Yb, La/Sm and Dy/Yb) than the Nelungaloo shoshonitic andesitic volcanics and Early Ordovician intrusions (Fig. 9). This example suggests a cyclicity of this maturation process and may provide evidence of an older mature arc segment underlying the Northparkes Intrusive Complex and more regional Forbes–Parkes district sequence.

Source components and metallogeny of the Northparkes and Cadia district deposits

Mantle source components and degree of partial melting can be estimated using the diagram of Aldanmaz *et al.* (2000). On this diagram, Macquarie Arc rocks are displaced from the mantle array represented by the spinel–lherzolite melting trend to higher Sm/Yb ratios (Fig. 12d). Data plot between the melting trajectories for an inferred E-MORB source composition drawn for garnet– and spinel–lherzolite. Distribution of data forms three broad groupings. Data from Northparkes and Copper Hill plot between melting trajectories for 50:50 garnet–lherzolite and spinel–lherzolite, and the spinel–lherzolite end-member. Cadia Intrusive Complex, Nelungaloo intrusives and Cheesmans Creek data plot between garnet– and spinel–lherzolite along the 50:50 garnet–lherzolite and spinel–lherzolite melt trajectory. Yiddah (Rain Hill) and Bushman Volcanics data plot between similar trajectories but with lower degrees of partial melting. Mother Shipton Monzodiorite plots on the garnet–lherzolite melt trajectory alongside continental shoshonite examples from the Bingham district and Sunda arc. Greater contributions of the garnet–lherzolite source component between these groupings roughly correspond to decreasing extent of melting, and likely

reflect generation from thickening arc crust and changing conditions as well as extent of melt generation (Langmuir *et al.* 2006; Turner and Langmuir 2015; Guo *et al.* 2020; Niu 2021; Balqis Mazuir and Niu 2023).

A direct comparison between the Cadia and Northparkes intrusive complexes can be made and has implications for the contrasting metal endowments observed in these two porphyry systems. Measures of subduction flux are noticeably enriched in the Cadia Intrusive Complex when compared with Northparkes. Greater contributions of garnet–lherzolite source component, lower extent of melting and the SiO₂ near-saturated more alkaline composition of Cadia samples suggest generation beneath a thicker more developed arc crust. Crustal thickness calculations suggest the thickest crust within any studied districts occurred beneath the Cadia district (Supplementary File 5). Generation of melts below this thickened arc crust changed conditions of melt generation (Turner *et al.* 1996; Langmuir *et al.* 2006; Turner and Langmuir 2015; Guo *et al.* 2020; Niu 2021; Balqis Mazuir and Niu 2023), whereas development of this arc crust potentially led to greater enrichment of source regions.

A fundamental observation by Blevin (2002) about the silica undersaturated composition of Cadia when compared with the Northparkes Intrusive Complex is supported by the suggestion herein of greater contributions of the garnet–lherzolite component to melt generation. The contributions of deeply derived alkaline (?garnet influenced) melts to a subduction modified and enriched lithospheric mantle and lower crust may be significant when assessing fertility and metal endowments.

Chiaradia (2020, 2022) suggests a link between alkaline magmas and the high Au endowment and Au/Cu ratios in deposits such as Bingham and Cadia, whereas Sillitoe (2012) speaks of the importance of primitive mantle contributions to generating deposits. The distinctive geochemistry and metal endowment of the Cadia district deposits suggest a different source and processes to those of the Northparkes Intrusive Complex, despite coeval emplacement. The influence of a garnet–lherzolite source is consistent with the geochemical characteristics of Cadia, whereas proposed links between alkaline magmas and Au endowment (Chiaradia 2020, 2022) might suggest this source directly influenced the fertility of the district.

A general comparative model for the genesis of medium-K and shoshonitic magmas in the Copper Hill and Cadia intrusive complexes

The available geochemical, isotopic and geochronological evidence along with previous detailed studies

of the deposit (e.g. Blevin and Morrison 1997; Holliday *et al.* 2002; Wilson *et al.* 2003, 2007; Forster *et al.* 2004; Harris *et al.* 2020) is synthesized as a general model for the Middle Ordovician medium-K sequences (e.g. Copper Hill) and for Cadia, an early Silurian high-K to shoshonitic intrusive complex in the Molong Volcanic Belt (Fig. 13). The Copper Hill and Cadia intrusive complexes are, respectively, the most K/LILE poor and richly mineralized suites of the pre-syn Benambran Macquarie Arc and formed approximately 20 Ma apart. At Cadia and Goonumbula, Ni and Cr are strongly depleted, whereas Cr, Ni and Pd are relatively less depleted at Copper Hill (Blevin and Morrison 1997; Blevin 2002). The enrichment of Ni, Cr and, to a lesser extent, Sc at Copper Hill, as compared with several other suites such as Cadia, suggests that the Copper Hill Intrusive Complex is compositionally variable, possibly due to heterogeneity of magma sources. Clots of amphibole, pyroxene and opaques texturally reminiscent of symplectites after either olivine or a high-temperature pyroxene support this notion (Blevin and Morrison 1997) (Fig. 13), as does mixing of more and less radiogenic Pb sources (Forster *et al.* 2011).

This model is underpinned by the transition from an ocean arc subduction system to an accretionary terrane absent of any input from mature sediments (as indicated by multiple isotopic systems; Crawford *et al.* 2007b; Kemp *et al.* 2009, 2020; Forster *et al.* 2011, 2015; Huston *et al.* 2016, 2017). We also suggest that this prior subduction event was important in contributing LILE, including the Phase 1 Nelungaloo Volcanics, and may have also been an important event for enrichment of the sub-arc mantle. As a result, heterogeneity of sub-arc mantle sources was likely the primary control on generation of lower-K sequences such as Copper Hill. Cyclic enrichment and maturation trends are observed from Early Ordovician Phase 1 rocks through to the most evolved and enriched Phase 4 mineralized intrusions. Copper Hill and other medium-K sequences appear as exceptions to this trend (Crawford *et al.* 2007b).

The enrichment of the sub-arc mantle in Pt, Pd, Au and Fe during prior partial melting was key for enrichment of Cu and Au during the latest Cambrian–Early Ordovician. Based on recent drilling and geochronological and isotopic evidence, such substrate has proven more widespread than previously recognized (e.g. see Leslie 2021), confirming previous suggestions by Forster *et al.* (2011, 2015) and Kemp *et al.* (2020). Evidence for such a primitive, refractory source component (attributed to the latest Cambrian–Early Ordovician substrate) includes amphibole-olivine–pyroxene cumulates (e.g. symplectites) which contain sequestered Pt and Pd and are observed at Copper Hill (Blevin and Morrison 1997, 2002). Repeated subduction-related melting and the formation of sulfide-rich

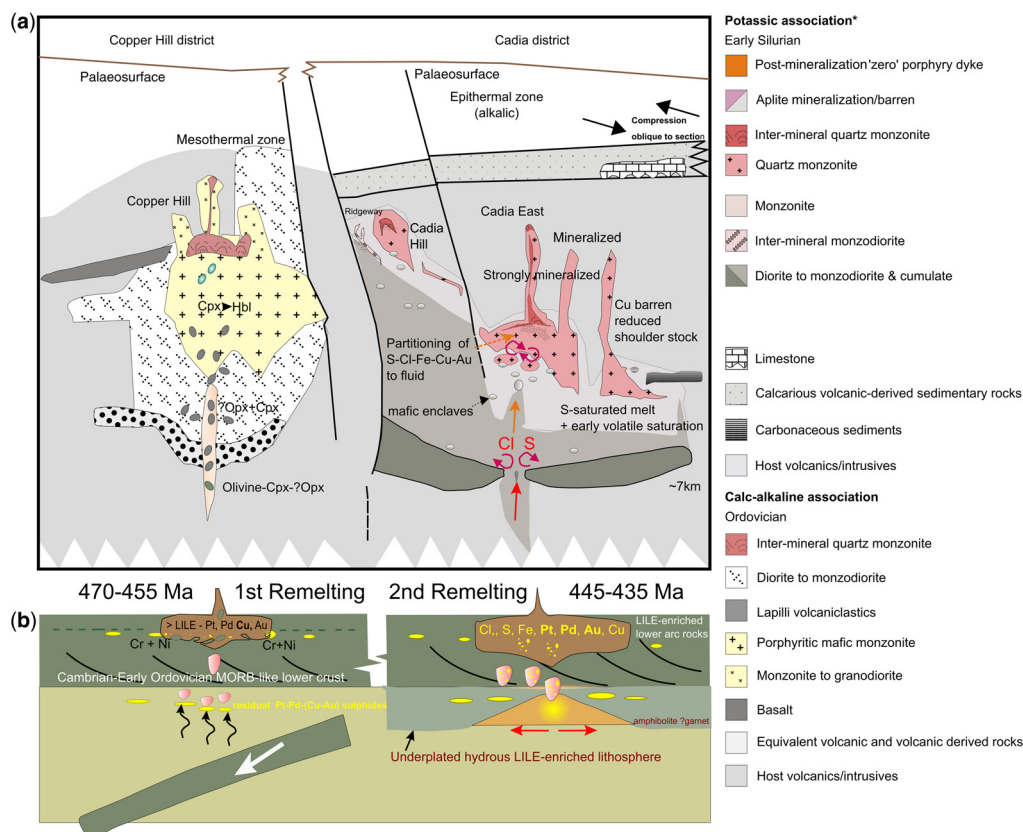


Fig. 13. General genetic model for medium-K to high-K calc-alkaline type Ordovician-aged porphyry deposits within the Molong Volcanic Belt. The diagram has a scale change from the lower crust and upper mantle to mid-upper crust near the brittle–ductile transition where complexes associated with porphyry mineralization assemble (Sillitoe 1973). **(a)** Melting in the Middle Ordovician (prior to emplacement of Copper Hill district) generates residual cumulate which sequester Ni, Cr, Fe, PGEs and Au in sulfides and silicate minerals. Remelting of these cumulates produces a moderately large ion lithophile Elements (LILE), platinum group elements (PGE) and Cu-rich magma which is emplaced in the crust (e.g. Copper Hill Intrusive Complex). Repeated tapping of this source depletes the sub-arc mantle of Ni, Cr and PGE. **(b)** An enriched mafic substrate continues to accrue under the Lachlan Orogen (see text for discussion of this). Later melting of the sub-arc mantle (here referred to as ‘second remelting’) during the earliest Silurian produces Cu–Au-rich magmas (e.g. the Cadia Intrusive Complex) during terrane accretion, and crustal thickening during the Benambran Orogeny. These magmas are more enriched in LILE due to greater ocean island basalt (OIB) magmatic input as well as Cl, S, Fe, Au and Cu with minor Pt and Pd.

cumulates resulted in the enrichment of the sub-arc mantle in Au and platinum group elements (PGEs) (see Hamlyn *et al.* 1985). Nickel, Sc and Fe are typically retained in the mantle within cumulates as solid phases within sulfide and bulk rock silicate minerals e.g. olivine, spinel, orthopyroxene and clinopyroxene (Wilson 1989).

During the Middle Ordovician, the sub-arc mantle, including these cumulates, was then subject to increasing temperature with episodic melt extraction at about approximately ~1100–1200°C at approximately 12–15 Kbar, which produced the parental

magmas for the Copper Hill Intrusive Complex (Supplementary File 5). In this model (Fig. 13a), we propose that Middle Ordovician (470–455 Ma) magmatism at Copper Hill was generated due to subduction-related dehydration melting of the weakly enriched sub-arc mantle beneath layered MORB-like Cambrian crust (Forster *et al.* 2011; Kemp *et al.* 2020). Magmas responsible for fluid exsolution and porphyry mineralization ponded above the brittle–ductile transition at this stage. Copper and Au-bearing sulfides preferentially partitioned into a sulfide-rich liquid during melting and

were an important source for the fertile magmas which produce porphyry mineralization at mid-crustal levels (Holwell *et al.* 2022).

Early Silurian magmas (445–435 Ma) were emplaced within a regionally compressive regime during the Benambran Orogeny (Fig. 13b). Note that the compression is oblique to the 2D section depicted in Fig. 13b. During the intervening period (post 455 Ma – Figure 13) thickening of the crust and lithospheric mantle occurred via continued underplating and evolution at the base of the crust with ongoing subduction prior to the peak compressional event at ~443 Ma (Glen 1998; Glen *et al.* 2007a; Harris *et al.* 2014; Kemp *et al.* 2020). During accretion, intrusions of high-K to shoshonitic affinity of diorite to quartz monzodiorite composition (Blevin 2002), such as those at Cadia, were emplaced. Low-percentage partial melts (compared with the pre-Benambran event) were accommodated by localized tearing and extension of the ductile lower crust (Richards 2009). Evidence for relatively low degree partial melts is evident from the enrichment in LILE and the high Dy/Yb in the Cadia Intrusive Complex, which suggests that rifting facilitated melting of OIB-type mantle (Davidson *et al.* 2013). This melting tapped a deeper, garnet bearing mantle source due to crustal thickening, and generated hydrous, more oxidized, and critically sulfur undersaturated melts which were favourable for mobilizing Au and Cu into the mid-crust.

Parental magmas then ponded in the competent mid-crust and underwent extensive fractional crystallization. The emplacement style of these fluid- and metal-bearing, more fractionated magmas was dependent on the host geology and local-structural regime, including a dyke at Cadia East, a plutonic suite around Cadia Hill and pipe-like intrusions at Ridgeway (Fig. 13b). Generally, the host rocks to these intrusions behaved very competently (Harris *et al.* 2014). Weakly mineralized and barren intrusions are features of the Cadia Intrusive Complex, where mineralization was inhibited by non-ideal fractionation v. fluid exsolution and/or oxidation histories.

In detail, the heterogeneity of mantle and lower-crustal sources may account for the medium-K affinity of Copper Hill and possible variability in enrichment within other suites (e.g. the Goonumbra district). The Copper Hill and Cadia intrusive complexes represent the evolution of a volcanic arc system and provide insight into the transition from an intraoceanic island arc terrane to continental accretion. The transition in orogenic setting is accompanied by thickening crust and significant mafic underplating, which is broadly applicable to the evolution of the Macquarie Arc from at least the Middle Ordovician. Our results strongly suggest that most high-K to shoshonitic rocks within the

Macquarie Arc are analogous to ‘primitive’ shoshonites generated within intraoceanic arc settings (e.g. the Izu–Bonin–Mariana Arc), and further support the role of subduction throughout much of its development.

Conclusion

New and existing geochemistry for potassic rocks of the Macquarie Arc suggests that it was enriched episodically from the Ordovician until the onset of Benambran orogenic collapse. Potassium enriched magmatism also occurred during the Late Silurian to Early Devonian, post accretion onto Gondwana, but should be considered distinct from the Macquarie Arc (*sensu stricto*). The general geochemical character is consistent with primitive high-K calc-alkaline rocks and shoshonites in a rear island arc setting. Most suites of pre- to syn-Benambran age may nonetheless be classified as fundamentally calc-alkaline. We consider the shoshonites in the Macquarie Arc, including notable examples in the Cadia Intrusive Complex, to be analogous to the ‘primitive’ shoshonites observed in other interoceanic arcs. Yiddah (Rain Hill) represents the only mineralized syn-Benambran aged district which can be satisfactorily classified as ‘shoshonitic’ in a typical sense, with geochemical characteristics more like well-described shoshonites in continental arcs and continental settings. Its presence in the southern extent of the Macquarie Arc may provide evidence of previously unrecognized variation in crustal architecture during accretion. Data for suspected post-Benambran suites also notably classify as shoshonitic. New U–Pb zircon ages suggest emplacement occurred post-subduction in a probable rift setting. This is strongly supported by Pb, Sm–Nd and Lu–Hf isotope data.

New geochemical data presented suggest that progressive enrichment of source regions occurred during arc maturation and development. Development and thickening of arc crust potentially led to greater enrichment of source regions but also changed conditions of melt generation. As a result of variation in crustal thickening, some early Silurian magmas within the Macquarie Arc show evidence of a higher degree of deeper garnet–lherzolite derived melts (e.g. Cadia Intrusive Complex), whilst others are dominated by spinel–lherzolite signatures reflecting along and across arc variability. The contributions of deeply derived garnet–lherzolite melts to enriched source regions may have influenced the fertility and metal endowment of mineralized districts.

Middle to Late Ordovician rocks were generated in an oceanic island arc setting during active subduction from a shallow E-MORB mantle reservoir. Critically, whilst the Macquarie Arc evolved, a mafic underplate continued to pool under the Lachlan

Orogen, providing a metal-rich substrate and thickening the crust. Significant porphyry Cu–Au mineralization, subject to modern mining operations, occurred in the early Silurian during accretion of the terrane during the Benambran Orogeny. Based on well-constrained models for the Lachlan Orogen published in the literature and the data from our study, pre- to syn-Benambran mineralized suites are fundamentally calc-alkaline and occurred within an oceanic arc setting synchronous with crustal thickening during terrane accretion.

Acknowledgements Ryan Dwyer, David Forster and Brenainn Simpson publish with the permission of the Chief Geoscientist and Head of the Geological Survey of New South Wales.

Competing interests The authors declare that they have no known competing financial interests or personal relationships that could have appeared to influence the work reported in this paper.

Author contributions RCD: formal analysis (lead); DBF: formal analysis (supporting), writing – original draft (supporting); BPS: writing – review & editing (lead); PLB: conceptualization (supporting), project administration (lead); HH: data curation (lead), investigation (supporting).

Funding New data presented in this chapter were funded by the Geological Survey of New South Wales.

Data availability All data generated or analysed during this study are included in this published article (and, if present, its supplementary information files).

References

- Aldanmaz, E., Pearce, J.A., Thirlwall, M.F. and Mitchell, J.G. 2000. Petrogenetic evolution of late Cenozoic, post-collision volcanism in western Anatolia, Turkey. *Journal of Volcanology and Geothermal Research*, **102**, 67–95, [https://doi.org/10.1016/S0377-0273\(00\)00182-7](https://doi.org/10.1016/S0377-0273(00)00182-7)
- Alkane Resources 2019. *ASX and Media Release: Discovery of Significant Porphyry Gold–Copper Mineralisation at Boda Prospect within Northern Molong Porphyry Project* NSW. Alkane Resources.
- Alkane Resources 2020. *ASX and Media Release: Significant High-Grade Gold–Copper Mineralisation Intersected at Boda*. Alkane Resources.
- Alkane Resources 2021. *ASX and Media Release: High Grade Continuity Northwest of Boda*. Alkane Resources.
- Amaral, J., Mata, J. and Santos, J.F. 2022. The Carboniferous shoshonitic (s.l.) gabbro–monzonitic stocks of Veiros and Vale de Maceira, Ossa-Morena Zone (SW Iberian Massif): evidence for diverse subduction-related lithospheric metasomatism. *Geochemistry*, **82**, article 125917, <https://doi.org/10.1016/j.chemer.2022.125917>
- Arundell, M.C. 1998. *The Geology and Mineralisation of the E31 Copper–Gold Prospect*. Master's thesis, University of Tasmania.
- Balqis Mazuir, R.A. and Niu, Y. 2023. Global volcanic arc magma composition correlates with thickness of both arc crust (Moho depth) and arc lithosphere (LAB depth): a revealing message on arc basement histories and arc magmatism. *Geoscience Frontiers*, **14**, article 101609, <https://doi.org/10.1016/j.gsf.2023.101609>
- Barron, L.M., Meffre, S. and Glen, R.A. 2007. Arc and mantle detritus in the post-collisional, Lower Silurian Kabadah Formation, Lachlan Orogen, New South Wales. *Australian Journal of Earth Sciences*, **54**, 353–362, <https://doi.org/10.1080/08120090701221698>
- Becker, H., Jochum, K.P. and Carlson, R.W. 2000. Trace element fractionation during dehydration of eclogites from high-pressure terranes and the implications for element fluxes in subduction zones. *Chemical Geology*, **163**, 65–99, [https://doi.org/10.1016/S0009-2541\(99\)00071-6](https://doi.org/10.1016/S0009-2541(99)00071-6)
- Bello, M., Cornwell, D.G., Rawlinson, N., Reading, A.M. and Likkason, O.K. 2021. Crustal structure of southeast Australia from teleseismic receiver functions. *Solid Earth*, **12**, 463–481, <https://doi.org/10.5194/se-12-463-2021>
- Blevin, P.L. 1998. A re-evaluation of mineralized Ordovician intrusives in the Lachlan Fold Belt: implications for tectonic and metallogenic models. *Geological Society of Australia Abstracts*, **49**, 43.
- Blevin, P.L. 2002. The petrographic and compositional character of variably K-enriched magmatic suites associated with Ordovician porphyry Cu–Au mineralisation in the Lachlan Fold Belt, Australia. *Mineralium Deposita*, **37**, 87–99, <https://doi.org/10.1007/s00126-001-0232-9>
- Blevin, P.L. and Morrison, G. 1997. *Magmatic and Hydrothermal Evolution of Major Intrusive Related Gold Deposits in Eastern Australia, P425 – Final Report*. Australian Mineral Industries Research Association Limited (AMIRA), Melbourne, unpublished.
- Blevin, P.L., Forster, D.B. and Downes, P.M. 2020. *A Mineral System Model for Porphyry Cu–Au Mineralisation in the Macquarie Arc, Eastern Lachlan Orogen, New South Wales*. Geological Survey of New South Wales Report **GS2019/0591**.
- Bryant, C.J., Arculus, R.J. and Eggins, S.M. 2003. The geochemical evolution of the Izu–Bonin arc system: a perspective from tephra recovered by deep-sea drilling. *Geochemistry, Geophysics, Geosystems*, **4**, article 2002GC000427, <https://doi.org/10.1029/2002GC000427>
- Burnham, C.W. and Ohmoto, H. 1980. Late-stage processes of felsic magmatism. *Mining Geology, Special Issue*, **8**, 1–11.
- Butera, K.M., Williams, I.S., Blevin, P.L. and Simpson, C.J. 2001. Zircon U–Pb dating of Early Palaeozoic monzonitic intrusives from the Goonumbla area, New South Wales. *Australian Journal of Earth Sciences*, **48**, 457–464, <https://doi.org/10.1046/j.1440-0952.2001.00870.x>

- Campbell, I.H., Stepanov, A.S., Liang, H.-Y., Allen, C.M., Norman, M.D., Zhang, Y.-Q. and Xie, Y.-W. 2014. The origin of shoshonites: new insights from the Tertiary high-potassium intrusions of eastern Tibet. *Contributions to Mineralogy and Petrology*, **167**, article 983, <https://doi.org/10.1007/s00410-014-0983-9>
- Carr, G.R., Dean, J.A., Suppel, D.W. and Heithersay, P.S. 1995. Precise lead isotope fingerprinting of hydrothermal activity associated with Ordovician to Carboniferous metallogenic events in the Lachlan fold belt of New South Wales. *Economic Geology*, **90**, 1467–1505, <https://doi.org/10.2113/gsecongeo.90.6.1467>
- Carroll, M.R. and Rutherford, M.J. 1987. The stability of igneous anhydrite: experimental results and implications for sulfur behavior in the 1982 El Chichon trachyandesite and other evolved magmas. *Journal of Petrology*, **28**, 781–801, <https://doi.org/10.1093/petrology/28.5.781>
- Chhun, E. 2004. *Ordovician Igneous Rocks of the Central Lachlan Fold Belt: Geochemical Signatures of Ore-Related Magmas*. The University of Sydney.
- Chiaradia, M. 2020. Gold endowments of porphyry deposits controlled by precipitation efficiency. *Nature Communications*, **11**, article 248, <https://doi.org/10.1038/s41467-019-14113-1>
- Chiaradia, M. 2022. Distinct magma evolution processes control the formation of porphyry Cu–Au deposits in thin and thick arcs. *Earth and Planetary Science Letters*, **599**, article 117864, <https://doi.org/10.1016/j.epsl.2022.117864>
- Chivas, A.R. and Nutter, A.H. 1975. Copper Hill porphyry copper prospect. *Australian Institute of Mining and Metallurgy Monograph*, **14**, 716–720.
- Clarke, R., Smith, D. and Naden, J. 2022. Source controls on mineralisation: regional geology and magmatic evolution of Fiji. *Lithos*, 432–433, article 106897, <https://doi.org/10.1016/j.lithos.2022.106897>
- Collins, W.J. 1994. Upper- and middle-crustal response to delamination: an example from the Lachlan fold belt, eastern Australia. *Geology*, **22**, 143–146, [https://doi.org/10.1130/0091-7613\(1994\)022<0143:UAMCRT>2.3.CO;2](https://doi.org/10.1130/0091-7613(1994)022<0143:UAMCRT>2.3.CO;2)
- Colquhoun, G.P., Hughes, K.S. *et al.* 2024. New South Wales (NSW) Seamless Geology Version 2.4. Geological Survey of New South Wales, Maitland, <https://search.geoscience.nsw.gov.au/product/9232>
- Cooke, D.R., Hollings, P. and Walshe, J.L. 2005. Giant porphyry deposits: characteristics, distribution, and tectonic controls. *Economic Geology*, **100**, 801–818, <https://doi.org/10.2113/gsecongeo.100.5.801>
- Cooke, D.R., Wilson, A.J., House, M.J., Wolfe, R.C., Walshe, J.L., Lickfold, V. and Crawford, A.J. 2007. Alkalic porphyry Au–Cu and associated mineral deposits of the Ordovician to early Silurian Macquarie Arc, New South Wales. *Australian Journal of Earth Sciences*, **54**, 445–463, <https://doi.org/10.1080/08120090601146771>
- Cox, K.G. 1980. A model for flood basalt volcanism. *Journal of Petrology*, **21**, 629–650, <https://doi.org/10.1093/petrology/21.4.629>
- Crawford, A.J., Glen, R.A., Cooke, D.R. and Percival, I.G. 2007a. Geological evolution and metallogenesis of the Ordovician Macquarie Arc, Lachlan Orogen, New South Wales. *Australian Journal of Earth Sciences*, **54**, 137–141, <https://doi.org/10.1080/08120090701221615>
- Crawford, A.J., Meffre, S., Squire, R.J., Barron, L.M. and Falloon, T.J. 2007b. Middle and Late Ordovician magmatic evolution of the Macquarie Arc, Lachlan Orogen, New South Wales. *Australian Journal of Earth Sciences*, **54**, 181–214, <https://doi.org/10.1080/08120090701227471>
- Crawford, A.J., Cooke, D.R. and Fanning, C.M. 2007c. Geochemistry and age of magmatic rocks in the unexposed Narromine, Cowal and Fairholme igneous complexes in the Ordovician Macquarie Arc, New South Wales. *Australian Journal of Earth Sciences*, **54**, 243–271, <https://doi.org/10.1080/08120090701221714>
- Cronin, D.E., Kitto, J., Mowat, B., Munro, S. and Scott, M.M. 2017. Temora copper–gold deposits. *Australian Institute of Mining and Metallurgy Monograph*, **32**, 771–774.
- Cyprus Amax Australia Corporation 1998. *Annual Report for the Year Ended 22 August 1998*. Geological Survey of New South Wales Report **GS1999/297**.
- Davidson, J., Turner, S. and Plank, T. 2013. Dy/Dy*: variations arising from mantle sources and petrogenetic processes. *Journal of Petrology*, **54**, 525–537, <https://doi.org/10.1093/petrology/egs076>
- Downes, P.M., McEvilly, R. and Raphael, N. 2004. Mineral deposits and models, Cootamundra 1:250 000 map sheet area. *Geological Survey of New South Wales Quarterly Notes*, **116**, 1–37.
- Edwards, C.M.H., Menzies, M.A., Thirlwall, M.F., Morris, J.D., Leeman, W.P. and Harmon, R.S. 1994. The transition to potassic alkaline volcanism in island arcs: the Ringgit–Besar Complex, East Java, Indonesia. *Journal of Petrology*, **35**, 1557–1595, <https://doi.org/10.1093/petrology/35.6.1557>
- Elliott, T. 2003. Tracers of the slab. *AGU Geophysical Monograph*, **138**, 23–46, <https://doi.org/10.1029/138GM03>
- Fergusson, C.L. 2009. Tectonic evolution of the Ordovician Macquarie Arc, central New South Wales: arguments for subduction polarity and anticlockwise rotation. *Australian Journal of Earth Sciences*, **56**, 179–193, <https://doi.org/10.1080/08120090802547017>
- Fergusson, C.L. 2014. Late Ordovician to mid-Silurian Benambran subduction zones in the Lachlan Orogen, southeastern Australia. *Australian Journal of Earth Sciences*, **61**, 587–606, <https://doi.org/10.1080/08120099.2014.903858>
- Forster, D.B. 2009. Pathways between skarns and porphyry deposits – a NSW perspective. Presented at Exploration in the House, June 2009.
- Forster, D.B. and Maas, R. 2015. *New Lead Isotope Data for the Macquarie Arc*. **GS2015/0994**.
- Forster, D.B., Seccombe, P.K. and Phillips, D. 2004. Controls on skarn mineralization and alteration at the Cadia deposits, New South Wales, Australia. *Economic Geology*, **99**, 761–788, <https://doi.org/10.2113/gsecongeo.99.4.761>
- Forster, D.B., Carr, G.R. and Downes, P.M. 2011. Lead isotope systematics of ore systems of the Macquarie Arc –

- implications for arc substrate. *Gondwana Research*, **19**, 686–705, <https://doi.org/10.1016/j.gr.2010.11.010>
- Forster, D.B., McInnes, P., Downes, P.M., Maas, R., Norman, R. and Blevin, P.L. 2015. New lead and isotopic and geochronologic constraints on mineralisation in the Macquarie Arc – insights from the Lake Cowal district, New South Wales. *Geological Survey of New South Wales Quarterly Notes*, **144**, 1–23.
- Fox, N., Cooke, D.R., Harris, A.C., Collett, D. and Eastwood, G. 2015. Porphyry Au–Cu mineralization controlled by reactivation of an arc-transverse volcanosedimentary subbasin. *Geology*, **43**, 811–814, <https://doi.org/10.1130/G36992.1>
- Gale, A., Dalton, C.A., Langmuir, C.H., Su, Y. and Schilling, J. 2013. The mean composition of ocean ridge basalts. *Geochemistry, Geophysics, Geosystems*, **14**, 489–518, <https://doi.org/10.1029/2012GC004334>
- Geoscience Australia 2024. Geoscience Australia Portal, <https://portal.ga.gov.au/> [last accessed 29 July 2024].
- Geological Survey of NSW 2024. NSW Whole Rock Geochemistry Samples, <https://meg.resourcesregulator.nsw.gov.au/geological-survey/products-and-data/geoscience-data-resources>
- Glen, R. 1998. Tectonic development of the Lachlan Orogen: a framework for mineral exploration. In: Lewis, P.C. (ed.) *Lachlan Fold Belt Conference '98*. Australian Institute of Geoscientists, 1–6.
- Glen, R.A. 2005. The Tasmanides of eastern Australia. *Geological Society, London, Special Publications*, **246**, 23–96, <https://doi.org/10.1144/GSL.SP.2005.246.01.02>
- Glen, R.A. 2013. Refining accretionary orogen models for the Tasmanides of eastern Australia. *Australian Journal of Earth Sciences*, **60**, 315–370, <https://doi.org/10.1080/08120099.2013.772537>
- Glen, R.A. and Blevin, P. 2019. *Porphyry and Vein Copper–Gold Deposits in the Ordovician Macquarie Volcanic Province, Lachlan Orogen: Mineralization in an Arc or a Rift? Mineral Systems of the Pacific Rim Congress 2019: Field Trip FT4 29 March–2 April 2019*. Geological Survey of New South Wales Report **GS 2019/0306**.
- Glen, R.A., Walshe, J.L., Barron, L.M. and Watkins, J.J. 1998. Ordovician convergent-margin volcanism and tectonism in the Lachlan sector of east Gondwana. *Geology*, **26**, 751–754, [https://doi.org/10.1130/0091-7613\(1998\)026<0751:OCMVAT>2.3.CO;2](https://doi.org/10.1130/0091-7613(1998)026<0751:OCMVAT>2.3.CO;2)
- Glen, R.A., Korsch, R.J. *et al.* 2002. Crustal structure of the Ordovician Macquarie Arc, Eastern Lachlan Orogen, based on seismic-reflection profiling. *Australian Journal of Earth Sciences*, **49**, 323–348, <https://doi.org/10.1046/j.1440-0952.2002.00925.x>
- Glen, R.A., Crawford, A.J., Percival, I.G. and Barron, L.M. 2007a. Early Ordovician development of the Macquarie Arc, Lachlan Orogen, New South Wales. *Australian Journal of Earth Sciences*, **54**, 167–179, <https://doi.org/10.1080/08120090601146797>
- Glen, R.A., Spencer, R., Willmore, A., David, V. and Scott, R.J. 2007b. June–Narromine Volcanic Belt, Macquarie Arc, Lachlan Orogen, New South Wales: components and structure. *Australian Journal of Earth Sciences*, **54**, 215–241, <https://doi.org/10.1080/08120090601146805>
- Glen, R.A., Meffre, S. and Scott, R.J. 2007c. Benambran Orogeny in the Eastern Lachlan Orogen, Australia. *Australian Journal of Earth Sciences*, **54**, 385–415, <https://doi.org/10.1080/08120090601147019>
- Glen, R.A., Crawford, A.J. and Cooke, D.R. 2007d. Tectonic setting of porphyry Cu–Au mineralisation in the Ordovician–early Silurian Macquarie Arc, Eastern Lachlan Orogen, New South Wales. *Australian Journal of Earth Sciences*, **54**, 465–479, <https://doi.org/10.1080/08120090701221672>
- Glen, R., Quinn, C. and Xiao, W. 2011a. Island arcs: their role in growth of accretionary orogens and mineral endowment. *Gondwana Research*, **19**, 567–570, <https://doi.org/10.1016/j.gr.2011.01.001>
- Glen, R.A., Saeed, A., Quinn, C.D. and Griffin, W.L. 2011b. U–Pb and Hf isotope data from zircons in the Macquarie Arc, Lachlan Orogen: implications for arc evolution and Ordovician palaeogeography along part of the east Gondwana margin. *Gondwana Research*, **19**, 670–685, <https://doi.org/10.1016/j.gr.2010.11.011>
- Glen, R.A., Quinn, C.D. and Cooke, D.R. 2012. The Macquarie Arc, Lachlan Orogen, New South Wales: its evolution, tectonic setting and mineral deposits. *Episodes*, **35**, 177–186, <https://doi.org/10.18814/epiugs/2012/v35i1/017>
- Goesch, E. 2011. *Petrology, Geochemistry, U–Pb Zircon Ages and Structure of the Yiddah Porphyry Cu–Au–Mo Prospect of the Late Macquarie Arc, NSW*. Bachelor of Science (Honours) thesis, University of Wollongong.
- Gradstein, F.M., Ogg, J.G. and Hilgen, F.J. 2012. On the Geologic Time Scale. *Newsletters on Stratigraphy*, **45**, 171–188, <https://doi.org/10.1127/0078-0421/2012/0020>
- Gray, N., Mandyczewsky, A. and Hine, R. 1995. Geology of the zoned gold skarn system at Junction Reefs, New South Wales. *Economic Geology*, **90**, 1533–1552, <https://doi.org/10.2113/gsecongeo.90.6.1533>
- Greenfield, J.E., Wang, Y. *et al.* 2022. *Ordovician Cu–Au Porphyry and Silurian Gold/Base Metal Mineral Deposits of the Eastern Lachlan Orogen: Discoveries in the Tasmanides 2022 Field Trip Guide*. Geological Survey of NSW Report **GS2021/1732**.
- Grondahl, C. and Zajacz, Z. 2017. Magmatic controls on the genesis of porphyry Cu–Mo–Au deposits: the Bingham Canyon example. *Earth and Planetary Science Letters*, **480**, 53–65, <https://doi.org/10.1016/j.epsl.2017.09.036>
- Groome, M., Tosdal, R.M., Harris, A.C. and Percival, I.G. 2021. Preservation of the Cadia Valley porphyry Au–Cu district, NSW, Australia: Silurian basin formation and subsequent inversion. *Australian Journal of Earth Sciences*, **68**, 799–817, <https://doi.org/10.1080/08120099.2021.1876165>
- Guo, P., Niu, Y., Sun, P., Gong, H. and Wang, X. 2020. Lithosphere thickness controls continental basalt compositions: an illustration using Cenozoic basalts from eastern China. *Geology*, **48**, 128–133, <https://doi.org/10.1130/G46710.1>
- Hamlyn, P.R., Keays, R.R., Cameron, W.E., Crawford, A.J. and Waldron, H.M. 1985. Precious metals in magnesian low-Ti lavas: implications for metallogenesis and sulfur saturation in primary magmas. *Geochimica et*

- Cosmochimica Acta*, **49**, 1797–1811, [https://doi.org/10.1016/0016-7037\(85\)90150-4](https://doi.org/10.1016/0016-7037(85)90150-4)
- Hao, H., Campbell, I.H., Park, J.-W. and Cooke, D.R. 2017. Platinum-group element geochemistry used to determine Cu and Au fertility in the Northparkes igneous suites, New South Wales, Australia. *Geochimica et Cosmochimica Acta*, **216**, 372–392, <https://doi.org/10.1016/j.gca.2017.05.009>
- Hao, H., Campbell, I.H., Cooke, D.R., Nakamura, E. and Sakaguchi, C. 2021. Geochronology, petrogenesis and oxidation state of the Northparkes Igneous Suite, New South Wales, Australia: implications for magma fertility. *Economic Geology*, **116**, 1161–1187, <https://doi.org/10.5382/econgeo.4825>
- Harris, A.C. and Golding, S.D. 2002. New evidence of magmatic-fluid-related phyllic alteration: implications for the genesis of porphyry Cu deposits. *Geology*, **30**, 335–338, [https://doi.org/10.1130/0091-7613\(2002\)030<0335:NEOMFR>2.0.CO;2](https://doi.org/10.1130/0091-7613(2002)030<0335:NEOMFR>2.0.CO;2)
- Harris, A.C., Percival, I.G. *et al.* 2014. Marine volcanosedimentary basins hosting porphyry Au–Cu deposits, Cadia Valley, New South Wales, Australia. *Economic Geology*, **109**, 1117–1135, <https://doi.org/10.2113/econgeo.109.4.1117>
- Harris, A.C., Cooke, D.R. *et al.* 2020. Geologic evolution of Late Ordovician to early Silurian alkalic porphyry Au–Cu deposits at Cadia, New South Wales, Australia. *Society of Economic Geologists Special Publication*, **23**, <https://doi.org/10.5382/SP.23.30>
- Hastie, A.R., Kerr, A.C., Pearce, J.A. and Mitchell, S.F. 2007. Classification of altered volcanic island arc rocks using immobile trace elements: development of the Th–Co discrimination diagram. *Journal of Petrology*, **48**, 2341–2357, <https://doi.org/10.1093/petrology/egm062>
- Heathersay, P.S. 1986. Endeavour 26 North copper–gold deposit, Goonumbra, N.S.W. – paragenesis and alteration zonation. In: Berkman, D.A. (ed.) CMMI congress, geology and exploration, 11–16 May, Singapore, **2**, 181–189, AusIMM Monograph.
- Heathersay, P.S. and Walshe, J.L. 1995. Endeavour 26 North; a porphyry copper–gold deposit in the Late Ordovician, shoshonitic Goonumbra Volcanic Complex, New South Wales, Australia. *Economic Geology*, **90**, 1506–1532, <https://doi.org/10.2113/gsecongeo.90.6.1506>
- Heathersay, P.S., O'Neill, W.J., van der Helder, P., Moore, C.R. and Harbon, P.G. 1990. Goonumbra porphyry copper district: Endeavour 26 North, Endeavour 22 and Endeavour 27 copper–gold deposits. *Australasian Institute of Mining and Metallurgy Monograph*, **14**, 1385–1398.
- Holliday, J., Wilson, A., Blevin, P., Tedder, I., Dunham, P. and Pfitzner, M. 2002. Porphyry gold–copper mineralisation in the Cadia district, eastern Lachlan Fold Belt, New South Wales, and its relationship to shoshonitic magmatism. *Mineralium Deposita*, **37**, 100–116, <https://doi.org/10.1007/s00126-001-0233-8>
- Hollings, P., Cooke, D.R., Waters, P.J. and Cousens, B. 2011. Igneous geochemistry of mineralized rocks of the Baguio district, Philippines: implications for tectonic evolution and the genesis of porphyry-style mineralization. *Economic Geology*, **106**, 1317–1333, <https://doi.org/10.2113/econgeo.106.8.1317>
- Holwell, D.A., Fiorentini, M.L. *et al.* 2022. Mobilisation of deep crustal sulfide melts as a first order control on upper lithospheric metallogeny. *Nature Communications*, **13**, article 573, <https://doi.org/10.1038/s41467-022-28275-y>
- Hooper, B., Heathersay, P.S., Mills, M.B., Lindhorst, J.W. and Freyberg, J. 1996. Shoshonite-hosted Endeavour 48 porphyry copper–gold deposit, Northparkes, central New South Wales. *Australian Journal of Earth Sciences*, **43**, 279–288, <https://doi.org/10.1080/08120099608728255>
- Huston, D.L., Champion, D.C. *et al.* 2016. Metallogenesis and geodynamics of the Lachlan Orogen: new (and old) insights from spatial and temporal variations in lead isotopes. *Ore Geology Reviews*, **76**, 257–267, <https://doi.org/10.1016/j.oregeorev.2015.07.005>
- Huston, D.L., Champion, D.C. *et al.* 2017. *Spatial Variations in Lead Isotopes, Tasman Element, Eastern Australia*. Geoscience Australia Record **2017/19**.
- Ishihara, S. 1977. The magnetite-series and ilmenite-series granitic rocks. *Mining Geology*, **27**, 293–305, <https://doi.org/10.11456/shigenchishitsu1951.27.293>
- Ishizuka, O., Taylor, R.N., Yuasa, M., Milton, J.A., Nesbitt, R.W., Uto, K. and Sakamoto, I. 2007. Processes controlling along-arc isotopic variation of the southern Izu–Bonin arc. *Geochemistry, Geophysics, Geosystems*, **8**, article 2006GC001475, <https://doi.org/10.1029/2006GC001475>
- Ishizuka, O., Yuasa, M. *et al.* 2010. Migrating shoshonitic magmatism tracks Izu–Bonin–Mariana intra-oceanic arc rift propagation. *Earth and Planetary Science Letters*, **294**, 111–122, <https://doi.org/10.1016/j.epsl.2010.03.016>
- Jamali, H. and Mehrabi, B. 2015. Relationships between arc maturity and Cu–Mo–Au porphyry and related epithermal mineralization at the Cenozoic Arasbaran magmatic belt. *Ore Geology Reviews*, **65**, 487–501, <https://doi.org/10.1016/j.oregeorev.2014.06.017>
- Johnson, K., Marsaglia, K.M. *et al.* 2021. Intra-oceanic submarine arc evolution recorded in an ~1-km-thick rear-arc succession of distal volcanoclastic lobe deposits. *Geosphere*, **17**, 957–980, <https://doi.org/10.1130/GES02321.1>
- Jones, G.J. 1985. The Goonumbra porphyry copper deposits, New South Wales. *Economic Geology*, **80**, 591–613, <https://doi.org/10.2113/gsecongeo.80.3.591>
- Jones, S.L., Bodorkos, S., Eastlate, M.A., Campbell, L.M., Hughes, K., Blevin, P.L. and Fitzherbert, J.A. 2023. *New SHRIMP U–Pb Zircon Ages from the Lachlan Orogen, NSW: Dubbo, Forbes and East Riverina Areas, July 2020–June 2021*. Geoscience Australia Report **GS2023/0017**, <https://doi.org/10.26186/147971>
- Kemp, A.I.S., Hawkesworth, C.J., Collins, W.J., Gray, C.M. and Blevin, P.L. 2009. Isotopic evidence for rapid continental growth in an extensional accretionary orogen: the Tasmanides, eastern Australia. *Earth and Planetary Science Letters*, **284**, 455–466, <https://doi.org/10.1016/j.epsl.2009.05.011>
- Kemp, A.I.S., Blevin, P.L. and Norman, M.D. 2020. A SIMS U–Pb (zircon) and Re–Os (molybdenite) isotope study of the early Paleozoic Macquarie Arc, southeastern Australia: implications for the tectono-magmatic evolution of the paleo-Pacific Gondwana margin.

- Gondwana Research*, **82**, 73–96, <https://doi.org/10.1016/j.gr.2019.12.015>
- Kincora Copper Ltd 2020. Kincora Provides Update on Expanded Drilling Program at Trundle. Kincora Copper Ltd, <https://kincoracopper.com/kincora-provides-update-on-expanded-drilling-program-at-trundle/> [last accessed 3 June 2024].
- Kirchenbaur, M., Schuth, S. *et al.* 2022. Sub-arc mantle enrichment in the Sunda rear-arc inferred from HFSE systematics in high-K lavas from Java. *Contributions to Mineralogy and Petrology*, **177**, article 8, <https://doi.org/10.1007/s00410-021-01871-9>
- Krmíček, L. and Chalapatthi Rao, N.V. 2022. Lamprophyres, lamproites and related rocks as tracers to supercontinent cycles and metallogenesis. *Geological Society, London, Special Publications*, **513**, 1–16, <https://doi.org/10.1144/SP513-2021-159>
- Krynan, J.P., Sherwin, L. and Clarke, I. 1990. Stratigraphy and structure. *Geological Survey of New South Wales Records*, **23**, 1–189.
- Langmuir, C.H., Bézoz, A., Escrig, S. and Parman, S.W. 2006. Chemical systematics and hydrous melting of the mantle in back-arc basins. *AGU Geophysical Monograph*, **166**, 87–146, <https://doi.org/10.1029/166GM07>
- Lawrie, K.C., Mernagh, T.P., Ryan, C.G., Achterbergh, E.V. and Black, L.P. 2007. Chemical fingerprinting of hydrothermal zircons: an example from the Gidginbung high sulphidation Au–Ag–(Cu) deposit, New South Wales, Australia. *Proceedings of the Geologists' Association*, **118**, 37–46, [https://doi.org/10.1016/S0016-7878\(07\)80045-9](https://doi.org/10.1016/S0016-7878(07)80045-9)
- Leitch, C.H. and Lentz, D.R. 1994. The Gresens approach to mass balance constraints of alteration systems: methods, pitfalls, examples. *Geological Association of Canada Short Course Notes*, **11**, 161–192.
- Le Maitre, R.W., Bateman, P. *et al.* 1989. *A classification of igneous rocks and glossary of terms*. Recommendation of the IUGS Subcommission on the Systematics of Igneous Rocks. Blackwell, Oxford.
- Leslie, C.D. 2021. *Metallogeny of the Cowal district, New South Wales, Australia*. PhD thesis, University of Tasmania.
- Leslie, R.A.J., Danyushevsky, L.V., Crawford, A.J. and Verbeeten, A.C. 2009. Primitive shoshonites from Fiji: geochemistry and source components. *Geochemistry, Geophysics, Geosystems*, **10**, article 2008GC002326, <https://doi.org/10.1029/2008GC002326>
- Li, X.-H., Li, Z.-X., Li, W.-X., Wang, X.-C. and Gao, Y. 2013. Revisiting the 'C-type adakites' of the Lower Yangtze River Belt, central eastern China: *in-situ* zircon Hf–O isotope and geochemical constraints. *Chemical Geology*, **345**, 1–15, <https://doi.org/10.1016/j.chemgeo.2013.02.024>
- Lickfold, V. 2002. *Intrusive History and Volatile Evolution of the Endeavour Porphyry Cu–Au Deposits, Goonumbla District*. PhD thesis, University of Tasmania.
- Lickfold, V., Cooke, D.R., Smith, S.G. and Ullrich, T.D. 2003. Endeavour copper–gold porphyry deposits, Northparkes, New South Wales: intrusive history and fluid evolution. *Economic Geology*, **98**, 1607–1636, <https://doi.org/10.2113/gsecongeo.98.8.1607>
- Lickfold, V., Cooke, D.R., Crawford, A.J. and Fanning, C.M. 2007. Shoshonitic magmatism and the formation of the Northparkes porphyry Cu–Au deposits, New South Wales. *Australian Journal of Earth Sciences*, **54**, 417–444, <https://doi.org/10.1080/08120090601175754>
- Loucks, R.R. 2014. Distinctive composition of copper–ore-forming arc magmas. *Australian Journal of Earth Sciences*, **61**, 5–16, <https://doi.org/10.1080/08120099.2013.865676>
- Lowczak, J.N., Campbell, I.H., Cocker, H., Park, J.-W. and Cooke, D.R. 2018. Platinum-group element geochemistry of the Forest Reef Volcanics, southeastern Australia: implications for porphyry Au–Cu mineralisation. *Geochimica et Cosmochimica Acta*, **220**, 385–406, <https://doi.org/10.1016/j.gca.2017.09.052>
- MacKenzie 1993. *The Geology of the Comobella Prospect near Wellington, New South Wales*. Honours thesis, University of New South Wales.
- Madeisky, H.E. and Stanley, C.R. 1993. Identifying metasomatic zones associated with volcanic-hosted massive sulphide deposits using Pearce element ratio analysis. *The Gangue. GAC – Mineral Deposits Division Newsletter*, **41**, 5–7.
- Mandyczewsky, A., Gray, N. and Hine, R. 1991. Junction Reefs gold deposits. *Geological Society of Australia – Abstracts*, **29**, 35.
- Mason, D.R. 2014. *Petrographic Descriptions for Rock Samples from Racecourse and Footrot Prospects Bushranger Project, New South Wales. Appendix V*. Annual report for Bushranger-EL5574 for the period 4th June 2013–2014. Geological Survey of New South Wales Records **GS2014/0962**.
- Maughan, D., Keith, J., Christiansen, E., Pulsipher, T., Hattori, K. and Evans, N. 2002. Contributions from mafic alkaline magmas to the Bingham porphyry Cu–Au–Mo deposit, Utah, USA. *Mineralium Deposita*, **37**, 14–37, <https://doi.org/10.1007/s00126-001-0228-5>
- McDonough, W.F. and Sun, S.-S. 1995. The composition of the Earth. *Chemical Geology*, **120**, 223–253, [https://doi.org/10.1016/0009-2541\(94\)00140-4](https://doi.org/10.1016/0009-2541(94)00140-4)
- Meffre, S., Scott, R.J., Glen, R.A. and Squire, R.J. 2007. Re-evaluation of contact relationships between Ordovician volcanic belts and the quartz-rich turbidites of the Lachlan Orogen. *Australian Journal of Earth Sciences*, **54**, 363–383, <https://doi.org/10.1080/08120090701221680>
- Meinert, L.D. 1992. Skarns and skarn deposits. *Geoscience Canada*, **19**.
- Meinert, L.D. 1995. Compositional variation of igneous rocks associated with skarn deposits – chemical evidence for a genetic connection between petrogenesis and mineralisation. *Mineralogical Society of Canada Short Course Series*, **23**, 401–418.
- Middlemost, E.A.K. 1994. Naming materials in the magma/igneous rock system. *Earth-Science Reviews*, **37**, 215–224, [https://doi.org/10.1016/0012-8252\(94\)90029-9](https://doi.org/10.1016/0012-8252(94)90029-9)
- Morrison, G.W. 1980. Characteristics and tectonic setting of the shoshonite rock association. *Lithos*, **13**, 97–108, [https://doi.org/10.1016/0024-4937\(80\)90067-5](https://doi.org/10.1016/0024-4937(80)90067-5)
- Müller, D. 2002. Gold–copper mineralization in alkaline rocks. *Mineralium Deposita*, **37**, 1–3, <https://doi.org/10.1007/s00126-001-0226-7>
- Müller, D. and Groves, D.I. 2019. *Potassic Igneous Rocks and Associated Gold–Copper Mineralization*. Springer, <https://doi.org/10.1007/978-3-319-92979-8>

- Müller, D., Groves, D.I. and Heathersay, P.S. 1994. The shoshonite porphyry Cu–Au association in the Goonumbra district, NSW, Australia. *Mineralogy and Petrology*, **51**, 299–321, <https://doi.org/10.1007/BF01159734>
- Mungall, J.E. 2002. Roasting the mantle: slab melting and the genesis of major Au and Au-rich Cu deposits. *Geology*, **30**, 915–918, [https://doi.org/10.1130/0091-7613\(2002\)030<0915:RTMSMA>2.0.CO;2](https://doi.org/10.1130/0091-7613(2002)030<0915:RTMSMA>2.0.CO;2)
- Musgrave, R.J. 2022. Structure of an accreted intra-oceanic arc: potential-field model of a crustal cross-section through the Macquarie Arc, Lachlan Orogen, southeastern Australia. *Australian Journal of Earth Sciences*, **69**, 47–60, <https://doi.org/10.1080/08120099.2021.1939158>
- Nayebi, N., Raeisi, D., Babazadeh, S., Xia, X. and Santosh, M. 2024. Zircon U–Pb–Hf and whole-rock Sr–Nd isotopic insights on the Silurian syenite–monzonite shoshonitic magmatism of Central Iran. *Geological Journal*, **59**, <https://doi.org/10.1002/gj.4876>
- Niu, Y. 2021. Lithosphere thickness controls the extent of mantle melting, depth of melt extraction and basalt compositions in all tectonic settings on Earth – a review and new perspectives. *Earth-Science Reviews*, **217**, article 103614, <https://doi.org/10.1016/j.earscirev.2021.103614>
- O'Neill, H., Berry, A.J., Danyushevsky, L.V., Falloon, T.J., Maas, R. and Feig, S.T. 2024. The relationship between iron redox states and H₂O contents in back-arc basin basaltic glasses from the North Fiji Basin. *Chemical Geology*, **655**, article 122062, <https://doi.org/10.1016/j.chemgeo.2024.122062>
- Overton, R. 1990. Sheahan–Grants gold deposit, Junction Reefs. *Australian Institute of Mining and Metallurgy Monograph*, **14**, 1403–1407.
- Pacey, A. 2016. *The Characteristics, Geochemistry and Origin of Propylitic Alteration in the Northparkes Porphyry Cu–Au System*. PhD thesis, Imperial College London.
- Pacey, A., Wilkinson, J.J., Owens, J., Priest, D., Cooke, D.R. and Millar, I.L. 2019. The anatomy of an alkalic porphyry Cu–Au system: geology and alteration at Northparkes Mines, New South Wales, Australia. *Economic Geology*, **114**, 441–472, <https://doi.org/10.5382/econgeo.4644>
- Packham, G.H. 1987. The eastern Lachlan Fold Belt of southeast Australia: a possible Late Ordovician to Early Devonian sinistral strike slip regime. *AGU Geodynamics Series*, **19**, 67–82, <https://doi.org/10.1029/GD019p0067>
- Pagen, R. 1998. *Ordovician Kaiser Cu–Au deposit, central west New South Wales*. University of Tasmania Research Project Report (Unpublished).
- Park, J.-W., Campbell, I.H., Chiaradia, M., Hao, H. and Lee, C.-T. 2021. Crustal magmatic controls on the formation of porphyry copper deposits. *Nature Reviews Earth and Environment*, **2**, 542–557, <https://doi.org/10.1038/s43017-021-00182-8>
- Pearce, J.A. 1982. Trace element characteristics of lavas from destructive plate boundaries. In: Thorpe, R. (ed.) *Andesites: Orogenic Andesites and Related Rocks*. Wiley, 525–548.
- Pearce, J.A. 1996. A users guide to basalt discrimination diagrams. *Geological Association of Canada Short Course Notes*, **12**, 79–113.
- Pearce, J.A. 2008. Geochemical fingerprinting of oceanic basalts with applications to ophiolite classification and the search for Archean oceanic crust. *Lithos*, **100**, 14–48, <https://doi.org/10.1016/j.lithos.2007.06.016>
- Pearce, J.A. 2014. Immobile element fingerprinting of ophiolites. *Elements*, **10**, 101–108, <https://doi.org/10.2113/gselements.10.2.101>
- Pearce, J.A., Stern, R.J., Bloomer, S.H. and Fryer, P. 2005. Geochemical mapping of the Mariana arc-basin system: implications for the nature and distribution of subduction components. *Geochemistry, Geophysics, Geosystems*, **6**, article 2004GC000895, <https://doi.org/10.1029/2004GC000895>
- Peate, D.W., Pearce, J.A., Hawkesworth, C.J., Colley, H., Edwards, C.M.H. and Hirose, K. 1997. Geochemical variations in Vanuatu arc lavas: the role of subducted material and a variable mantle wedge composition. *Journal of Petrology*, **38**, 1331–1358, <https://doi.org/10.1093/ptro/38.10.1331>
- Peccerillo, A. and Taylor, S.R. 1976. Geochemistry of eocene calc-alkaline volcanic rocks from the Kastamonu area, Northern Turkey. *Contributions to Mineralogy and Petrology*, **58**, 63–81, <https://doi.org/10.1007/BF00384745>
- Percival, I.G. and Glen, R.A. 2007. Ordovician to earliest Silurian history of the Macquarie Arc, Lachlan Orogen, New South Wales. *Australian Journal of Earth Sciences*, **54**, 143–165, <https://doi.org/10.1080/08120090601146789>
- Percival, I.G., Morgan, E.J. and Scott, M.M. 1999. Ordovician to earliest Silurian history of the Macquarie Arc, Lachlan Orogen, New South Wales. *Geological Survey of New South Wales Quarterly Notes*, **108**, 8–27.
- Perkins, C., McDougall, I., Claoue-Long, J. and Hithersay, P. 1990. ⁴⁰Ar–³⁹Ar and U–Pb geochronology of the Goonumbra copper–gold and Gidginbung gold deposits, New South Wales, Australia. *Economic Geology*, **85**, 1808–1824, <https://doi.org/10.2113/gsecongeo.85.8.1808>
- Perkins, C., McDougall, I. and Walshe, J.L. 1992. Timing of shoshonitic magmatism and gold mineralization, Sheahan–Grants and Glendale, New South Wales. *Australian Journal of Earth Sciences*, **39**, 99–110, <https://doi.org/10.1080/08120099208728004>
- Perkins, C., Walshe, J.L. and Morrison, G. 1995. Metallogenic episodes of the Tasman fold belt system, eastern Australia. *Economic Geology*, **90**, 1443–1466, <https://doi.org/10.2113/gsecongeo.90.6.1443>
- Pettke, T., Oberli, F. and Heinrich, C.A. 2010. The magma and metal source of giant porphyry-type ore deposits, based on lead isotope microanalysis of individual fluid inclusions. *Earth and Planetary Science Letters*, **296**, 267–277, <https://doi.org/10.1016/j.epsl.2010.05.007>
- Pickett, J.W. and Ingpen, I.A. 1990. Ordovician and Silurian strata south of Trundle, New South Wales. *Geological Survey of New South Wales Quarterly Notes*, **78**, 1–14.
- Plank, T. and Langmuir, C.H. 1993. Tracing trace elements from sediment input to volcanic output at subduction zones. *Nature*, **362**, 739–743, <https://doi.org/10.1038/362739a0>
- Plank, T. and Langmuir, C.H. 1998. The chemical composition of subducting sediment and its consequences for the crust and mantle. *Chemical Geology*, **145**,

- 325–394, [https://doi.org/10.1016/S0009-2541\(97\)00150-2](https://doi.org/10.1016/S0009-2541(97)00150-2)
- Plank, T., Kelley, K.A., Zimmer, M.M., Hauri, E.H. and Wallace, P.J. 2013. Why do mafic arc magmas contain ~4 wt% water on average? *Earth and Planetary Science Letters*, **364**, 168–179, <https://doi.org/10.1016/j.epsl.2012.11.044>
- Richards, J.P. 2009. Postsubduction porphyry Cu–Au and epithermal Au deposits: products of remelting of subduction-modified lithosphere. *Geology*, **37**, 247–250, <https://doi.org/10.1130/G25451A.1>
- Richards, J.P., Spell, T., Rameh, E., Razique, A. and Fletcher, T. 2012. High Sr/Y magmas reflect arc maturity, high magmatic water content, and porphyry Cu \pm Mo \pm Au potential: examples from the Tethyan arcs of central and eastern Iran and western Pakistan. *Economic Geology*, **107**, 295–332, <https://doi.org/10.2113/econgeo.107.2.295>
- Rosenbaum, G. 2018. The Tasmanides: Phanerozoic tectonic evolution of eastern Australia. *Annual Review of Earth and Planetary Sciences*, **46**, 291–325, <https://doi.org/10.1146/annurev-earth-082517-010146>
- Saccani, E. 2015. A new method of discriminating different types of post-Archean ophiolitic basalts and their tectonic significance using Th–Nb and Ce–Dy–Yb systematics. *Geoscience Frontiers*, **6**, 481–501, <https://doi.org/10.1016/j.gsf.2014.03.006>
- Savov, I.P., Ryan, J.G., D'Antonio, M., Kelley, K. and Mattie, P. 2005. Geochemistry of serpentized peridotites from the Mariana Forearc Conical Seamount, ODP Leg 125: implications for the elemental recycling at subduction zones. *Geochemistry, Geophysics, Geosystems*, **6**, article 2004GC000777, <https://doi.org/10.1029/2004GC000777>
- Scarrow, J.H., Bea, F., Montero, P. and Molina, J.F. 2008. Shoshonites, vagnerites and potassic lamprophyres: similarities and differences between 'ultra'-high-K rocks. *Earth and Environmental Science Transactions of the Royal Society of Edinburgh*, **99**, 159–175, <https://doi.org/10.1017/S1755691009008032>
- Scheibner, E. 1987. Paleozoic development of eastern Australia in relation to the Pacific region. *AGU Geodynamic Series*, **18**, 133–165.
- Scott, K.M. 1978. Geochemical aspects of the alteration–mineralization at Copper Hill, New South Wales, Australia. *Economic Geology*, **73**, 966–976, <https://doi.org/10.2113/gsecongeo.73.5.966>
- Sherwin, L. 1976. The Secrets section through the Cotton Beds north of Parkes. *Geological Survey of New South Wales Quarterly Notes*, **24**, 6–10.
- Sherwin, L. 1996. *Narrowmire 1:250 000 Geological Sheet SI/55-3: Explanatory Notes* Geological Survey of New South Wales, Sydney.
- Sherwin, L. 2000. Cotton formation. In: Lyons, P., Raymond, O.L. and Duggan, M.B. (eds) *Forbes 1:250 000 Geological Sheet 2nd Edition SI/55-7 Explanatory Notes*. Australian Geological Survey Organisation Record **2000/20**, 230.
- Sillitoe, R.H. 1972. A plate tectonic model for the origin of porphyry copper deposits. *Economic Geology*, **67**, 184–197, <https://doi.org/10.2113/gsecongeo.67.2.184>
- Sillitoe, R.H. 1973. The tops and bottoms of porphyry copper deposits. *Economic Geology*, **68**, 799–815, <https://doi.org/10.2113/gsecongeo.68.6.799>
- Sillitoe, R.H. 1997. Characteristics and controls of the largest porphyry copper–gold and epithermal gold deposits in the circum-Pacific region. *Australian Journal of Earth Sciences*, **44**, 373–388, <https://doi.org/10.1080/08120099708728318>
- Sillitoe, R.H. 2000. Gold-rich porphyry deposits: descriptive and genetic models and their role in exploration and discovery. *Reviews in Economic Geology*, **13**, 215–345, <https://doi.org/10.5382/Rev.13.09>
- Sillitoe, R.H. 2010. Porphyry copper systems. *Economic Geology*, **105**, 3–41, <https://doi.org/10.2113/gsecongeo.105.1.3>
- Sillitoe, R.H. 2012. Copper provinces. *Society of Economic Geologists, Special Publication*, **16**, 1–18.
- Simpson, B.P. and Sutherland, F.L. 2022. Cenozoic volcanism in New South Wales. *Geological Survey of New South Wales Quarterly Notes*, **156**, 1–40.
- Simpson, C.J., Cas, R.A.F. and Arundell, M.C. 2005. Volcanic evolution of a long-lived Ordovician island-arc province in the Parkes region of the Lachlan Fold Belt, southeastern Australia. *Australian Journal of Earth Sciences*, **52**, 863–886, <https://doi.org/10.1080/08120090500304273>
- Simpson, C.J., Scott, R.J., Crawford, A.J. and Meffre, S. 2007. Volcanology, geochemistry and structure of the Ordovician Cargo Volcanics in the Cargo–Walli region, central New South Wales. *Australian Journal of Earth Sciences*, **54**, 315–352, <https://doi.org/10.1080/08120090701221706>
- Singer, D.A. 2017. Future copper resources. *Ore Geology Reviews*, **86**, 271–279, <https://doi.org/10.1016/j.oregeorev.2017.02.022>
- Squire, R.J. and Crawford, A.J. 2007. Magmatic characteristics and geochronology of Ordovician igneous rocks from the Cadia–Neville region, New South Wales: implications for tectonic evolution. *Australian Journal of Earth Sciences*, **54**, 293–314, <https://doi.org/10.1080/08120090601147001>
- Squire, R.J. and McPhie, J. 2007. Complex volcanic facies architecture of the Forest Reefs Volcanics near Cadia, New South Wales, associated with prolonged arc-related volcanism. *Australian Journal of Earth Sciences*, **54**, 273–292, <https://doi.org/10.1080/08120090601146995>
- Stern, R.J. and Arima, M. 1998. Introduction to the special volume on the Izu–Bonin–Mariana arc system. *Island Arc*, **7**, 295–300, <https://doi.org/10.1111/j.1440-1738.1998.00190.x>
- Sun, S.S. 1980. Lead isotopic study of young volcanic rocks from mid-ocean ridges, ocean islands and island arcs. *Philosophical Transactions of the Royal Society of London Series A: Mathematical and Physical Sciences*, **297**, 409–445, <https://doi.org/10.1098/rsta.1980.0224>
- Sun, C.H. and Stern, R.J. 2001. Genesis of Mariana shoshonites: contribution of the subduction component. *Journal of Geophysical Research: Solid Earth*, **106**, 589–608, <https://doi.org/10.1029/2000JB900342>
- Tamura, Y., Busby, C.J., and Blum, P. and Expedition 350 Scientists 2015. *Proceedings of the International Ocean Discovery Program. Volume 350: Izu–Bonin–Mariana Rear Arc*. International Ocean Discovery Program, <https://doi.org/10.14379/iodp.proc.350.2015>

- Tani, K., Fiske, R.S., Dunkley, D.J., Ishizuka, O., Oikawa, T., Isobe, I. and Tatsumi, Y. 2011. The Izu Peninsula, Japan: zircon geochronology reveals a record of intra-oceanic rear-arc magmatism in an accreted block of Izu–Bonin upper crust. *Earth and Planetary Science Letters*, **303**, 225–239, <https://doi.org/10.1016/j.epsl.2010.12.052>
- Tatsumi, Y. and Eggins, S. 1995. *Subduction Zone Magmatism*. Blackwell Science; Frontiers in Earth Sciences.
- Till, C.B., Grove, T.L. and Withers, A.C. 2012. The beginnings of hydrous mantle wedge melting. *Contributions to Mineralogy and Petrology*, **163**, 669–688, <https://doi.org/10.1007/s00410-011-0692-6>
- Torabi, G. 2011. Middle Eocene volcanic shoshonites from western margin of Central–East Iranian Microcontinent (CEIM), a mark of previously subducted CEIM-confining oceanic crust. *Petrology*, **19**, 675–689, <https://doi.org/10.1134/S0869591111030039>
- Turner, S.J. and Langmuir, C.H. 2015. What processes control the chemical compositions of arc front stratovolcanoes? *Geochemistry, Geophysics, Geosystems*, **16**, 1865–1893, <https://doi.org/10.1002/2014GC005633>
- Turner, S., Arnaud, N. *et al.* 1996. Post-collision, shoshonitic volcanism on the Tibetan plateau: implications for convective thinning of the lithosphere and the source of ocean island basalts. *Journal of Petrology*, **37**, 45–71, <https://doi.org/10.1093/petrology/37.1.45>
- Veevers, J.J. 2013. Pangea: geochronological correlation of successive environmental and strati-tectonic phases in Europe and Australia. *Earth-Science Reviews*, **127**, 48–95, <https://doi.org/10.1016/j.earscirev.2013.09.001>
- Wallace, P.J. 2005. Volatiles in subduction zone magmas: concentrations and fluxes based on melt inclusion and volcanic gas data. *Journal of Volcanology and Geothermal Research*, **140**, 217–240, <https://doi.org/10.1016/j.jvolgeores.2004.07.023>
- Wells, T.J. 2016. *Geology and Genesis of the Two-Thirty Prospect, Northparkes, NSW*. Honours thesis, University of Tasmania.
- Wells, T.J., Meffre, S., Cooke, D.R., Steadman, J.A. and Hoyer, J.L. 2020. Porphyry fertility in the Northparkes district: indicators from whole-rock geochemistry. *Australian Journal of Earth Sciences*, **67**, 717–738, <https://doi.org/10.1080/08120099.2020.1715477>
- Wells, T.J., Cooke, D.R. *et al.* 2021. Geology and geochronology of the Two-Thirty prospect, Northparkes district, NSW. *Australian Journal of Earth Sciences*, **68**, 659–683, <https://doi.org/10.1080/08120099.2021.1861095>
- Wilkinson, J.J. 2013. Triggers for the formation of porphyry ore deposits in magmatic arcs. *Nature Geoscience*, **6**, 917–925, <https://doi.org/10.1038/ngo1940>
- Wilson, A.J., Cooke, D.R. and Harper, B.L. 2003. The Ridgeway gold–copper deposit: a high-grade alkalic porphyry deposit in the Lachlan Fold Belt, New South Wales, Australia. *Economic Geology*, **98**, 1637–1666, <https://doi.org/10.2113/gsecongeo.98.8.1637>
- Wilson, A.J., Cooke, D.R., Stein, H.J., Fanning, C.M., Holliday, J.R. and Tedder, I.J. 2007. U–Pb and Re–Os geochronologic evidence for two alkalic porphyry ore-forming events in the Cadia district, New South Wales, Australia. *Economic Geology*, **102**, 3–26, <https://doi.org/10.2113/gsecongeo.102.1.3>
- Wilson, M. (ed.) 1989. *Igneous Petrogenesis*. Springer, <https://doi.org/10.1007/978-1-4020-6788-4>
- Wilson, M. 2003. *The Geology, Genesis and Exploration Context of the Cadia Gold–Copper Porphyry Deposits, New South Wales, Australia*. PhD thesis, University of Tasmania.
- Winter, J.D. 2014. *Principles of Igneous and Metamorphic Petrology*. 2nd edn. Harlow, UK, Pearson education.
- Wormald, R.J. 1993. *The petrology and geochemistry of mid to late Palaeozoic magmatism in the Temora region, New South Wales*. PhD thesis, Department of Geology, La Trobe University.
- Wyborn, D. 1992. The tectonic significance of Ordovician magmatism in the eastern Lachlan Fold Belt. *Tectonophysics*, **214**, 177–192, [https://doi.org/10.1016/0040-1951\(92\)90196-D](https://doi.org/10.1016/0040-1951(92)90196-D)
- Wyborn, D. 1996. *Geology, Chemistry and Gold/Copper Potential of the Temora Belt and Adjacent Gilmore Fault System*. Australian Mineral Industries Research Association Ltd (AMIRA) Project Report **P425**.
- Wyborn, D. 1997. Regional geology of the Forest Reefs Volcanic Complex. In: Lawrie, K.C. *Porphyry–Epithermal Deposits of the Lachlan Fold Belt*. Pre-conference field trip 27–29 January 1997. Specialist group in Economic Geology, Geological Society of Australia.
- Wyborn, D. and Sun, S.S. 1993. Nd-isotopic ‘fingerprinting’ of the Cu/Au mineralisation in the Lachlan Fold Belt. *AGSO Research Newsletter*, **19**, 13–14.
- Yutani, T., Hirano, N. *et al.* 2023. An intraoceanic juvenile arc of shoshonite and adakitic andesite in the Nemuro Belt, the Lesser Kuril Arc, across the K/Pg boundary. *Cretaceous Research*, **147**, article 105510, <https://doi.org/10.1016/j.cretres.2023.105510>
- Zhang, Q., Buckman, S., Bennett, V.C. and Nutman, A. 2019. Inception and early evolution of the Ordovician Macquarie Arc of eastern Gondwana margin: zircon U–Pb–Hf evidence from the Molong Volcanic Belt, Lachlan Orogen. *Lithos*, 326–327, 513–528, <https://doi.org/10.1016/j.lithos.2019.01.008>
- Zhang, Q., Nutman, A., Buckman, S. and Bennett, V.C. 2020. What is underneath the juvenile Ordovician Macquarie Arc (eastern Australia)? A question resolved using Silurian intrusions to sample the lower crust. *Gondwana Research*, **81**, 362–377, <https://doi.org/10.1016/j.gr.2019.11.018>
- Zhen, Y.Y. and Percival, I.G. 2023. Late Ordovician conodonts from subsurface carbonates near Quandialla and inferred depositional age of the Currumburrumba Volcanics in south–central New South Wales. *Proceedings of the Linnean Society of New South Wales*, **145**, 35–54.
- Zukowski, W. 2010. *Geology and Mineralisation of the Endeavour 41 Gold Deposit Cowal District, NSW*. PhD thesis, University of Tasmania.